

University of Kentucky

UKnowledge

Theses and Dissertations--Molecular and Cellular Biochemistry

Molecular and Cellular Biochemistry


2019

SEMISYNTHETIC AURONES: A FAMILY OF NEWLY DISCOVERED TUBULIN INHIBITORS AS ANTINEOPLASTIC AGENTS

Yanqi Xie

University of Kentucky, yqxiexie@gmail.com

Author ORCID Identifier:

 <https://orcid.org/0000-0002-9887-0084>

Digital Object Identifier: <https://doi.org/10.13023/etd.2019.387>

[Right click to open a feedback form in a new tab to let us know how this document benefits you.](#)

Recommended Citation

Xie, Yanqi, "SEMISYNTHETIC AURONES: A FAMILY OF NEWLY DISCOVERED TUBULIN INHIBITORS AS ANTINEOPLASTIC AGENTS" (2019). *Theses and Dissertations--Molecular and Cellular Biochemistry*. 44. https://uknowledge.uky.edu/biochem_etds/44

This Doctoral Dissertation is brought to you for free and open access by the Molecular and Cellular Biochemistry at UKnowledge. It has been accepted for inclusion in Theses and Dissertations--Molecular and Cellular Biochemistry by an authorized administrator of UKnowledge. For more information, please contact UKnowledge@lsv.uky.edu.

STUDENT AGREEMENT:

I represent that my thesis or dissertation and abstract are my original work. Proper attribution has been given to all outside sources. I understand that I am solely responsible for obtaining any needed copyright permissions. I have obtained needed written permission statement(s) from the owner(s) of each third-party copyrighted matter to be included in my work, allowing electronic distribution (if such use is not permitted by the fair use doctrine) which will be submitted to UKnowledge as Additional File.

I hereby grant to The University of Kentucky and its agents the irrevocable, non-exclusive, and royalty-free license to archive and make accessible my work in whole or in part in all forms of media, now or hereafter known. I agree that the document mentioned above may be made available immediately for worldwide access unless an embargo applies.

I retain all other ownership rights to the copyright of my work. I also retain the right to use in future works (such as articles or books) all or part of my work. I understand that I am free to register the copyright to my work.

REVIEW, APPROVAL AND ACCEPTANCE

The document mentioned above has been reviewed and accepted by the student's advisor, on behalf of the advisory committee, and by the Director of Graduate Studies (DGS), on behalf of the program; we verify that this is the final, approved version of the student's thesis including all changes required by the advisory committee. The undersigned agree to abide by the statements above.

Yanqi Xie, Student

Dr. Chunming Liu, Major Professor

Dr. Trevor P. Creamer, Director of Graduate Studies

SEMISYNTHETIC AURONES: A FAMILY OF NEWLY
DISCOVERED TUBULIN INHIBITORS AS ANTINEOPLASTIC AGENTS

DISSERTATION

A dissertation submitted in partial fulfillment of the
requirements for the degree of Doctor of Philosophy in the
College of Medicine
at the University of Kentucky

By

Yanqi Xie

Lexington, Kentucky

Co-Directors: Dr. Chunming Liu, Professor of Biochemistry
and Dr. David S. Watt, Professor of Biochemistry

Lexington, Kentucky

2019

Copyright ©Yanqi Xie 2019

ABSTRACT OF DISSERTATION

SEMISYNTHETIC AURONES: A FAMILY OF NEWLY DISCOVERED TUBULIN INHIBITORS AS ANTINEOPLASTIC AGENTS

Aurones belong to an uncommon class of plant flavonoids that provide the bright yellow coloration of some ornamental flowers and that possess a range of biological activities. Structure-activity relationships (SAR) in the aurone pharmacophore identified heterocyclic variants of the (*Z*)-2-benzylidene-6-hydroxybenzofuran-3(*2H*)-one scaffold that possessed low nanomolar *in vitro* potency in cell proliferation assays using various cancer cell lines, *in vivo* potency in prostate cancer PC-3 xenograft and zebrafish models, selectivity for the colchicine-binding site on tubulin, and absence of appreciable toxicity. Among biologically active analogs developed in the course of this dissertation work were (*Z*)-2-((2-((1-ethyl-5-methoxy-1*H*-indol-3-yl)methylene)-3-oxo-2,3-dihydrobenzofuran-6-yl)oxy)acetonitrile (**5a**) and (*Z*)-6-((2,6-dichlorobenzyl)oxy)-2-(pyridin-4-ylmethylene)benzofuran-3(*2H*)-one (**5r**). These two aurones **5a** and **5r** inhibited *in vitro* PC-3 prostate cancer cell proliferation with IC₅₀ values below 100 nM. A xenograft study in nude mice using 10 mg/kg of **5a** for 18 days had no effect on mice weight, and aurone **5a** did not inhibit, as desired, the human ether-à-go-go-related (hERG) potassium channel. Cell cycle arrest data, comparisons of the inhibition of cancer cell proliferation by aurones and known antineoplastic agents, and *in vitro* inhibition of tubulin polymerization indicated that aurone **5a** disrupted tubulin dynamics. Based on a National Cancer Institute COMPARE analysis, studies using computer-based molecular docking and liquid chromatography-electrospray ionization-tandem mass spectrometry studies, aurone **5a** targets the colchicine-binding site on tubulin. In addition to solid tumors, aurones **5a** and **5r** strongly inhibited *in vitro* a panel of human leukemia cancer cell lines and the *in vivo* myc-induced T cell acute lymphoblastic leukemia (T-ALL) in a zebrafish model. In summary, aurones possess a pharmacophore of considerable potential in the search for new antineoplastic agents for the clinical treatment of human cancers.

KEYWORDS: Aurones, Cancer, Tubulins, Microtubules

Yanqi Xie

Student's Signature

09-25-2019

Date

SEMISYNTHETIC AURONES: A FAMILY OF NEWLY
DISCOVERED TUBULIN INHIBITORS AS ANTINEOPLASTIC AGENTS

By

Yanqi Xie

Dr. Chunming Liu

Co-Director of Dissertation

Dr. David S. Watt

Co-Director of Dissertation

Dr. Trevor P. Creamer

Director of Graduate Studies

09-25-2019

Date

To my father for his unwavering trust in me

ACKNOWLEDGEMENTS

First, I need to thank my co-mentors Dr. Chunming Liu and Dr. David Watt for a unique environment for my Ph.D. training in the application of organic chemistry and biology to drug development. I am grateful for their guidance, suggestions, and patience. I would also like to thank my Graduate Research Committee members Dr. Chang-Guo Zhan and Dr. Tianyan Gao, as well as my outside examiner Dr. Kyung Bo Kim, who provided constructive advice on my research project and dissertation.

I express thanks to my colleagues, Wen Zhang, Dr. Tianxin Yu, Xuehe Xu, Muxian Liu, and Zack Martin for their help. I thank Dr. Stefan Kwiatkowski, Dr. Vitaliy Sviripa, Liliia Kril, and Dr. Przemyslaw Wyrebek, for their supportive help in this project. A special thanks goes to Dr. Mykhaylo Frasinuk for providing an initial set of aurone compounds for screening. I appreciated help from Dr. Yinan Zhang and Dr. Lei Qi for technical discussions in organic synthesis and biology, respectively. Thanks also go to collaborators including Dr. Jing Chen, Dr. Haining Zhu, Elizabeth Hausman, Dr. Jessica Blackburn, Agripina Deaciuc, and Dr. Linda P. Dwoskin; I thank all the Biochemistry faculty, staff, and students for their support. I thank my undergraduate advisers Dr. Haiyan Hu and Dr. Guangmei Yan for my early training in science.

Finally, I am grateful to my family for their love and support. The trust, encouragement, understanding that my father and my mother put in me is the mighty power that drives me forward. I thank my sisters and their families for looking after my parents when I am away from home. Lastly, I thank my wife, Ying, for her unconditional love and support over the years.

TABLE OF CONTENTS

ACKNOWLEDGEMENTS	iii
TABLE OF CONTENTS.....	iv
LIST OF TABLES	vii
LIST OF FIGURES	viii
Chapter 1 Background and Introduction.....	1
Society’s cancer burden	1
The development of cancer therapeutics.....	2
Microtubules and tubulin inhibitors	4
Microtubule structure	4
Importance of microtubule dynamics	5
Examples of microtubule-targeting agents	8
Resistance to microtubule-targeting agents.....	9
Aurones	10
Dissertation objectives	13
Chapter 2 Materials and Methods.....	15
Chemistry	15
General procedure for the synthesis of aurones 3a-3f and 4a-4o	15
General procedure for the synthesis of aurones 5d-5q	25
Procedure for the synthesis of biotinylated aurone analog 6d	34
Biology.....	37
Cell lines and cell culture	37
Cell proliferation inhibition assay	37
Biotin-streptavidin pull-down assay.....	38
Silver staining.....	38
NCI-60 cell lines	38
Immunofluorescence imaging.....	38
<i>In vivo</i> microtubule assembly assay	39
<i>In vitro</i> tubulin polymerization assay.....	39
Molecular docking studies	40
Competitive tubulin binding assay	41

Cell cycle assay by flow cytometry.....	42
hERG binding studies.....	42
hERG-HEK Cell Culture.....	43
[³ H]-Dofetilide binding assay.....	43
<i>Membrane preparation</i>	43
<i>[³H]-Dofetilide binding assay</i>	44
<i>In vivo</i> evaluation of anti-leukemia activity in the zebrafish model	44
<i>In vivo</i> evaluation of antineoplastic activity and gross toxicity in PC-3 xenografts	45
Statistics	45
Chapter 3 Structure-activity relationships of semisynthetic aurones.....	47
Introduction	47
Results	48
Synthesis of semisynthetic aurones modified at C-2.....	48
Synthesis of semisynthetic aurones modified at C-6.....	50
Aurones 5a and 5r showed broad antineoplastic activities	54
Discussion	54
Chapter 4 Mechanism of action of semisynthetic aurones	57
Introduction	57
Results	58
Attempted affinity-based approach to purify aurone 5a 's binding partner	58
Use of NCI COMPARE analysis.....	61
Disruption microtubule networks	63
Effects on cell cycle.....	66
Tubulin polymerization in vivo and in vitro.....	66
Molecular docking analysis	69
Synergistic effects of aurones with a cyclin dependent kinase inhibitor.....	73
hERG inhibition.....	75
Discussion	76
Chapter 5 <i>In vivo</i> evaluation of the antineoplastic activity of aurones.....	80
Introduction	80
Results	81
Mouse xenograft model.....	81

Effects on leukemia cells and T-ALL.....	82
Discussion	85
Chapter 6 Conclusions and future directions	86
Conclusions	86
Future directions.....	88
APPENDIX A: Abbreviations	90
APPENDIX B: Collaborations	92
REFERENCES	93
VITA.....	98

LIST OF TABLES

Table 1. Abbreviated Structure-activity relationship (SAR) study involving modifications aurone at the C-2 and C-6 positions using prostate cancer PC-3 cell proliferation assays.

Table 2. SAR study involving modifications of the C-6 alkoxy group in aurones **5** *versus* modifications of the C-2 heteroaryl-substituted methylene subunit using prostate cancer PC-3 cell proliferation assays.

Table 3. IC₅₀ values of aurones **5a** and **5r** in cancer cell line proliferation inhibition assays.

Table 4. IC₅₀ values of aurone **5a** in National Cancer Institute (NCI) - 60 cell line proliferation inhibition assays (Data generated by the National Cancer Institute (Maryland, USA)).

Table 5. Results of an NCI COMPARE analysis.

Table 6. IC₅₀ values of aurone **5a** in leukemia cell line proliferation inhibition assays.

LIST OF FIGURES

Figure 1.1: Most common cancers in 2018 (source: World Health Organization).

Figure 1.2: Most common causes of cancer-related death in 2018 (source: World Health Organization).

Figure 1.3: The four binding sites of tubulin inhibitors on tubulins and microtubules. This figure is from Lu et al. *Pharm Res.* 2012, 29(11):2943-2971.

Figure 1.4: Structurally diverse colchicine-site binders: colchicine, ABT751, and TN16.

Figure 1.5: Aurone synthase converts chalcones through hydroxylation and oxidative cyclization to aureusidin through the shikimate pathway. This figure is adapted from Vogt T., *Molecular Plant*, 2010, 3(1):2-20.

Figure 3.1: **A**, Representative, naturally occurring aurones, sulfuretin (**1a**) and aureusidin (**1b**). **B**, Synthesis of aurones **3-5**. Legend: *a*, heterocyclic-substituted benzaldehydes or heteroarylcarboxaldehydes, 50% aq. potassium hydroxide, 1:1 ethanol: *N,N*-dimethylformamide (DMF), *b*, bromoacetonitrile, potassium carbonate, DMF; *c*, halogenated benzyl bromide, potassium carbonate, DMF. **C**, Leading aurone candidate. (*Z*)-2-((2-((1-ethyl-5-methoxy-1*H*-indol-3-yl) methylene)-3-oxo-2,3-dihydrobenzofuran-6-yl) oxy) acetonitrile (**5a**).

Figure 4.1: Synthesis scheme of biotinylated aurone analog **6d**. *a*, 1-ethyl-3-(3-dimethylaminopropyl)carbodiimide (EDC).

Figure 4.2: Biotinylated aurone analog **6d** inhibited PC-3 cell growth.

Figure 4.3: Pull-down assay results. Left lane, dimethyl sulfoxide (DMSO); Right lane, biotinylated aurone analog **6d**.

Figure 4.4: Aurone **5a** and **5r** treatment (6 hours) inhibited microtubule structures and caused cell morphology change in PC-3 cells as shown in panels A, DMSO; B, **5a** (1 μ M); C, **5a** (300 nM); D, **5r** (1 μ M); E, **5r** (300 nM). Red immunofluorescence: α -tubulin; blue immunofluorescence: 4', 6-diamidino-2-phenylindole (DAPI).

Figure 4.5: Aurones **5a** and **5r** induced cell cycle arrest in PC-3 cells.

Figure 4.6: Aurones **5a** and **5r** decreased tubulin polymerization in HEK293T cells.

Figure 4.7: Aurone **5a** (5 μ M) and colchicine (5 μ M) inhibited tubulin polymerization *in vitro* in a similar fashion.

Figure 4.8: (A) Structures of aurone **5a**, aurone **4d**, and colchicine. (B) Aurone **5a** bound to the colchicine-binding site (CBS) at the interface of $\alpha\beta$ -tubulin dimers (cyan for β , green for α). (C) Close-up view of the interaction environment of **5a** (gray sticks) and tubulin (cartoon). (D) Superimposition of **5a** (gray sticks) and **4d** (magenta sticks) in the colchicine-binding site. Hydrogen bonding is represented by yellow, dashed lines. (E) Superimposition of **5a** (gray sticks) and colchicine (purple sticks) in the colchicine-binding site.

Figure 4.9: Competitive tubulin binding assay with colchicine in the presence of increasing concentrations of aurones **5a** and **5r**.

Figure 4.10: Aurone **5a** induced cdc2 (CDK1) activation by decreasing phosphorylation at tyrosine 15.

Figure 4.11: Aurone **5a** had synergistic effects with a cdc2 inhibitor RO3306 on the proliferation of LS174T colon and PC-3 prostate cancer cells.

Figure 5.1: (A) Effects of aurone **5a** on PC-3 tumor xenografts in nude mice (n=5) at 10 mg/kg/day. (B) Effect on aurone **5a** on body weights of the treated mice: * $p < 0.05$, t-test.

Figure 5.2: Aurones **5a** and **5r** inhibited myc-induce T-ALL in a zebrafish model. (A and D). Treatment of green fluorescence protein (GFP)-labeled thymic lymphoma cells with DMSO alone at day 0 and day 5, respectively. (B and E) Treatment of GFP-labeled thymic lymphoma cells with aurone **5a** in DMSO at day 0 and day 5, respectively. (C and F) Treatment of GFP-labeled thymic lymphoma cells with aurone **5r** at day 0 and day 5, respectively. (G) Percent change in fluorescence (*i.e.*, number of GFP-labeled thymic lymphoma cells) as a function of time from administration of DMSO alone to the administration of aurone **5r** in each zebrafish (n=8).

Chapter 1 Background and Introduction

Society's cancer burden

Cancer is a collection of different diseases that are characterized by abnormal cell proliferation and cell metastasis to other parts of the body. Due to the genomic instability and heterogeneity of tumors, current treatments often fail to eradicate all malignant cancer cells and thus set the stage for cancer relapse as well as metastasis leading to premature death. According to the World Health Organization, cancer is the second leading cause of death with an estimated 9.6 million deaths worldwide in 2018. The most common organs that develop cancers and the organ-specific cancers causing deaths are shown in Figure 1.1 and Figure 1.2, respectively.

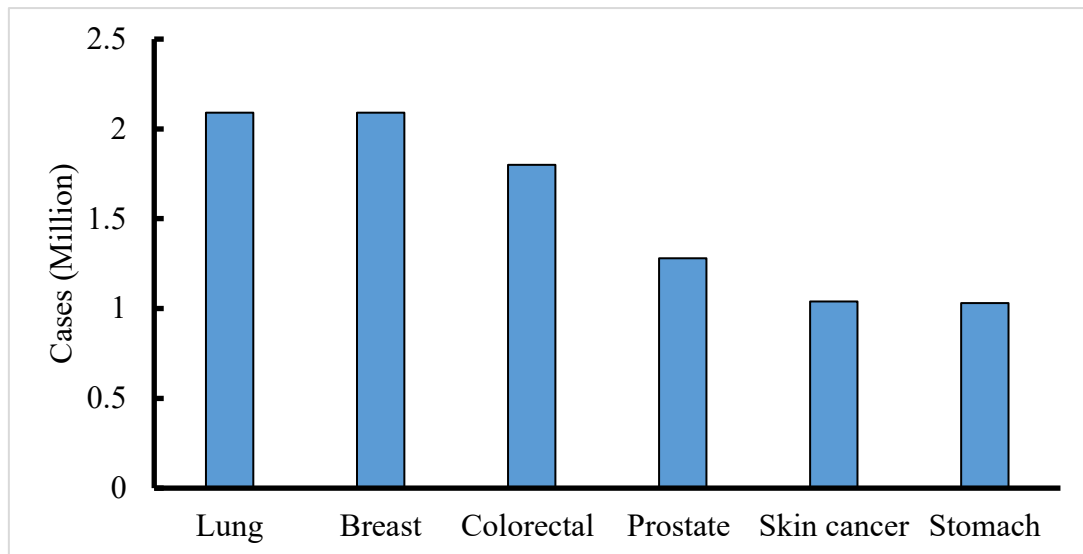


Figure 1.1: Most common cancers in 2018 (source: World Health Organization)

Although medical advances in cancer treatment have succeeded in extending human lifetimes, cancer remains as a significant financial burden for society. The total annual costs of cancer diagnosis and treatment in 2010 in the United States was estimated at approximately \$1.16 trillion¹. The projected total cost of cancer care in 2020 is estimated at \$173 billion, a 39% increase compared with the costs in 2010². Cancer represent an enormous burden to the patients, their families, and their societies, and efforts to treat these diseases represent an important, intellectually intriguing goal for science.

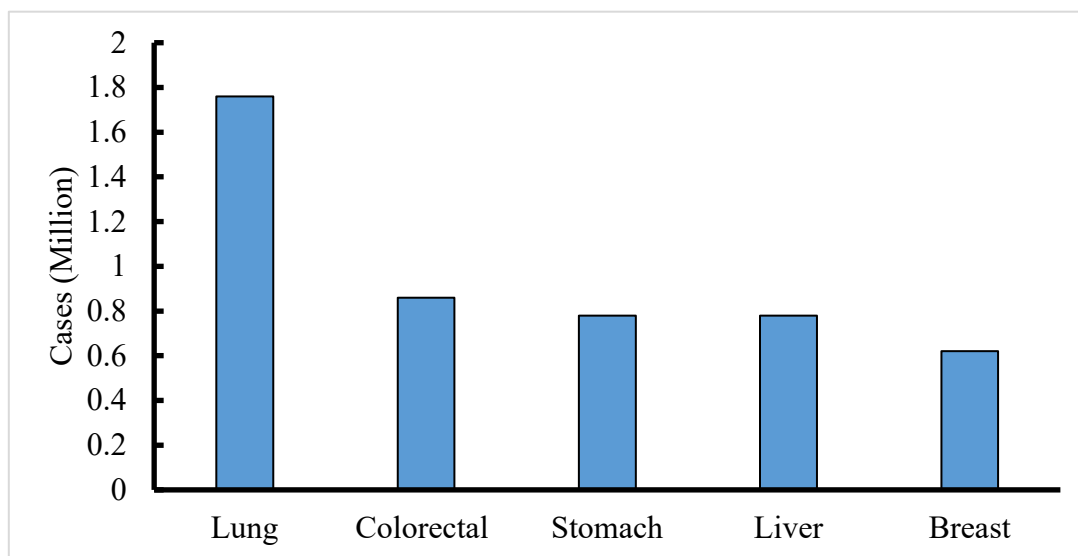


Figure 1.2: Most common causes of cancer-related death in 2018 (source: World Health Organization)

The development of cancer therapeutics

To reduce this cancer burden, the development of new therapeutics, including traditional “small molecules” and inventive “large molecules” such as antibodies, continuously evolved as we learned more about tumor molecular biology than we knew in the past. The transition from traditional, nonspecific chemotherapeutics such as cellular poisons modifying DNA to targeted therapies such as kinase inhibitors selectively affecting

signaling pathways in cancer cells represents a dramatic change. In addition, as our understanding of cancer biology increases, we gained a capacity to design treatments possessing specificity for cancer cells and avoiding significant side-effects on normal cells. Even these modern-day approaches are not without problems because targeted inhibitors are often effective during initial treatments but patients subsequently develop resistance to them during their long-term use.

The development of epidermal growth factor receptor (EGFR) tyrosine kinase inhibitors (TKIs) for the treatment of EGFR mutant Non-Small Cell Lung Cancers (NSCLCs) is an important example that showcases drug resistance and resistance-driven drug development. The EGFR tyrosine kinase regulates cell growth and proliferation and activating mutations drive NSCLC malignancy³. First generation EGFR TKIs gefitinib and erlotinib as well as second generation irreversible TKIs, afatinib and dacomitinib, are effective for about a year in most patients but then develop minimal effects due to a new acquired ATP pocket “gatekeeper” point mutation T790M⁴. To address the resistance caused by the mutant EGFR harboring T790M, third generation EGFR TKIs including WZ4002⁵ and CO1686⁶ were developed to target T790M EGFR selectively and spare the wild type EGFR as a means for reducing side-effects such as diarrhea and rash. The third generation EGFR TKIs are irreversible inhibitors that covalently bind to ATP pocket Cys797. Unfortunately, resistance to these third generation EGFR TKIs was found and EGFR C797S was revealed as a leading mechanism of resistance⁷. Recently, a fourth generation of EGFR TKIs were developed to target C797S/T790M EGFR mutant. One of the examples is an allosteric EGFR inhibitor EAI045, in which binding to EGFR is distant from the ATP-binding site⁸.

In addition to the success of “small-molecule” chemotherapeutics, antineoplastic antibodies such as the immune checkpoint blockers achieved impressive results with patients achieving a cancer-free state in some rare cases. However, only a small portion of patients respond to cancer immunotherapies and the cost of immunotherapies at “\$1 million per patient”⁹ is probably unsustainable. Small-molecule therapeutics will continue to enhance immunotherapies with respect to the resistance to cancer immunotherapies and their cost. Continued efforts focused on discovering novel small molecules remains as a worthy goal.

Microtubules and tubulin inhibitors

Microtubule structure

Microtubules are key components of the cellular cytoskeleton and perform important functions in cellular processes including cell cycle, cell morphology, intracellular transport and cell migration¹⁰. Microtubules are hollow, cylindrical polymeric structures with a diameter of approximately 25 nm, and are assembled from 13 protofilaments per microtubule¹⁰. These protofilaments polymerize from alpha-tubulin and beta-tubulin dimers in a head-to-tail fashion as shown in Figure 1.3. The $\alpha\beta$ -tubulin heterodimers are two 50-kDa proteins and show about 50% similarity.

The polarity of microtubules is defined as (+)- and (-)-ends¹¹ in which the (+)-end is the one ringed with beta-tubulin and the (-)-end is the one ringed with alpha-tubulin (Figure 1.3). Microtubules bind to microtubule-associated proteins that form the microtubule-organizing center. The (-)-ends of microtubules are anchored to the microtubule-organizing center whereas the (+)-ends are the dynamic locus for adding or removing tubulin dimers¹¹.

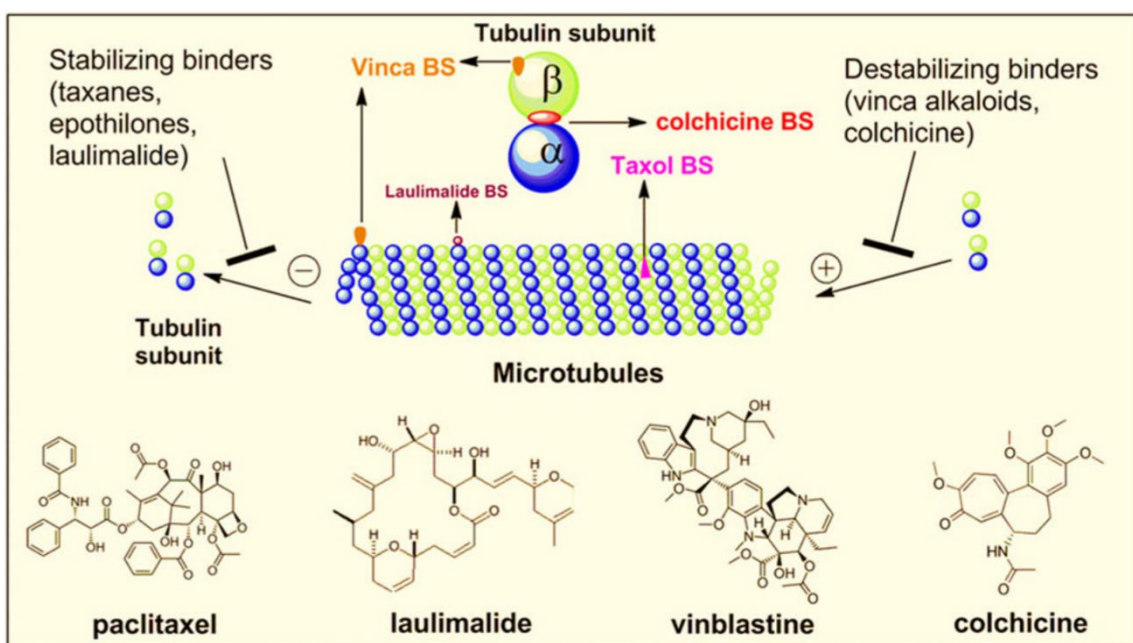


Figure 1.3: The four binding sites of tubulin inhibitors on tubulins and microtubules. This figure is from Lu et al. Pharm Res. 2012, 29(11):2943-2971.

Importance of microtubule dynamics

One key feature of microtubules is their dynamic instability, meaning that microtubules are constantly either growing or shortening in length by adding or removing tubulin dimers¹². Tubulins are guanosine triphosphate (GTP)-binding proteins although the GTP in alpha-tubulin is neither hydrolyzed nor exchanged with guanosine diphosphate

(GDP). For beta-tubulins, the bound GTP is hydrolyzed to guanosine diphosphate (GDP) after polymerization¹³. When the (+)-ends of microtubules are capped with GTP-bound beta-tubulins, then these microtubules will grow. If beta-tubulin-bound GTP hydrolysis faster than the rate of tubulin addition, the (+)-ends of microtubules are capped with GDP-bound beta-tubulins and these microtubules depolymerize to shorten the length.

Apart from the GTP-GDP cycling, tubulins also undergo structural changes in the microtubule assembly-disassembly process. Crystallography studies show that tubulins dimers are in a “curved conformation” while tubulins after polymerization into microtubules are in a “straight conformation”^{12,14}. Structural changes that occur during tubulin polymerization are within each alpha and beta-tubulin heterodimer and the inter-heterodimer interface. These reorientations are accompanied by structural rearrangements within tubulin subdomains.

Structural changes within tubulin heterodimers occur in the presence and absence of tubulin polymerization inhibitors. Colchicine is a well-established tubulin inhibitor (Figure 1.4) that binds to a specific colchicine-binding site (Figure 1.3) lying at the interface of alpha and beta-tubulin heterodimers. This site also accommodates chemically diverse ligands such as ABT751, TN16 (Figure 1.4) and others (reviewed in reference¹⁵). With or without colchicine occupying the colchicine-binding site, tubulin heterodimers are in a curved conformation. However, the T7 loop that links helix H7 and helix H8 (*i.e.*,

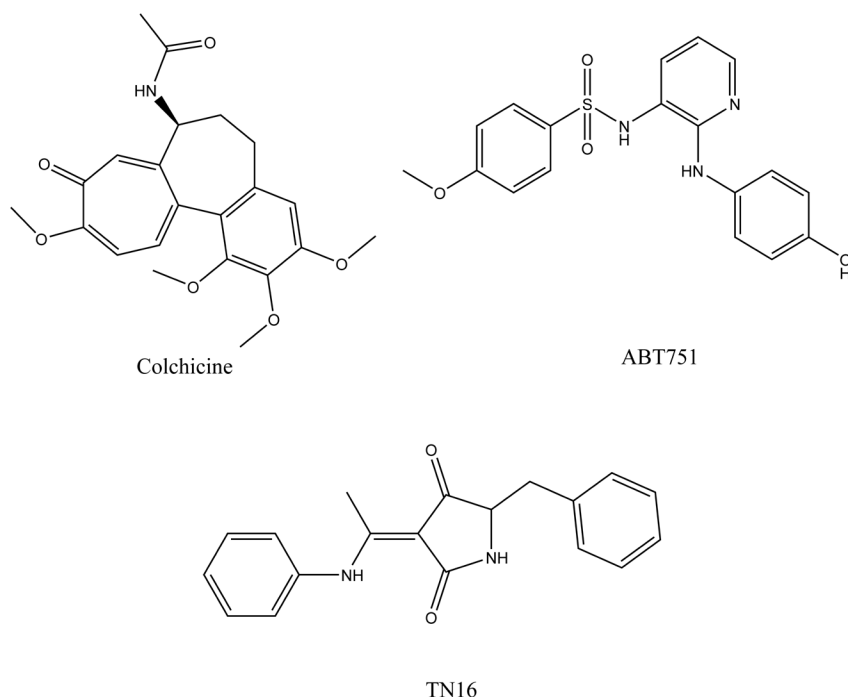


Figure 1.4: Structurally diverse colchicine site binders: colchicine, ABT751, and TN16.

helical designations in tubulin secondary structure nomenclature described in reference¹⁴) in beta-tubulin flips into the colchicine-binding site during the conformational change from curved to straight¹⁶. When the colchicine-binding site is occupied by a ligand, the conformational change in the T7 loop cannot occur, and tubulins cannot transition to the straight conformation. These circumstances inhibit tubulin polymerization¹⁶.

Tubulin polymerization is a critical part of tubulin dynamics, and tubulin inhibitors that disrupt this process lead to fatal effects for cells. During the cell cycle, a cell forms a mitotic spindle in which microtubules are the main components. During metaphase and anaphase, chromosomes are quickly aligned and then segregated into daughter cells by

mitotic spindle. Tubulin inhibitors disrupt this process and lead to cell cycle arrest at G2/M phase and ultimately cell death¹⁷.

Examples of microtubule-targeting agents

Tubulin inhibitors function by disrupting microtubule dynamics, either by inhibiting tubulin polymerization or by stabilizing microtubules. Over the years, many tubulin inhibitors were identified and categorized into four classes according to the natural products that target specific binding sites¹⁵: the laulimalide, taxane, Vinca alkaloid, and colchicine sites (Figure 1.3). Colchicine binds to the colchicine-binding site at the interface of tubulin heterodimers and Vinca alkaloids such as vinblastine bind to beta-tubulins. These two classes of inhibitors both inhibit tubulin polymerization. Taxanes bind to polymerized microtubules at the inner surface and stabilizes microtubules while laulimalide stabilizes microtubules but binds to a different site of microtubules.

Taxanes are a structurally complex but valuable class of diterpenes, and important representatives of this class include paclitaxel and docetaxel that are used in chemotherapy for breast cancer and prostate cancer¹⁸. These compounds have poor water-solubility and require polyethoxylated castor oil and ethanol for intravenous administration. Patients develop resistance to taxanes due to the expression of ABC drug transporters¹⁹, which decrease intracellular drug concentrations and reduces bioavailability. Another class of tubulin-stabilizing agents are the Vinca alkaloids (*i.e.*, vincristine, vinblastine, vindesine and vinorelbine) that are isolated from the periwinkle plant, *Catharanthus rosea*, and are the chronologically oldest of that microtubule-targeting agents. One of the fluorinated vinorelbine analogs, vinflunine, is approved to treat bladder cancer, and vinblastine was

used to treat a number of cancers including Hodgkin's lymphoma, non-small cell lung cancer, bladder cancer, brain cancer, melanoma, and testicular cancer²⁰.

Colchicine finds frequent use in the treatment of gout²¹, but its toxicity precludes its use in cancer treatment. Although the literature describes a number of colchicine-site binders as tubulin inhibitors¹⁹, none of these agents has yet gained FDA-approval for cancer chemotherapy. One of the advantages of colchicine-site binders is that many of these compounds are not substrates of P-glycoprotein (Pgp) drug efflux pumps¹⁹. Therefore, resistance that plagues drugs such as those in the taxane class may be less of an issue for colchicine-site binders. Combretastatin A-4 phosphate (CA4P) is a prodrug developed by Oxigene to treat solid tumors¹⁹. CA4P is dephosphorylated *in vivo* to the active metabolite CA4 that binds to the colchicine-binding site. Despite multiple clinical trials²², CA4P has yet to receive regulatory approval.

Resistance to microtubule-targeting agents

Several resistance mechanisms affect microtubule-targeting agents. Overexpression of the MDR1 gene is a major setback for tubulin inhibitors including taxanes and Vinca alkaloids. MDR1 encodes a Pgp drug efflux transporter that decreases intracellular drug concentrations and reduces bioavailability. Secondly, because there are at least 13 isotypes of tubulins, different compositions of microtubules show different sensitivity to tubulin inhibitors. Overexpression of tubulin isotype β III resulted in a slower polymerization rate in comparison with other tubulin isotypes. This altered microtubule dynamics lead to resistance to taxane and vinorelbine^{23,24}. Thirdly, microtubule dynamics

are regulated by cellular proteins such as stathmin and microtubule associated protein 4. Stathmin destabilizes microtubules while microtubule associated protein 4 promotes microtubule formation. Overexpression of stathmin decreases paclitaxel sensitivity in breast cancer and microtubule associated protein 4 overexpression reduces cytotoxicity of Vinca alkaloids^{25,26}. Overall, these resistance mechanisms warrant further efforts to develop new tubulin inhibitors that may overcome these types of drug resistance.

Aurones

Aurones are a sub-class of naturally occurring flavonoids that feature a common structural scaffold described as (*Z*)-2-benzylidenebenzofuran-3(*2H*)-one. The bright yellow color of ornamental flowers such as the snapdragon (*Antirrhinum majus*) derives from aurones. The biosynthesis of aurones involves the shikimate pathway leading first to phenylalanine and hence to from *p*-coumaroyl CoA²⁷. The addition of malonyl CoA extends the *p*-coumaroyl to a chalcone, and the enzyme, aurone synthase, catalyzes the conversion of chalcones, using hydroxylation and oxidative cyclization reactions, to aurones (Figure 1.5)^{28,29}. The main biological functions of aurones in plants are coloration of flowers and fruits and defense against insects and viruses³⁰.

Aurones are not as widely distributed in nature as other common flavonoids³¹, which is probably the reason why they have received less attention in comparison to the structurally similar and widely investigated flavones and isoflavones. Still, a number of interesting biological activities of aurones or semisynthetic aurones analogs were reported^{30,31}. The terminology “semisynthetic” refers to compounds bearing the parent

aurone pharmacophore found in nature but also possessing unnatural fragments introduced by chemists in a laboratory setting.

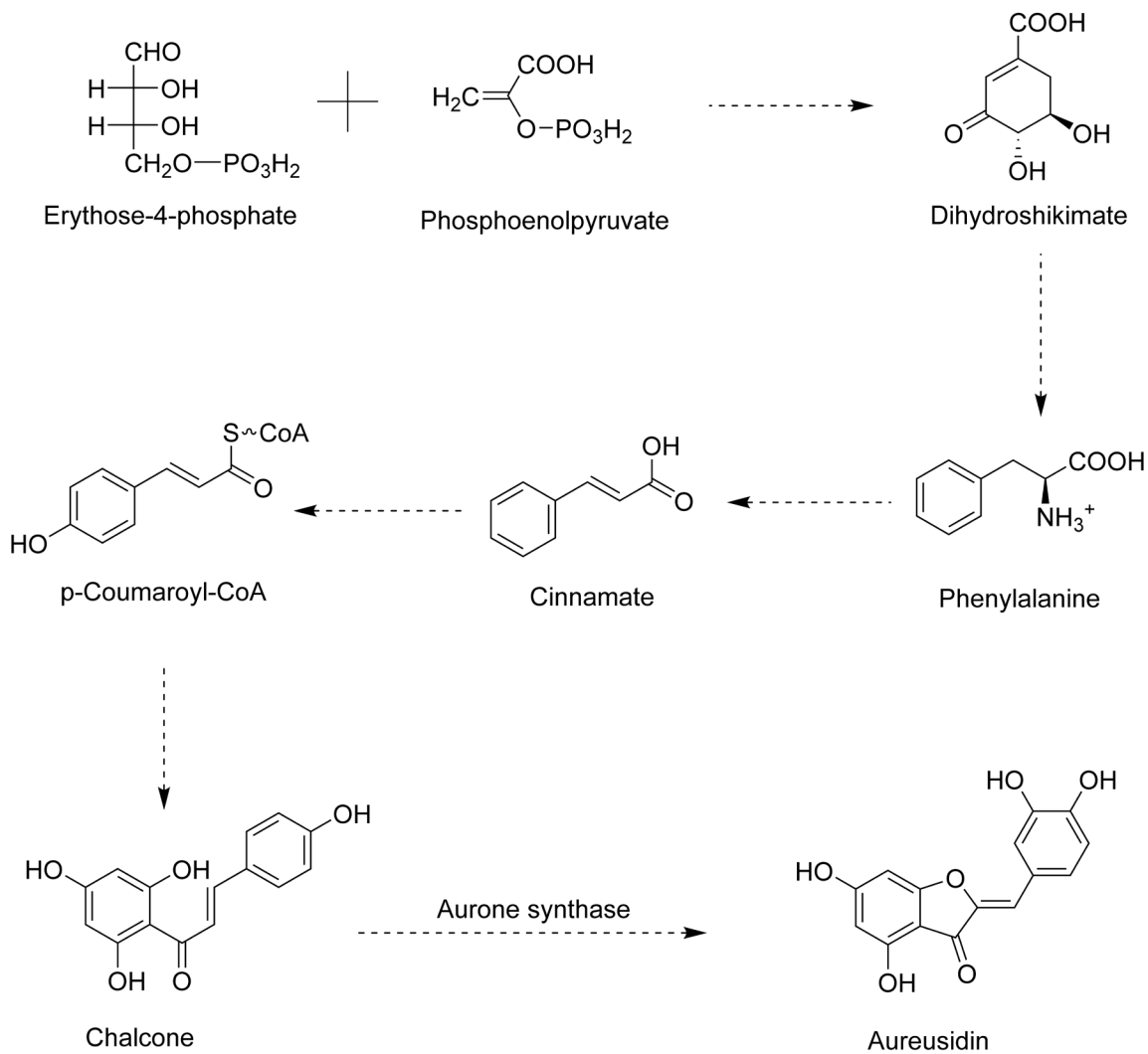


Figure 1.5: Aurone synthase converts chalcones through hydroxylation and oxidative cyclization to aureusidin through the shikimate pathway. This figure is adapted from Vogt T., *Molecular Plant*, 2010, 3(1):2-20.

Aurones possess antiparasitic, antimicrobial, anti-viral, anti-inflammatory, and antineoplastic bioactivities³¹, and aurone analogs as potential cancer therapeutics are the focus of this dissertation. Past research in aurones for cancer treatment involves several unrelated areas of research. A transmembrane drug transporter, P-glycoprotein (Pgp), was shown to mediate antineoplastic drug resistance by unwanted export of drugs from tumor cells³², and a number of aurone analogs based on 4-hydroxy-6-methoxyaurones were reported to bind to the cytosolic domain of P-glycoprotein³³. One of these reported compounds, 5,7-dimethoxyaurone, inhibited Pgp and thereby increased daunorubicin cytotoxicity on resistant K562 cells.

Cyclin-dependent kinases are well-established targets in cancer therapy³⁴ and a flavonoid cyclin-dependent kinase inhibitor flavopiridol, was approved by the FDA for the treatment of acute myeloid leukemia³⁵. Novartis developed an aurone mimic of flavopiridol and this mimic was as potent as flavopiridol as a cyclin-dependent kinase inhibitor³⁶.

Telomerase, the enzyme responsible for maintaining the length of telomeres, was activated in many human cancers and was extensively studied as a target for cancer treatment³⁷. A series of aurone analogs, namely 6,7-dihydroxyaurones, were reported as telomerase inhibitors³⁰ and the most potent one, 3',4'-dichloro-6,7-dihydroxyaurone, showed an IC₅₀ of 300 nM.

Finally, Wyeth reported an interesting set of benzofuran-3-one indole aurone derivatives as inhibitors of PI3 kinase- α and the mammalian target of rapamycin³⁸. Analog 32 showed strong potency against PI3 kinase-alpha with an IC₅₀ of 40 nM and displayed an IC₅₀ of 3 μ M on PC-3 cell proliferation inhibition assays. Because the related targets

were determined by looking at the downstream signaling of phosphorylated Akt and computational docking, the exact mechanism of action was unclear.

In summary, despite these unrelated prior studies, the naturally occurring aurone scaffold represents a valuable starting point for identifying novel antineoplastic agents and warrants further effort to address following problems. Firstly, the exact mechanism of action and direct binding targets of previous aurones are often unclear. Secondly, the potency of the reported aurone analogs requires improvement to the low nanomolar range. Developing aurone analogs with clear mechanisms of action requires aurones with a level of chemical complexity that will result in strong binding affinity to a specific target. This reduction to the low nanomolar range will also reduce possible off-target side effects. Thirdly, although tumor cell lines were used in the testing of the reported aurone analogs, the *in vivo* antineoplastic potential these agents must be explored.

Dissertation objectives

The long-term goal of this project is to develop specific aurone analogs as potential antineoplastic drugs. There are three specific aims of this dissertation

Aim 1: To synthesize new aurone derivatives and identify promising, potent leading compounds suitable for pharmaceutical development.

Aim 2a: To understand the precise molecular mechanisms and identify the direct biological target(s) of the potent leading compounds using biotinylated aurone derivatives.

Aim 2b: To perform target characterization and validation.

Aim 3: To perform *in vivo* evaluation of the antineoplastic effects of potent leading compounds.

Chapter 2 Materials and Methods

Chemistry

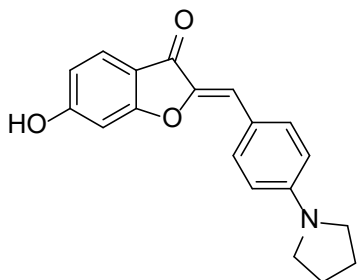
Chemicals were purchased from Sigma-Aldrich (St. Louis, MO) or Fisher Scientific (Pittsburgh, PA) unless otherwise noted or were synthesized according to literature procedures. Solvents were used from commercial vendors without further purification unless otherwise noted. Nuclear magnetic resonance spectra were determined on Varian instruments (^1H , 400 or 500MHz; ^{13}C , 100 or 126Mz). Low-resolution mass spectra were obtained using an Agilent 1100 (atmospheric pressure, chemical ionization) instrument. High resolution mass data were obtained by direct infusion electrospray ionization mass spectrometry (-MS) using a LTQ-Orbitrap mass spectrometer coupled with a Heated Electrospray Ionization (HESI-II) Probe (Thermo Fisher Scientific, Waltham, MA) and an FT analyzer at a resolution of 100,000. The reported m/z mass was a mean of 20 scans. Melting points were determined in open capillarity tubes with a Buchi B-535 apparatus and are uncorrected. Compounds were purified by chromatography on preparative layer Merck silica gel F254 unless otherwise noted.

General procedure for the synthesis of aurones **3a-3f** and **4a-4o**

To a suspension of 10 mmol of 6-hydroxybenzofuran-3(2H)-one (2) (Ark Pharm, Arlington Heights, IL USA) in 20 mL of a 1:1 mixture of DMF and absolute ethanol was added 2.3 mL of 50% aqueous potassium hydroxide. To this clear solution, obtained after stirring for ca. 30 min, was added 10 mmol of the appropriate carboxaldehyde. The mixture was stirred for 6-8 hours at 25°C. The mixture was diluted with 100 mL of hot water,

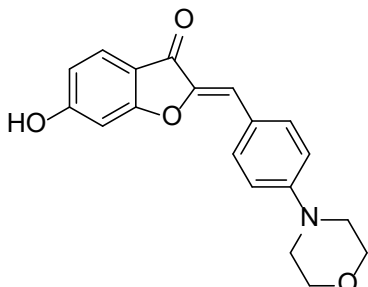
acidified with glacial acetic acid pH 5. The resulting precipitate was collected by filtration, washed with water, dried and re-crystallized from DMF-methanol.

(2Z)-6-Hydroxy-2-(4-pyrrolidin-1-ylbenzylidene)-1-benzofuran-3(2H)-one (3a).



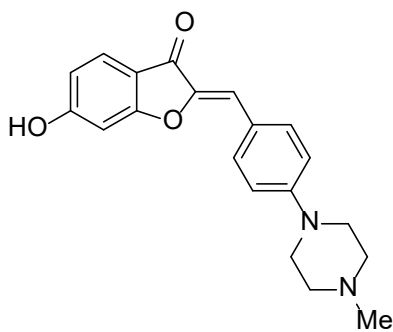
Yellow crystals (83% yield); mp >220°C; ¹H NMR (400 MHz, DMSO-*d*₆) δ 1.83-2.07 (m, 4H), 3.26-3.32 (m, 4H), 6.61 (d, *J* = 8.9 Hz, 2H), 6.66-6.72 (m, 2H), 6.77 (d, *J* = 1.9 Hz, 1H), 7.57 (d, *J* = 8.4 Hz, 1H), 7.77 (d, *J* = 8.9 Hz, 2H), 11 ppm (s, 1H); ¹³C NMR (100 MHz, DMSO-*d*₆) δ 24.95, 47.24, 98.42, 111.97, 112.58, 112.94, 113.69, 118.62, 125.39, 133.16, 144.73, 148.49, 165.58, 166.87, 180.64 ppm; MS (ACPI) *m/z* 308.1 (MH⁺, 100); HRMS (ESI/HESI) *m/z*: [M+H]⁺ Calcd for C₁₉H₁₇NO₃ 308.1281; Found 308.1279.

(2Z)-6-Hydroxy-2-(4-morpholin-4-ylbenzylidene)-1-benzofuran-3(2H)-one (3b).



Yellow crystals (78% yield); mp >220°C; ¹H NMR (400 MHz, DMSO-*d*₆) δ 3.15-3.30 (m, 4H), 3.63-3.80 (m, 4H), 6.70 (dd, *J* = 8.4, 2 Hz, 1H), 6.73 (s, 1H), 6.78 (d, *J* = 1.9 Hz, 1H), 7.02 (d, *J* = 9 Hz, 2H), 7.59 (d, *J* = 8.4 Hz, 1H), 7.82 (d, *J* = 9 Hz, 2H), 11.09 ppm (s, 1H); ¹³C NMR (100 MHz, DMSO-*d*₆) δ 47.04, 65.89, 98.52, 111.66, 112.78, 113.35, 114.27, 121.93, 125.64, 132.71, 145.65, 151.64, 165.98, 167.29, 181.02 ppm; MS (ACPI) *m/z* 324.1 (MH⁺, 100); HRMS (ESI/HESI) *m/z*: [M+H]⁺ Calcd for C₁₉H₁₇NO₄ 324.1230; Found 324.1228.

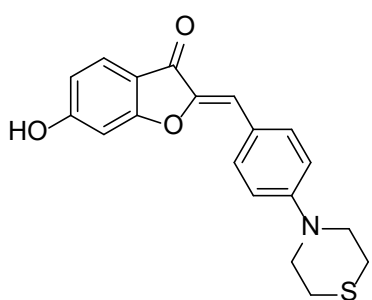
(2Z)-6-Hydroxy-2-[4-(4-methylpiperazin-1-yl)benzylidene]-1-benzofuran-3(2H)-one hydrochloride (3c). Yellow crystals (77% yield); mp >220°C; ¹H NMR (400 MHz, DMSO-*d*₆) δ 2.83 (s, 3H), 3.04-3.24 (m, 4H), 3.4-3.6 (m, 2H), 3.9-4.2 (m, 2H), 6.72 (dd, *J*



= 8.4, 2 Hz, 1H), 6.75 (s, 1H), 6.8 (d, $J = 2$ Hz, 1H), 7.11 (d, $J = 9.2$ Hz, 2H), 7.60 (d, $J = 8.4$ Hz, 1H), 7.86 (d, $J = 9.2$ Hz, 2H), 10.2 (s, 1H), 11.16 ppm (s, 1H); ^{13}C NMR (100 MHz, $\text{DMSO-}d_6$) δ 41.9, 44.3, 51.7, 98.5, 111.2, 112.9, 113.2, 115.2, 122.8, 125.7, 132.7, 145.9, 150.1,

166.3, 167.4, 181.1 ppm; MS (ACPI) m/z 337.1 (MH^+ , 100); HRMS (ESI/HESI) m/z : $[\text{M}+\text{H}]^+$ Calcd for $\text{C}_{20}\text{H}_{20}\text{N}_2\text{O}_3$ 337.1547; Found 337.1543.

(Z)-6-Hydroxy-2-[(4-thiomorpholin-4-yl)methylidene]-1-benzofuran-3(2H)-one (3d).

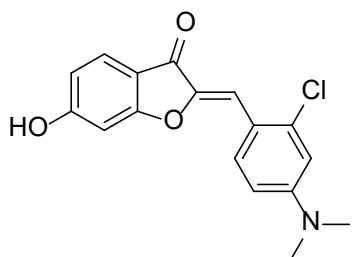


Yellow crystals (84% yield); mp $>220^\circ\text{C}$; ^1H NMR (400 MHz, $\text{DMSO-}d_6$) δ 2.58-2.68 (m, 4H), 3.56-3.86 (m, 4H), 6.7 (dd, $J = 8.4, 1.9$ Hz, 1H), 6.72 (s, 1H), 6.77 (d, $J = 1.9$ Hz, 1H), 7 (d, $J = 9$ Hz, 2H), 7.59 (d, $J = 8.4$ Hz, 1H), 7.81 (d, $J = 9$ Hz, 2H), 11.05 ppm (s, 1H); ^{13}C NMR (100 MHz,

$\text{DMSO-}d_6$) δ 24.82, 49.69, 98.44, 111.76, 112.72, 113.39, 114.64, 120.9, 125.56, 133.02, 145.47, 150.15, 165.87, 167.16, 180.89 ppm; MS (ACPI) m/z 340.1 (MH^+ , 100); HRMS (ESI/HESI) m/z : $[\text{M}+\text{H}]^+$ Calcd for $\text{C}_{19}\text{H}_{17}\text{NO}_3\text{S}$ 340.1002; Found 340.0998.

(Z)-2-[2-Chloro-4-(dimethylamino)benzylidene]-6-hydroxy-1-benzofuran-3(2H)-

one (3e). Yellow crystals (83% yield); mp $>220^\circ\text{C}$; ^1H NMR (400 MHz, $\text{DMSO-}d_6$) δ 3.01



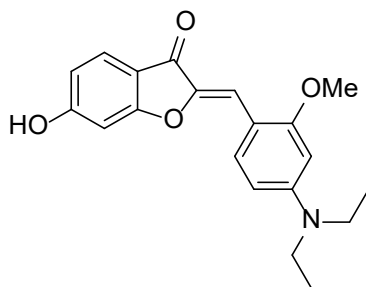
(s, 6H), 6.71 (dd, $J = 8.4, 2$ Hz, 1H), 6.77 (d, $J = 1.9$ Hz, 1H), 6.79-6.84 (m, 2H), 6.95 (s, 1H), 7.6 (d, $J = 8.4$ Hz, 1H), 8.16 (d, $J = 9.7$ Hz, 1H), 11.1 ppm (s, 1H); ^{13}C NMR (100 MHz, $\text{DMSO-}d_6$) δ 39.59, 98.52, 106.31, 111.27, 111.86, 112.86,

113.14, 115.87, 125.69, 132.51, 136.25, 145.7, 151.44, 166.02, 167.2, 180.77 ppm; MS

(ACPI) m/z 316.2 (MH^+ , 100); HRMS (ESI/HESI) m/z : $[M+H]^+$ Calcd for $C_{17}H_{14}ClNO_3$ 316.0735; Found 316.0733.

(2Z)-2-[4-(Diethylamino)-2-methoxybenzylidene]-6-hydroxy-1-benzofuran-3(2H)-

one (3f). Yellow crystals (75% yield); mp $>220^\circ C$; 1H NMR (400 MHz, $DMSO-d_6$) δ 1.15



(t, $J = 7$ Hz, 7H), 3.44 (q, $J = 7$ Hz, 4H), 3.88 (s, 3H), 6.22

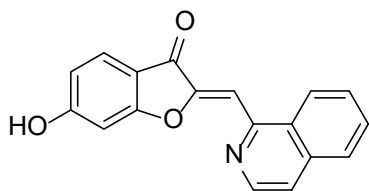
(d, $J = 2.4$ Hz, 1H), 6.43 (dd, $J = 9, 2.4$ Hz, 1H), 6.68 (dd,

$J = 8.4, 2$ Hz, 1H), 6.75 (d, $J = 2$ Hz, 1H), 7.05 (s, 1H), 7.56

(d, $J = 8.4$ Hz, 1H), 8.03 (d, $J = 9$ Hz, 1H), 10.93 ppm (s,

1H); ^{13}C NMR (100 MHz, $DMSO-d_6$) δ 12.55, 43.96, 55.47, 93.64, 98.34, 104.78, 106.17, 107.43, 112.46, 113.8, 125.26, 132.59, 144.45, 150.55, 160.29, 165.33, 166.56, 180.43 ppm; MS (ACPI) m/z 340.2 (MH^+ , 100); HRMS (ESI/HESI) m/z : $[M+H]^+$ Calcd for $C_{20}H_{21}NO_4$ 340.1543; Found 340.1540.

(2Z)-6-Hydroxy-2-(isoquinolin-1-ylmethylene)-1-benzofuran-3(2H)-one (4a). Yellow



crystals (78% yield); mp $>220^\circ C$; 1H NMR (400 MHz,

$DMSO-d_6$) δ 6.71-6.76 (m, 2H), 7.43 (s, 1H), 7.69 (d, $J =$

8.3 Hz, 1H), 7.7-7.77 (m, 1H), 7.79-7.85 (m, 1H), 7.87 (d,

$J = 5.6$ Hz, 1H), 8.03 (d, $J = 8.1$ Hz, 1H), 8.35 (d, $J = 8.9$ Hz, 1H), 8.69 (d, $J = 5.6$ Hz, 1H),

11.3 ppm (s, 1H); ^{13}C NMR (100 MHz, $DMSO-d_6$) δ 98.78, 105.12, 112.39, 113.23,

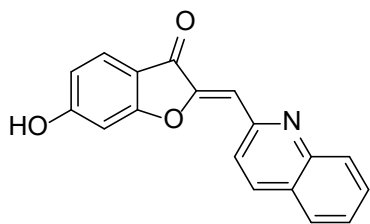
120.99, 125, 126.42, 127.44, 128.25, 130.59, 135.8, 142.65, 149.81, 151.34, 167.15,

169.05, 182.01 ppm; MS (ACPI) m/z 290.2 (MH^+ , 100); HRMS (ESI/HESI) m/z : $[M+H]^+$

Calcd for $C_{18}H_{11}NO_3$ 290.0812; Found 290.0810.

(2Z)-6-Hydroxy-2-(quinolin-2-ylmethylene)-1-benzofuran-3(2H)-one (4b). Yellow

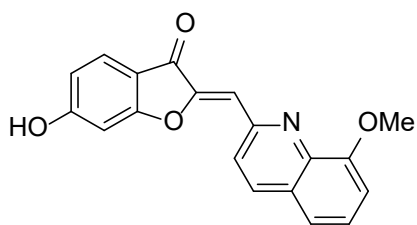
crystals (72% yield); mp $249-251^\circ C$; 1H NMR (400 MHz, $DMSO-d_6$) δ 6.75 (dd, $J = 8.4,$



2 Hz, 1H), 6.78-6.9 (m, 2H), 7.56-7.73 (m, 2H), 7.75-7.88 (m, 1H), 7.93-8.13 (m, 2H), 8.29 (d, $J = 8.7$ Hz, 1H), 8.48 (d, $J = 8.7$ Hz, 1H), 11.39 ppm (s, 1H); ^{13}C NMR (126 MHz, DMSO- d_6) δ 98.84, 110, 112.29, 113.41, 122.62, 126.29, 126.88, 127.47, 127.79, 129.08, 130.11, 136.72, 147.82, 149.55, 151.88, 167.13, 168.36, 181.53 ppm; MS (ACPI) m/z 290.0 (MH^+ , 100); HRMS (ESI/HESI) m/z : $[\text{M}+\text{H}]^+$ Calcd for $\text{C}_{18}\text{H}_{11}\text{NO}_3$ 290.0812; Found 290.0806.

(2Z)-6-Hydroxy-2-[(8-methoxyquinolin-2-yl)methylene]-1-benzofuran-3(2H)-one

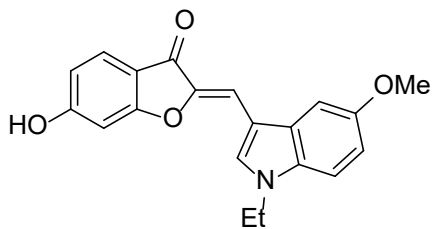
(4c). Yellow crystals (68% yield); mp 250-252°C; ^1H NMR (400 MHz, DMSO- d_6) δ 4 (s,



3H), 6.75 (dd, $J = 8.5$, 2 Hz, 1H), 6.81 (s, 1H), 6.85 (d, $J = 2$ Hz, 1H), 7.09-7.30 (m, 1H), 7.45-7.62 (m, 2H), 7.67 (d, $J = 8.5$ Hz, 1H), 8.3 (d, $J = 8.7$ Hz, 1H), 8.42 (d, $J = 8.7$ Hz, 1H), 11.38 ppm (s, 1H); ^{13}C NMR (100 MHz, DMSO- d_6) δ 55.75, 98.59, 109.12, 110.09, 112.2, 113.21, 119.05, 122.67, 125.9, 127.71, 127.77, 136.19, 139.81, 149.11, 150.13, 155.13, 166.87, 168.12, 181.22 ppm; MS (ACPI) m/z 320.0 (MH^+ , 100); HRMS (ESI/HESI) m/z : $[\text{M}+\text{H}]^+$ Calcd for $\text{C}_{19}\text{H}_{13}\text{NO}_4$ 320.0917; Found 320.0919.

(2Z)-2-[(1-Ethyl-5-methoxy-1H-indol-3-yl)methylene]-6-hydroxy-1-benzofuran-3(2H)-one (4d).

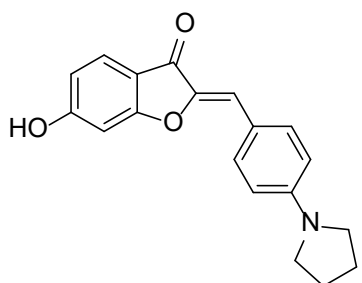
Yellow crystals (77% yield); mp 265-267°C; ^1H NMR (400 MHz, DMSO-



d_6); δ 1.39 (t, $J = 7.2$ Hz, 3H), 3.85 (s, 3H), 4.27 (q, $J = 7.2$ Hz, 2H), 6.72 (dd, $J = 8.4$, 2 Hz, 1H), 6.83 (d, $J = 2$ Hz, 1H), 6.87 (dd, $J = 8.9$, 2.4 Hz, 1H), 7.23 (s, 1H), 7.42 (d, $J = 8.8$ Hz, 1H), 7.56-7.64 (m, 2H), 8.18

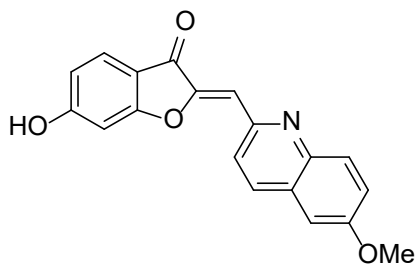
(s, 1H), 10.98 ppm (s, 1H); ^{13}C NMR (126 MHz, DMSO- d_6); δ 15.38, 41.3, 55.46, 98.49, 101.1, 105.37, 107.42, 111.41, 112.56, 112.76, 114.38, 125.36, 128.22, 130.74, 133.5, 144.76, 155.02, 165.47, 166.52, 180.12 ppm; MS (ACPI) m/z 336.0 (MH^+ , 100); HRMS (ESI/HESI) m/z : $[\text{M}+\text{H}]^+$ Calcd for $\text{C}_{20}\text{H}_{17}\text{NO}_4$ 336.1230; Found 336.1224.

(2Z)-6-Hydroxy-2-(4-pyrrolidin-1-ylbenzylidene)-1-benzofuran-3(2H)-one (4e).



Yellow crystals (83% yield); mp $>220^\circ\text{C}$; ^1H NMR (400 MHz, DMSO- d_6) δ 1.83-2.07 (m, 4H), 3.26-3.32 (m, 4H), 6.61 (d, $J = 8.9$ Hz, 2H), 6.66-6.72 (m, 2H), 6.77 (d, $J = 1.9$ Hz, 1H), 7.57 (d, $J = 8.4$ Hz, 1H), 7.77 (d, $J = 8.9$ Hz, 2H), 11 ppm (s, 1H); ^{13}C NMR (100 MHz, DMSO- d_6) δ 24.95, 47.24, 98.42, 111.97, 112.58, 112.94, 113.69, 118.62, 125.39, 133.16, 144.73, 148.49, 165.58, 166.87, 180.64 ppm; MS (ACPI) m/z 308.1 (MH^+ , 100); HRMS (ESI/HESI) m/z : $[\text{M}+\text{H}]^+$ Calcd for $\text{C}_{19}\text{H}_{17}\text{NO}_3$ 308.1281; Found 308.1279.

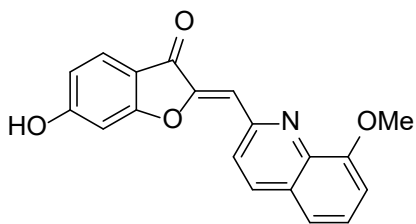
(2Z)-6-Hydroxy-2-[(6-methoxyquinolin-2-yl)methylene]-1-benzofuran-3(2H)-one (4f).



Yellow crystals (70% yield); mp $269\text{-}271^\circ\text{C}$; ^1H NMR (400 MHz, DMSO- d_6) δ 3.91 (s, 3H), 6.74 (dd, $J = 8.4, 2$ Hz, 1H), 6.77 (s, 1H), 6.83 (d, $J = 2$ Hz, 1H), 7.34-7.48 (m, 2H), 7.65 (d, $J = 8.4$ Hz, 1H), 7.94 (d, $J = 9$ Hz, 1H), 8.24 (d, $J = 8.7$ Hz, 1H), 8.35 ppm (d, $J = 8.7$ Hz, 1H); ^{13}C NMR (100 MHz, DMSO- d_6) δ 55.43, 98.57, 105.61, 110.07, 112.12, 113.27, 122.35, 122.71, 125.84, 128.02, 130.45, 135.1, 143.82, 148.85, 149.1, 158.02, 167.07, 168.12, 181.16 ppm; MS (ACPI) m/z 320.0 (MH^+ , 100); HRMS (ESI/HESI) m/z : $[\text{M}+\text{H}]^+$ Calcd for $\text{C}_{19}\text{H}_{13}\text{NO}_4$ 320.0917; Found 320.0912.

(2Z)-6-Hydroxy-2-[(8-methoxyquinolin-2-yl)methylene]-1-benzofuran-3(2H)-one

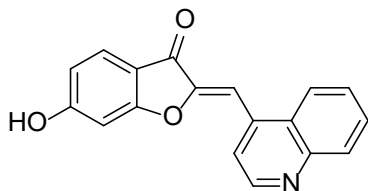
(4g). Yellow crystals (68% yield); mp 250-252°C; ¹H NMR (400 MHz, DMSO-*d*₆) δ 4 (s,



3H), 6.75 (dd, *J* = 8.5, 2 Hz, 1H), 6.81 (s, 1H), 6.85 (d, *J* = 2 Hz, 1H), 7.09-7.30 (m, 1H), 7.45-7.62 (m, 2H), 7.67 (d, *J* = 8.5 Hz, 1H), 8.3 (d, *J* = 8.7 Hz, 1H), 8.42 (d, *J* = 8.7 Hz, 1H), 11.38 ppm (s, 1H); ¹³C NMR (100

MHz, DMSO-*d*₆) δ 55.75, 98.59, 109.12, 110.09, 112.2, 113.21, 119.05, 122.67, 125.9, 127.71, 127.77, 136.19, 139.81, 149.11, 150.13, 155.13, 166.87, 168.12, 181.22 ppm; MS (ACPI) *m/z* 320.0 (MH⁺, 100); HRMS (ESI/HESI) *m/z*: [M+H]⁺ Calcd for C₁₉H₁₃NO₄ 320.0917; Found 320.0919.

(2Z)-6-Hydroxy-2-(quinolin-4-ylmethylene)-1-benzofuran-3(2H)-one (4h). Yellow

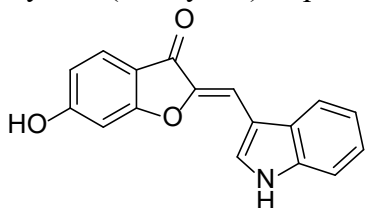


crystals (64% yield); mp 278-280°C; ¹H NMR (400 MHz, DMSO-*d*₆) δ 6.76 (dd, *J* = 8.5, 2 Hz, 1H), 6.81 (d, *J* = 2 Hz, 1H), 7.39 (s, 1H), 7.61-7.75 (m, 2H), 7.78-7.91 (m,

1H), 8.09 (dd, *J* = 8.4, 1.3 Hz, 1H), 8.15 (d, *J* = 4.6 Hz, 1H), 8.34 (dd, *J* = 8.5, 1.4 Hz, 1H), 9.03 (d, *J* = 4.6 Hz, 1H), 11.4 ppm (s, 1H); ¹³C NMR (100 MHz, DMSO-*d*₆) δ 98.54, 102.42, 112.17, 113.13, 121.61, 123.19, 125.5, 125.84, 126.86, 129.12, 129.49, 135.85, 147.94, 149.72, 150.05, 166.79, 168.06, 180.62 ppm; MS (ACPI) *m/z* 290.0 (MH⁺, 100); HRMS (ESI/HESI) *m/z*: [M+H]⁺ Calcd for C₁₈H₁₁NO₃ 290.0812; Found 290.0812.

(2Z)-6-Hydroxy-2-(1H-indol-3-ylmethylene)-1-benzofuran-3(2H)-one (4i). Yellow

crystals (55% yield); mp 280-282°C; ¹H NMR (400 MHz, DMSO-*d*₆) δ 6.72 (dd, *J* = 8.5,

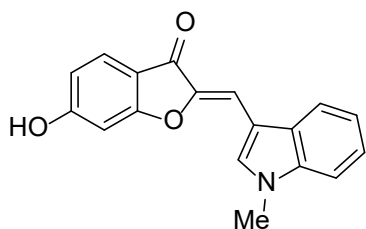


2 Hz, 1H), 6.85 (d, *J* = 2 Hz, 1H), 7.11-7.28 (m, 3H), 7.51 (d, *J* = 7.8 Hz, 1H), 7.62 (d, *J* = 8.5 Hz, 1H), 8.01 (d, *J* = 7.7

Hz, 1H), 8.21 (d, $J = 2.8$ Hz, 1H), 10.99 (s, 1H), 11.99 ppm (s, 1H); ^{13}C NMR (126 MHz, DMSO- d_6) δ 98.75, 105.36, 108.49, 112.4, 112.76, 114.45, 118.98, 120.86, 122.74, 125.52, 126.9, 131.31, 136.43, 145.43, 165.79, 166.9, 180.52 ppm; MS (ACPI) m/z 278.2 (MH^+ , 100); HRMS (ESI/HESI) m/z : $[\text{M}+\text{H}]^+$ Calcd for $\text{C}_{17}\text{H}_{11}\text{NO}_3$ 278.0812; Found 278.0813.

(2Z)-6-Hydroxy-2-[(1-methyl-1H-indol-3-yl)methylene]-1-benzofuran-3(2H)-one

(4j). Yellow crystals (78% yield); mp 272-274°C; ^1H NMR (400 MHz, DMSO- d_6) δ 3.9

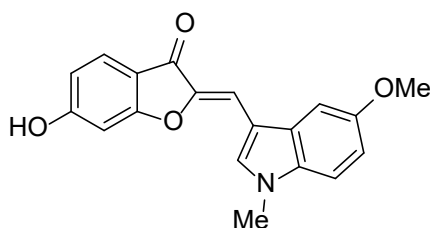


(s, 3H), 6.72 (d, $J = 8.4$ Hz, 1H), 6.83 (s, 1H), 7.13-7.32 (m, 3H), 7.51 (d, $J = 8$ Hz, 1H), 7.6 (d, $J = 8.1$ Hz, 1H), 7.99 (d, $J = 7.8$ Hz, 1H), 8.19 (s, 1H), 11.02 ppm (s, 1H); ^{13}C NMR (126 MHz, DMSO- d_6) δ 33.13, 98.48, 104.67, 107.3,

110.54, 112.6, 114.26, 118.96, 120.96, 122.64, 125.41, 127.2, 134.74, 136.76, 145.12, 165.57, 166.65, 180.17 ppm; MS (ACPI) m/z 292.0 (MH^+ , 100); HRMS (ESI/HESI) m/z : $[\text{M}+\text{H}]^+$ Calcd for $\text{C}_{18}\text{H}_{13}\text{NO}_3$ 292.0968; Found 292.0962.

(2Z)-6-Hydroxy-2-[(5-methoxy-1-methyl-1H-indol-3-yl)methylene]-1-benzofuran-

3(2H)-one (4k). Yellow crystals (82% yield); mp 301-303°C; ^1H NMR (400 MHz,

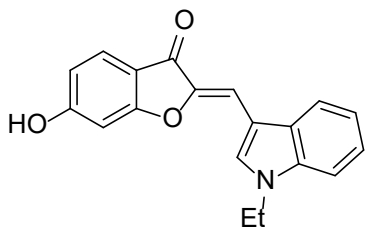


DMSO- d_6) δ 3.84 (s, 3H), 3.86 (s, 3H), 6.71 (dd, $J = 8.5, 2$ Hz, 1H), 6.82 (d, $J = 2$ Hz, 1H), 6.88 (dd, $J = 8.7, 2.4$ Hz, 1H), 7.21 (s, 1H), 7.39 (d, $J = 8.8$ Hz, 1H), 7.53-7.64 (m, 2H), 8.12 (s, 1H), 11.03 ppm (s, 1H); ^{13}C

NMR (126 MHz, DMSO- d_6) δ 33.28, 55.45, 98.41, 100.92, 105.32, 107.19, 111.38, 112.54, 112.73, 114.33, 125.32, 127.99, 131.82, 134.99, 144.74, 155.05, 165.48, 166.48, 180.07 ppm; MS (ACPI) m/z 322.0 (MH^+ , 100); HRMS (ESI/HESI) m/z : $[\text{M}+\text{H}]^+$ Calcd for $\text{C}_{19}\text{H}_{15}\text{NO}_4$ 322.1074; Found 322.1067.

(2Z)-2-[(1-Ethyl-5-methoxy-1H-indol-3-yl)methylene]-6-hydroxy-1-benzofuran-

3(2H)-one (4l). Yellow crystals (77% yield); mp 265-267°C; ¹H NMR (400 MHz, DMSO-

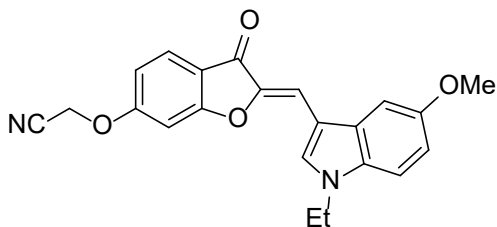


*d*₆); δ 1.39 (t, *J* = 7.2 Hz, 3H), 3.85 (s, 3H), 4.27 (q, *J* = 7.2 Hz, 2H), 6.72 (dd, *J* = 8.4, 2 Hz, 1H), 6.83 (d, *J* = 2 Hz, 1H), 6.87 (dd, *J* = 8.9, 2.4 Hz, 1H), 7.23 (s, 1H), 7.42 (d, *J* = 8.8 Hz, 1H), 7.56-7.64 (m, 2H), 8.18 (s, 1H), 10.98 ppm (s, 1H);

¹³C NMR (126 MHz, DMSO-*d*₆); δ 15.38, 41.3, 55.46, 98.49, 101.1, 105.37, 107.42, 111.41, 112.56, 112.76, 114.38, 125.36, 128.22, 130.74, 133.5, 144.76, 155.02, 165.47, 166.52, 180.12 ppm; MS (ACPI) *m/z* 336.0 (MH⁺, 100); HRMS (ESI/HESI) *m/z*: [M+H]⁺ Calcd for C₂₀H₁₇NO₄ 336.1230; Found 336.1224.

(Z)-2-((2-((1-Ethyl-5-methoxy-1H-indol-3-yl)methylene)-3-oxo-2,3-

dihydrobenzofuran-6-yl)oxy)acetonitrile (5a). To a solution of 670 mg (2 mmol) of (2Z)-



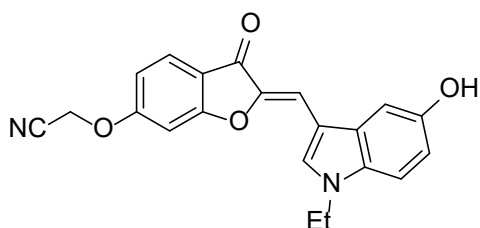
2-[(1-ethyl-5-methoxy-1H-indol-3-yl)methylene]-6-hydroxy-1-benzofuran-3(2H)-one (**4d**) in 10 mL of DMF was added 830 mg (6 mmol, 3 eq) of anhydrous potassium carbonate.

The mixture was heated to 60°C and 0.152 mL (2.4 mmol, 1.2 eq) of chloroacetonitrile was added. The mixture was stirred at 60°C for an additional 8 hours, cooled, and poured into 100 mL of 0.1N aqueous sulfuric acid. The precipitate was collected by filtration, washed with water, dried and re-crystallized from DMF-methanol to afford 487 mg (65%) of **5a** as yellow crystals: mp 230-232°C; ¹H NMR (400 MHz, DMSO-*d*₆) δ 1.44 (d, *J* = 7.2 Hz, 3H), 3.86 (s, 3H), 4.33 (q, *J* = 7.2 Hz, 2H), 5.39 (s, 2H), 6.9 (dd, *J* = 8.9, 2.4 Hz, 1H), 6.97 (dd, *J* = 8.6, 2.2 Hz, 1H), 7.29 (d, *J* = 2.2 Hz, 1H), 7.37 (s, 1H), 7.51 (d, *J* = 8.9 Hz, 1H), 7.63

(d, $J = 2.4$ Hz, 1H), 7.77 (d, $J = 8.6$ Hz, 1H), 8.23 ppm (s, 1H); ^{13}C NMR (100 MHz, DMSO- d_6) δ 14.67, 40.97, 53.89, 55.34, 98.17, 101.45, 106.18, 107.17, 110.99, 111.68, 112.46, 115.45, 116.87, 124.84, 127.89, 130.8, 133.46, 144.2, 154.96, 162.6, 165.49, 179.58 ppm; MS (ACPI) m/z 375.2 (MH^+ , 100); HRMS (ESI/HESI) m/z : $[\text{M}+\text{H}]^+$ Calcd for $\text{C}_{22}\text{H}_{19}\text{N}_2\text{O}_4$ 375.1339; Found 375.1337.

(Z)-2-((2-((1-Ethyl-5-hydroxy-1H-indol-3-yl)methylene)-3-oxo-2,3-

dihydrobenzofuran-6-yl)oxy)acetonitrile (5b). To 36 mg (0.11 mmol, 1 eq) of 5-(tert-

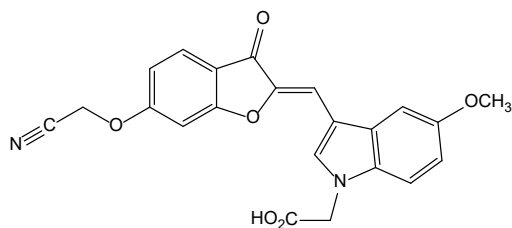


butyldimethylsilyloxy)-1-ethyl-1H-indole-3-

carboxaldehyde in 2 mL of anhydrous dichloromethane was added 30 mg (0.16 mmol, 1.4 eq) of 2-((3-oxo-2,3-dihydrobenzofuran-6-

yl)oxy)acetonitrile and 366 mg (3.6 mmol, 32 eq) of alumina (Sigma-Aldrich, St. Louis, MO.). The mixture was stirred at 25°C for 6 hours, filtered and concentrated. The residue was treated with 824 μL of a 1M (2.5 eq) solution of tetra(n-butyl)ammonium fluoride in tetrahydrofuran for 1 hour at 25°C. The product was recrystallized from *ca.* 1:1 methanol-dichloromethane to afford 24 mg (60%) of **4b** as yellow crystals: mp 208-210°C; ^1H NMR (400 MHz, DMSO- d_6) δ 1.43 (t, $J = 7.2$ Hz, 4H), 4.29 (q, $J = 7.2$ Hz, 2H), 5.38 (s, 2H), 6.8 (dd, $J = 8.8, 2.2$ Hz, 1H), 6.96 (dd, $J = 8.6, 2.1$ Hz, 1H), 7.11 (s, 1H), 7.3 (dd, $J = 6.4, 2.1$ Hz, 2H), 7.76 (d, $J = 8.5$ Hz, 1H), 8.17 (s, 1H), 9.16 ppm (s, 1H); ^{13}C NMR (100 MHz, DMSO- d_6) δ 15.35, 41.35, 54.05, 98.26, 103.37, 106.73, 106.76, 111.45, 112.11, 112.83, 116.19, 117.02, 125.35, 128.45, 134.08, 144.17, 152.8, 162.79, 165.73, 179.84 ppm; HRMS (ESI/HESI) m/z : $[\text{M}+\text{H}]^+$ Calcd for $\text{C}_{21}\text{H}_{16}\text{N}_2\text{O}_4$ 361.1183; Found 361.1180.

(Z)-2-(3-((6-(Cyanomethoxy)-3-oxobenzofuran-2(3H)-ylidene)methyl)-5-methoxy-1H-indol-1-yl)acetic acid (5c). To a solution of 45 mg (0.24 mmol, 1.2 eq) of 2-(3-oxo-



2,3-dihydrobenzofuran-6-yl)oxy)acetonitrile in 3 mL of anhydrous dichloromethane was added 58 mg (0.2 mmol, 1 eq) of tert-butyl 2-(3-formyl-5-methoxy-1H-indol-1-yl)acetate and 646 mg

(6.4 mmol, 32 eq) of alumina. The mixture was stirred at 25°C for 6 hours, filtered, concentrated and recrystallized from *ca.* 1:4 methanol-dichloromethane, to afford pure tert-butyl (Z)-2-(3-((6-(cyanomethoxy)-3-oxobenzofuran-2(3H)-ylidene)methyl)-5-methoxy-1H-indol-1-yl)acetate. This product was refluxed in 2 mL of formic acid at 60°C for 2 hours. The solution was concentrated to afford, 48 mg (60%) of **5c** as yellow crystals: mp >220°C; ¹H NMR (400 MHz, DMSO-*d*₆) δ 3.85 (s, 3H), 5.18 (s, 2H), 5.38 (s, 2H), 6.88 (dd, *J* = 8.9, 2.4 Hz, 1H), 6.97 (dd, *J* = 8.5, 2.2 Hz, 1H), 7.23 (d, *J* = 2.1 Hz, 1H), 7.37 (s, 1H), 7.43 (d, *J* = 8.9 Hz, 1H), 7.63 (d, *J* = 2.4 Hz, 1H), 7.78 (d, *J* = 8.5 Hz, 1H), 8.22 (s, 1H), 13.18 ppm (s, 1H); ¹³C NMR (100 MHz, DMSO-*d*₆) δ 54.04, 55.56, 98.11, 100.99, 106.62, 107.83, 111.63, 112.24, 113.01, 116.17, 116.94, 125.52, 128.02, 131.69, 135.55, 144.83, 155.23, 162.94, 165.92, 169.99, 180.10 ppm; MS (ACPI) *m/z* 391.2 (MH⁺, 100); HRMS (ESI/HESI) *m/z*: [M+H]⁺ Calcd for C₂₂H₁₇N₂O₆ 405.1081; Found 405.1075.

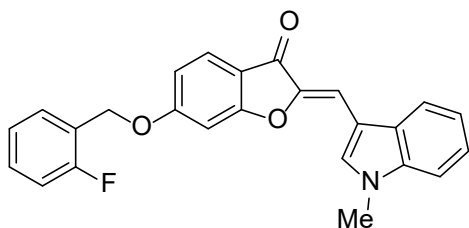
General procedure for the synthesis of aurones 5d-5q

To a solution of 2 mmol of aurones **4** in 10 mL of *N,N*-dimethylformamide was added 830 mg (6 mmol) of anhydrous potassium carbonate. The mixture was heated to 60°C and 2.4 mmol of the appropriate benzyl chloride was added. The mixture was stirred at 60°C for 8 hours, cooled, and poured into 100 mL of aqueous 0.1N sulfuric acid. The

precipitate was collected by filtration, washed with water, dried and re-crystallized from *ca.* 1:1 *N,N*-dimethylformamide-methanol.

(2*Z*)-6-[(2-Fluorobenzyl)oxy]-2-[(1-methyl-1*H*-indol-3-yl)methylene]-1-benzofuran-

3(2*H*)-one (5d). Yellow crystals (76% yield); mp 241-243°C; ¹H NMR (400 MHz,

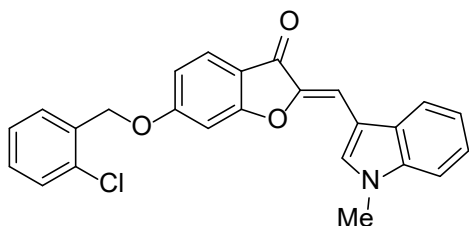


DMSO-*d*₆) δ 3.93 (s, 3H), 5.34 (s, 2H), 6.93 (dd, *J* = 8.4, 2.2 Hz, 1H), 7.14-7.35 (m, 6H), 7.39-7.72 (m, 4H), 8.02 (d, *J* = 7.8 Hz, 1H), 8.15 ppm (s, 1H); ¹³C NMR (126 MHz, CDCl₃) δ 33.47, 64.31 (d, *J* = 4.6

Hz), 97.42, 105.95, 108.57, 109.8, 112.12, 115.52 (d, *J* = 21.1 Hz), 116.62, 119.17, 121.28, 123.01, 124.44 (d, *J* = 3.4 Hz), 125.55, 127.87, 129.61, 129.64, 130.18 (d, *J* = 8.4 Hz), 134.01, 136.96, 146.01, 160.43 (d, *J* = 247.5 Hz), 165.36, 167, 181.75 ppm; MS (ACPI) *m/z* 400.0 (MH⁺, 100); HRMS (ESI/HESI) *m/z*: [M+H]⁺ Calcd for C₂₅H₁₈FNO₃ 400.1343; Found 400.1334.

(2*Z*)-6-[(2-Chlorobenzyl)oxy]-2-[(1-methyl-1*H*-indol-3-yl)methylene]-1-benzofuran-

3(2*H*)-one (5e). Yellow crystals (69% yield); mp 206-208°C; ¹H NMR (400 MHz,

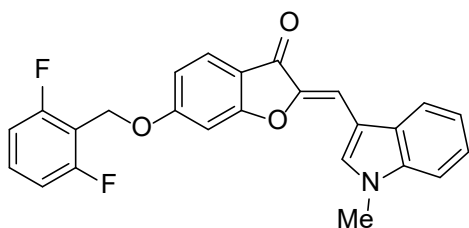


DMSO-*d*₆) δ 3.93 (s, 3H), 5.35 (s, 2H), 6.93 (dd, *J* = 8.5, 2.2 Hz, 1H), 7.17-7.36 (m, 4H), 7.38-7.49 (m, 2H), 7.5-7.59 (m, 2H), 7.6-7.73 (m, 2H), 8.04 (d, *J* = 7.7 Hz, 1H), 8.21 ppm (s, 1H); ¹³C NMR (126

MHz, CDCl₃) δ 33.53, 67.78, 97.54, 106.03, 108.61, 109.92, 112.24, 116.72, 119.18, 121.36, 123.08, 125.56, 127.24, 127.96, 128.82, 129.51, 129.64, 132.74, 133.67, 134.17, 137.01, 146.08, 165.37, 167.04, 181.78 ppm; MS (ACPI) *m/z* 416.0 (MH⁺, 100); HRMS (ESI/HESI) *m/z*: [M+H]⁺ Calcd for C₂₅H₁₈ClNO₃ 416.1048; Found 416.1044.

(2Z)-6-[(2,6-Difluorobenzyl)oxy]-2-[(1-methyl-1H-indol-3-yl)methylene]-1-

benzofuran-3(2H)-one (5f). Yellow crystals (73% yield); mp >220°C; ¹H NMR (400

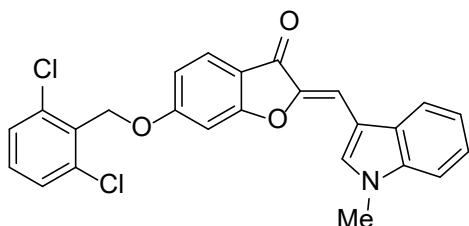


MHz, DMSO-*d*₆) δ 3.94 (s, 3H), 5.31 (s, 2H), 6.9 (dd, *J* = 8.5, 2.1 Hz, 1H), 7.19-7.40 (m, 6H), 7.54-7.61 (m, 2H), 7.69 (d, *J* = 8.5 Hz, 1H), 8.08 (d, *J* = 7.8 Hz, 1H), 8.21 ppm (s, 1H); ¹³C NMR (100 MHz,

DMSO-*d*₆) δ 33.67, 58.99, 98.11, 106.19, 107.8, 111.09, 111.95 (t, *J* = 18.7 Hz), 112.36 (d, *J* = 24.2 Hz), 112.88, 116.21, 119.65, 121.54, 123.22, 125.56, 127.5, 132.56 (t, *J* = 10.2 Hz), 135.55, 137.28, 145.29, 161.63 (dd, *J* = 256.8, 7.1 Hz), 165.48, 166.82, 180.58 ppm; MS (ACPI) *m/z* 418.2 (MH⁺, 100); HRMS (ESI/HESI) *m/z*: [M+H]⁺ Calcd for C₂₅H₁₇F₂NO₃ 418.1249; Found 418.1246.

(2Z)-6-[(2,6-Dichlorobenzyl)oxy]-2-[(1-methyl-1H-indol-3-yl)methylene]-1-

benzofuran-3(2H)-one (5g). Yellow crystals (65% yield); mp 247-249°C; ¹H NMR (400

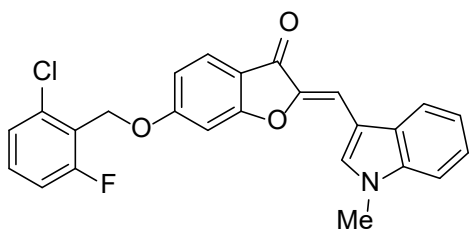


MHz, CDCl₃) δ 3.9 (s, 3H), 5.4 (s, 2H), 6.84 (dd, *J* = 8.5, 2.1 Hz, 1H), 6.95 (d, *J* = 2.1 Hz, 1H), 7.18-7.48 (m, 7H), 7.75 (d, *J* = 8.5 Hz, 1H), 7.92 (d, *J* = 7.7 Hz, 1H), 7.97 ppm (s, 1H); ¹³C NMR (100 MHz,

CDCl₃) δ 33.63, 65.82, 97.65, 106.12, 108.75, 109.96, 112.23, 116.81, 119.33, 121.43, 123.16, 125.67, 128.01, 128.72, 131, 131.28, 134.2, 137.1, 137.18, 146.18, 165.83, 167.1, 181.94 ppm; MS (ACPI) *m/z* 450.0 (MH⁺, 100); HRMS (ESI/HESI) *m/z*: [M+H]⁺ Calcd for C₂₅H₁₇Cl₂NO₃ 450.0658; Found 450.0650.

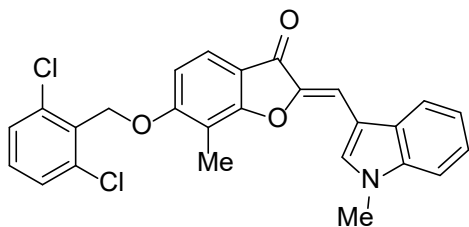
(2Z)-6-[(2-Chloro-6-fluorobenzyl)oxy]-2-[(1-methyl-1H-indol-3-yl)methylene]-1-

benzofuran-3(2H)-one (5h). Yellow crystals (76% yield); mp 225-227°C; ¹H NMR



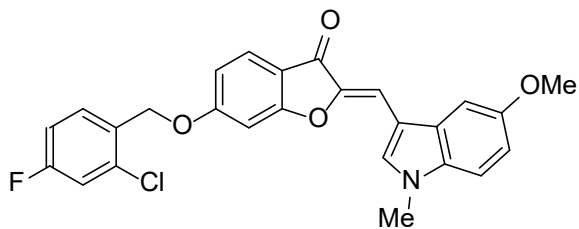
(400 MHz, CDCl₃) δ 3.87 (s, 3H), 5.28 (d, J = 1.8 Hz, 2H), 6.8 (dd, J = 8.5, 2.1 Hz, 1H), 6.91 (d, J = 2.1 Hz, 1H), 7.03-7.13 (m, 1H), 7.24-7.41 (m, 6H), 7.72 (d, J = 8.5 Hz, 1H), 7.90 (d, J = 7.6 Hz, 1H), 7.94 ppm (s, 1H); ¹³C NMR (126 MHz, CDCl₃) δ 33.59, 61.83 (d, J = 4.1 Hz), 97.63, 106.05, 108.73, 109.94, 112.17, 114.57 (d, J = 22.5 Hz), 116.79, 119.3, 121.41, 121.61 (d, J = 17.4 Hz), 123.14, 125.62, 125.82 (d, J = 3.3 Hz), 128, 131.31 (d, J = 9.7 Hz), 134.18, 136.74 (d, J = 4.6 Hz), 137.09, 146.16, 162.12 (d, J = 251.8 Hz), 165.64, 167.07, 181.89 ppm; MS (ACPI) m/z 434.0 (MH⁺, 100); HRMS (ESI/HESI) m/z : [M+H]⁺ Calcd for C₂₅H₁₇ClFNO₃ 434.0954; Found 434.0949.

(2Z)-6-[(2,6-Dichlorobenzyl)oxy]-7-methyl-2-[(1-methyl-1H-indol-3-yl)methylene]-1-benzofuran-3(2H)-one (5i). Yellow crystals (87% yield); mp 232-234°C; ¹H NMR (400



MHz, DMSO-*d*₆) δ : 2.25 (s, 3H), 3.93 (s, 3H), 5.40 (s, 2H), 7.15-7.33 (m, 4H), 7.46-7.62 (m, 4H), 7.66 (d, J = 8.5 Hz, 1H), 8.05 (d, J = 7.9 Hz, 1H), 8.12 ppm (s, 1H); ¹³C NMR (126 MHz, CDCl₃) δ 8.16, 33.57, 66.25, 105.45, 107.75, 108.88, 109.85, 110.91, 116.61, 119.22, 121.23, 122.6, 123.01, 127.89, 128.62, 130.73, 131.71, 134, 136.96, 137.05, 146.24, 163.15, 164.54, 182.64 ppm; MS (ACPI) m/z 464.0 (MH⁺, 100); HRMS (ESI/HESI) m/z : [M+H]⁺ Calcd for C₂₆H₁₉Cl₂NO₃ 464.0815; Found 464.0811.

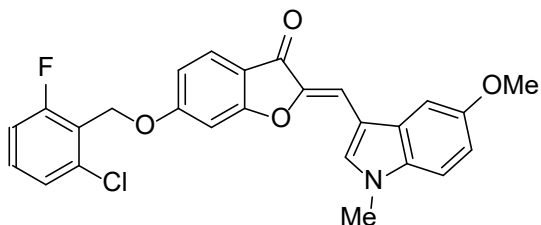
(2Z)-6-[(2-Chloro-4-fluorobenzyl)oxy]-2-[(5-methoxy-1-methyl-1H-indol-3-yl)methylene]-1-benzofuran-3(2H)-one (5j). Yellow crystals (85% yield); mp 184-186°C; ¹H NMR (400 MHz, DMSO-*d*₆) δ 3.85 (s, 3H), 3.89 (s, 3H), 5.3 (s, 2H), 6.85-



6.97 (m, 2H), 7.20 (d, $J = 2.1$ Hz, 1H),
7.26-7.37 (m, 2H), 7.45 (d, $J = 8.9$ Hz,
1H), 7.56 (dd, $J = 8.9, 2.6$ Hz, 1H), 7.61
(d, $J = 2.4$ Hz, 1H), 7.65-7.75 (m, 2H),

8.16 ppm (s, 1H); ^{13}C NMR (126 MHz, CDCl_3) δ 33.66, 55.84, 67.19, 97.45, 100.58, 106.26, 108.23, 110.78, 111.98, 113.39, 114.44 (d, $J = 21.1$ Hz), 116.8, 117.08 (d, $J = 24.9$ Hz), 125.4, 128.63, 129.66 (d, $J = 3.6$ Hz), 130.14 (d, $J = 9$ Hz), 132.03, 133.55 (d, $J = 10.5$ Hz), 134.43, 145.67, 155.62, 162.34 (d, $J = 250.5$ Hz), 165.03, 166.78, 181.59 ppm; MS (ACPI) m/z 464.0 (MH^+ , 100); HRMS (ESI/HESI) m/z : $[\text{M}+\text{H}]^+$ Calcd for $\text{C}_{26}\text{H}_{19}\text{ClFNO}_4$ 464.1059; Found 464.1049.

(2Z)-6-[(2-Chloro-6-fluorobenzyl)oxy]-2-[(5-methoxy-1-methyl-1H-indol-3-yl)methylene]-1-benzofuran-3(2H)-one (5k). Yellow crystals (71% yield); mp 200-

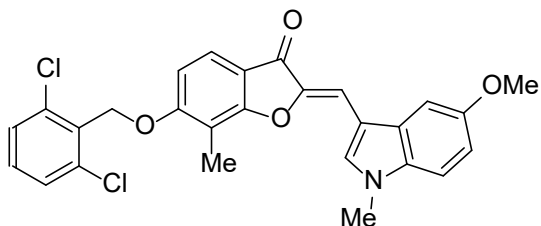


202°C; ^1H NMR (400 MHz, DMSO-d_6) δ
3.85 (s, 3H), 3.9 (s, 3H), 5.33 (d, $J = 1.8$ Hz,
2H), 6.86-6.95 (m, 2H), 7.26-7.4 (m, 3H),
7.42-7.49 (m, 2H), 7.51-7.6 (m, 1H), 7.62 (d,

$J = 2.4$ Hz, 1H), 7.69 (d, $J = 8.5$ Hz, 1H), 8.15 ppm (s, 1H); ^{13}C NMR (126 MHz, CDCl_3) δ 33.56, 55.78, 61.65 (d, $J = 4.2$ Hz), 97.38, 100.51, 106.13, 108.18, 110.73, 111.96, 113.29, 114.43 (d, $J = 22.6$ Hz), 116.63, 121.47 (d, $J = 17.2$ Hz), 125.31, 125.67 (d, $J = 3.4$ Hz), 128.54, 131.18 (d, $J = 9.9$ Hz), 131.95, 134.42, 136.56 (d, $J = 4.8$ Hz), 145.63, 155.52, 161.96 (d, $J = 251.9$ Hz), 165.39, 166.75, 181.59 ppm; MS (ACPI) m/z 464.2 (MH^+ , 100); HRMS (ESI/HESI) m/z : $[\text{M}+\text{H}]^+$ Calcd for $\text{C}_{26}\text{H}_{19}\text{ClFNO}_4$ 464.1059; Found 464.1050.

(2Z)-6-[(2,6-Dichlorobenzyl)oxy]-2-[(5-methoxy-1-methyl-1H-indol-3-yl)methylene]-1-benzofuran-3(2H)-one (5l). Yellow crystals (69% yield); mp 233-235°C; ¹H NMR (400 MHz, CDCl₃) δ 3.8 (s, 3H), 3.89 (s, 3H), 5.34 (s, 2H), 6.8 (dd, *J* = 8.5, 2.1 Hz, 1H), 6.89 (d, *J* = 2.1 Hz, 1H), 6.93 (dd, *J* = 8.8, 2.4 Hz, 1H), 7.15-7.41 (m, 6H), 7.71 (d, *J* = 8.5 Hz, 1H), 7.87 ppm (s, 1H); ¹³C NMR (126 MHz, CDCl₃) δ 33.69, 55.9, 65.74, 97.58, 100.66, 106.22, 108.31, 110.8, 112.07, 113.45, 116.79, 125.49, 128.63, 130.91, 131.23, 132.07, 134.43, 137.09, 145.77, 155.63, 165.68, 166.89, 181.71 ppm; MS (ACPI) *m/z* 480.0 (MH⁺, 100); HRMS (ESI/HESI) *m/z*: [M+H]⁺ Calcd for C₂₆H₁₉Cl₂NO₄ 480.0764; Found 480.0754.

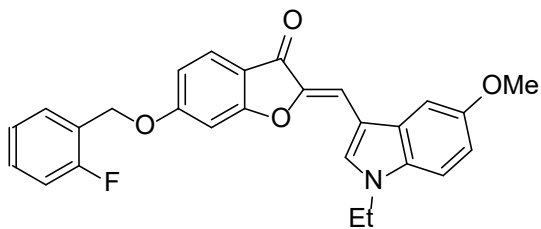
(2Z)-6-[(2,6-Dichlorobenzyl)oxy]-2-[(5-methoxy-1-methyl-1H-indol-3-yl)methylene]-7-methyl-1-benzofuran-3(2H)-one (5m). Yellow crystals (74% yield); mp 241-243°C;



¹H NMR (400 MHz, DMSO-*d*₆) δ 2.25 (s, 3H), 3.84 (s, 3H), 3.9 (s, 3H), 5.41 (s, 2H), 6.9 (dd, *J* = 8.8, 2.4 Hz, 1H), 7.2 (d, *J* = 8.5 Hz, 1H), 7.29 (s, 1H), 7.41-7.55 (m, 2H),

7.57-7.63 (m, 3H), 7.66 (d, *J* = 8.5 Hz, 1H), 8.08 ppm (s, 1H); ¹³C NMR (126 MHz, CDCl₃) δ 8.21, 33.83, 55.97, 66.32, 100.72, 105.78, 107.83, 108.59, 110.8, 110.96, 113.51, 116.75, 122.66, 128.66, 128.7, 130.76, 131.77, 132.1, 134.27, 137.11, 146.02, 155.62, 163.16, 164.55, 182.67 ppm; MS (ACPI) *m/z* 494.2 (MH⁺, 100); HRMS (ESI/HESI) *m/z*: [M+H]⁺ Calcd for C₂₇H₂₁Cl₂NO₄ 494.0920; Found 494.0911.

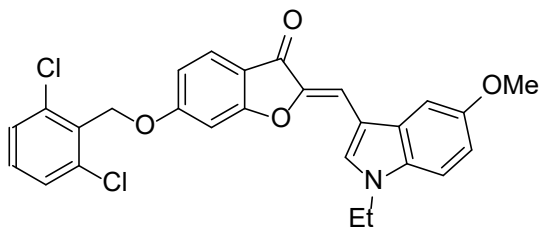
(2Z)-2-[(1-Ethyl-5-methoxy-1H-indol-3-yl)methylene]-6-[(2-fluorobenzyl)oxy]-1-benzofuran-3(2H)-one (5n). Yellow crystals (63% yield); mp 139-141°C; ¹H NMR (400 MHz, DMSO-*d*₆) δ 1.42 (t, *J* = 7.2 Hz, 3H), 3.85 (s, 3H), 4.29 (q, *J* = 7.2 Hz, 2H),



5.31 (s, 2H), 6.83-6.94 (m, 2H), 7.18-7.33 (m, 4H), 7.4-7.53 (m, 2H), 7.56-7.64 (m, 2H), 7.67 (d, $J = 8.5$ Hz, 1H), 8.19 ppm (s, 1H); ^{13}C NMR (126 MHz, CDCl_3) δ 15.39,

41.93, 55.79, 64.27 (d, $J = 4.6$ Hz), 97.36, 100.63, 106.29, 108.29, 110.81, 112.06, 113.32, 115.48 (d, $J = 21.1$ Hz), 116.63, 123.03 (d, $J = 14.2$ Hz), 124.43 (d, $J = 3.6$ Hz), 125.4, 128.78, 129.61 (d, $J = 3.6$ Hz), 130.15 (d, $J = 8.2$ Hz), 130.97, 132.69, 145.6, 155.48, 160.41 (d, $J = 247.2$ Hz), 165.25, 166.82, 181.64 ppm; MS (ACPI) m/z 444.2 (MH^+ , 100); HRMS (ESI/HESI) m/z : $[\text{M}+\text{H}]^+$ Calcd for $\text{C}_{27}\text{H}_{22}\text{FNO}_4$ 444.1606; Found 444.1600.

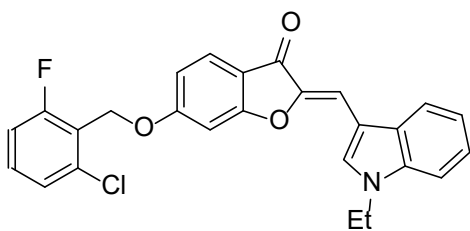
(2Z)-6-[(2,6-Dichlorobenzyl)oxy]-2-[(1-ethyl-5-methoxy-1H-indol-3-yl)methylene]-1-benzofuran-3(2H)-one (5o). Yellow crystals (73% yield); mp 211-213°C; ^1H NMR (400



MHz, CDCl_3) δ 1.54 (t, $J = 7.2$ Hz, 3H), 3.9 (s, 3H), 4.2 (q, $J = 7.2$ Hz, 2H), 5.36 (s, 2H), 6.82 (dd, $J = 8.6, 2.1$ Hz, 1H), 6.89-6.97 (m, 2H), 7.2-7.42 (m, 6H), 7.73 (d, $J = 8.5$ Hz,

1H), 7.97 ppm (s, 1H); ^{13}C NMR (126 MHz, CDCl_3) δ 15.46, 42.02, 55.91, 65.75, 97.62, 100.76, 106.33, 108.42, 110.91, 112.09, 113.41, 116.82, 125.51, 128.63, 128.9, 130.91, 131.09, 131.22, 132.76, 137.09, 145.75, 155.59, 165.68, 166.89, 181.74 ppm; MS (ACPI) m/z 494.2 (MH^+ , 100); HRMS (ESI/HESI) m/z : $[\text{M}+\text{H}]^+$ Calcd for $\text{C}_{27}\text{H}_{21}\text{Cl}_2\text{NO}_4$ 494.0920; Found 494.0917.

(2Z)-6-[(2-Chloro-6-fluorobenzyl)oxy]-2-[(1-ethyl-1H-indol-3-yl)methylene]-1-benzofuran-3(2H)-one (5p). Yellow crystals (74% yield); mp 198-200°C; ^1H NMR

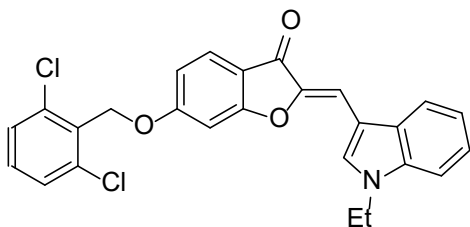


(400 MHz, DMSO-*d*₆) δ 1.46 (t, J = 7.2 Hz, 3H),
 4.36 (q, J = 7.2 Hz, 2H), 5.35 (d, J = 1.8 Hz, 2H),
 6.91 (dd, J = 8.5, 2.1 Hz, 1H), 7.21-7.33 (m, 3H),
 7.33-7.41 (m, 2H), 7.47 (d, J = 8.1 Hz, 1H), 7.52-

7.59 (m, 1H), 7.61 (d, J = 8.1 Hz, 1H), 7.7 (d, J = 8.5 Hz, 1H), 8.08 (d, J = 7.8 Hz, 1H),
 8.28 ppm (s, 1H); ¹³C NMR (126 MHz, CDCl₃) δ 15.31, 41.73, 61.68, 97.46, 105.98,
 108.61, 109.95, 112.02, 114.42 (d, J = 22.7 Hz), 116.6, 119.18, 121.22, 121.44 (d, J =
 17.2 Hz), 122.88, 125.36, 125.66, 128.06, 131.18 (d, J = 9.8 Hz), 132.51, 135.96, 136.55
 (d, J = 4.8 Hz), 145.95, 161.95 (d, J = 252.5 Hz), 165.46, 166.87, 181.69 ppm; MS
 (ACPI) m/z 448.2 (MH⁺, 100); HRMS (ESI/HESI) m/z : [M+H]⁺ Calcd for C₂₆H₁₉ClFNO₃
 448.1110; Found 448.1108.

(2Z)-6-[(2,6-Dichlorobenzyl)oxy]-2-[(1-ethyl-1H-indol-3-yl)methylene]-1-

benzofuran-3(2H)-one (5q). Yellow crystals (68% yield); mp 213-215°C; ¹H NMR

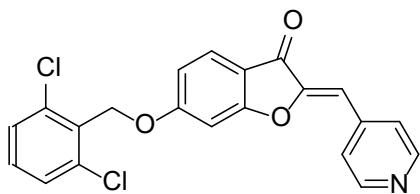


(400 MHz, DMSO-*d*₆) δ 1.46 (t, J = 7.2 Hz, 3H),
 3.35 (s, 3H), 4.37 (q, J = 7.2 Hz, 2H), 5.43 (s,
 2H), 6.92 (dd, J = 8.5, 2.2 Hz, 1H), 7.18-7.34 (m,

3H), 7.40 (d, J = 2.2 Hz, 1H), 7.52 (dd, J = 8.9, 7.2 Hz, 1H), 7.59-7.65 (m, 3H), 7.71 (d, J
 = 8.5 Hz, 1H), 8.05-8.13 (m, 1H), 8.29 ppm (s, 1H); ¹³C NMR (126 MHz, CDCl₃) δ
 15.43, 41.85, 65.77, 97.6, 106.13, 108.76, 110.03, 112.17, 116.75, 119.35, 121.33,
 122.99, 125.55, 128.17, 128.66, 130.93, 131.22, 132.58, 136.08, 137.11, 146.07, 165.75,
 167, 181.83 ppm; MS (ACPI) m/z 464.2 (MH⁺, 100); HRMS (ESI/HESI) m/z : [M+H]⁺
 Calcd for C₂₆H₁₉Cl₂NO₃ 464.0815; Found 464.0806.

(2Z)-6-[(2,6-Dichlorobenzyl)oxy]-2-(pyridin-4-ylmethylene)-1-benzofuran-3(2H)-one

(5r). To a solution of 1.5 g (10 mmol) of 6-hydroxybenzofuran-3(2H)-one (**2**) in 30 mL of



DMF was added 4.14 g (30 mmol, 3 eq) of anhydrous potassium carbonate followed by 2.35 g (12 mmol, 1.2 eq) of 2,6-dichlorobenzyl chloride (Thermofisher

Acros Organics, Geel, Belgium). The mixture was stirred at 25°C for 8 hours and diluted

with 200 mL of water. The precipitate was collected, washed with water, dried and purified

by column chromatography using 1:100 dichloromethane-methanol to afford 1.79 g (58%)

of 6-((2,6-dichlorobenzyl)oxy)benzofuran-3(2H)-one as pale yellow crystals: mp 153-155

°C. ¹H NMR (400 MHz, CDCl₃) δ 4.64 (s, 2H), 5.34 (s, 2H), 6.67-6.77 (m, 2H), 7.29 (d,

J = 7.2 Hz, 1H), 7.33-7.42 (m, 2H), 7.58 (d, *J* = 9 Hz, 1H); ¹³C NMR (100 MHz, CDCl₃)

δ 65.57, 75.56, 97.32, 111.98, 114.76, 125.15, 128.56, 130.9, 130.96, 136.97, 167.18,

176.32, 197.49 ppm; MS (ACPI) *m/z* 309.2 (MH⁺, 100). To 50 mL of a freshly prepared

0.2 M (5 eq) solution of sodium methoxide was added a solution of 618 mg (2 mmol) of 6-

((2,6-dichlorobenzyl)oxy)benzofuran-3(2H)-one and 214 mg (2 mmol, 1 eq) of 4-

pyridinecarboxaldehyde in 5 mL of methanol. The mixture was stirred at 25°C for 12 hours.

The solution was concentrated and poured into 100 mL of water at 0°C. The mixture was

acidified with 1N aqueous hydrochloric acid solution to *ca.* pH 6. The precipitate was

collected by filtration and recrystallized from 2:1 DMF-methanol to afford 445 mg (56%)

of **5r**: mp 219-222°C; ¹H NMR (400 MHz, CDCl₃) δ 5.41 (s, 2H), 6.7 (s, 1H), 6.88 (dd, *J*

= 8.6, 2.2 Hz, 1H), 6.96 (d, *J* = 2.2 Hz, 1H), 7.28-7.36 (m, 1H), 7.36-7.45 (m, 2H), 7.68-

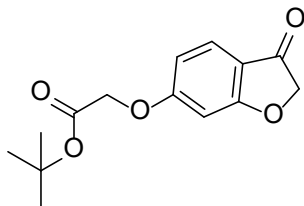
7.78 (m, 3H), 8.7 ppm (d, *J* = 5.2 Hz, 2H); ¹³C NMR (126 MHz, CDCl₃) δ 66.04, 98, 108.3,

113.23, 114.8, 124.74, 126.45, 128.78, 130.92, 131.17, 137.19, 139.95, 150.3, 150.36,

167.19, 168.85, 182.73 ppm; MS (ACPI) m/z 398.0 (MH^+ , 100); HRMS (ESI/HESI) m/z : $[M+H]^+$ Calcd for $C_{21}H_{13}Cl_2NO_3$ 398.0345; Found 398.0349.

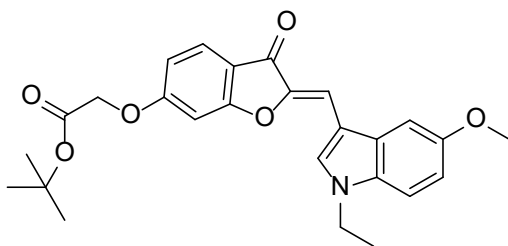
Procedure for the synthesis of biotinylated aurone analog **6d**

Tert-butyl 2-((3-oxo-2,3-dihydrobenzofuran-6-yl)oxy)acetate (6a). To a flask



containing 0.5 mL of DMF, and 30 mg (0.2 mmol) of 6-hydroxybenzofuran-3(2H)-one (Ark pharm, IL, USA) was added 37 μ L (0.24 mmol, 1.2 eq) of tert-Butyl bromoacetate (Sigma, MO, USA), and 55 mg (0.4 mmol, 2 eq) of potassium carbonate. The mixture was stirred at 25°C for 16 hours, extracted with DCM (dichloromethane), washed, dried and chromatographed on SiO_2 using 1:10-1:2 ethyl acetate: hexane to afford 31 mg (58%) of **6a** as yellow solid. 1H NMR (400 MHz, $DMSO-d_6$) δ 1.43 (s, 9H), 4.77(s, 2H), 4.82(s, 2H), 6.69-6.77 (m, 2H), 7.53-7.55 ppm (d, 2H); ^{13}C NMR (126 MHz, $DMSO-d_6$) δ 27.72, 65.31, 75.55, 81.82, 97.57, 111.54, 114.55, 124.72, 165.96, 167.09, 175.47, 197.26 ppm.

(Z)-tert-butyl 2-((2-((1-ethyl-5-methoxy-1H-indol-3-yl)methylene)-3-oxo-2,3-



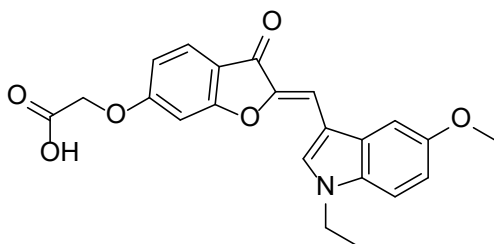
dihydrobenzofuran-6-yl)oxy)acetate (6b). To

a flask containing 26 mg (0.1 mmol) of tert-butyl 2-((3-oxo-2,3-dihydrobenzofuran-6-yl)oxy)acetate (**6a**) in 1 mL of DCM was added 20.3 mg (0.1 mmol, 1 eq) of commercially available 1-ethyl-5-methoxy-1H-indole-3-carbaldehyde and 320 mg (3.2 mmol, 32 eq) of aluminum oxide. The mixture was stirred at 25°C for 16 hours, filtered, concentrated, crystallized in methanol to afford 27 mg (60%) of **6b** as yellow solid. 1H NMR (400 MHz, $DMSO-d_6$) δ 1.41-1.45 (m, 12H), 3.48 (s, 3H),

4.28-4.34 (q, 2H), 4.88 (s, 2H), 6.83-6.90 (m, 2H), 7.07 (d, 1H), 7.30 (s, 1H), 7.49-7.51 (d, 1H), 7.62-7.69 (m, 2H), 8.19 ppm (s, 1H); ¹³C NMR (126 MHz, DMSO-d₆) δ 15.79, 28.15, 41.78, 55.92, 65.89, 82.27, 98.27, 101.55, 106.78, 107.82, 111.99, 112.52, 113.30, 116.73, 125.45, 128.63, 131.18, 134.11, 144.97, 155.52, 165.02, 166.48, 167.59, 180.45 ppm.

(Z)-2-((2-((1-ethyl-5-methoxy-1H-indol-3-yl)methylene)-3-oxo-2,3-

dihydrobenzofuran-6-yl)oxy)acetic acid (6c). (Z)-tert-butyl 2-((2-((1-ethyl-5-methoxy-



1H-indol-3-yl)methylene)-3-oxo-2,3-

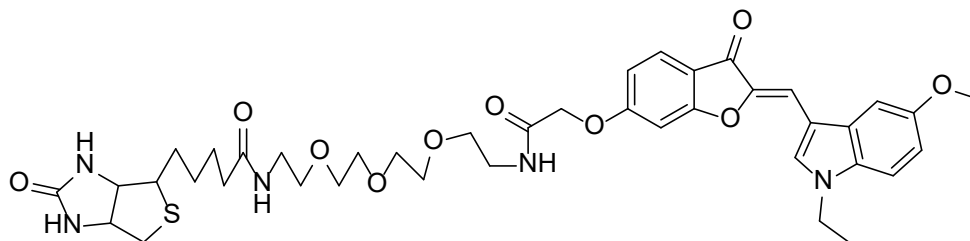
dihydrobenzofuran-6-yl)oxy)acetate (**6b**) was refluxed in 2 mL of formic acid at 60 °C for 2 hours. The solution was concentrated by

evaporation and further dried in a desiccator to afford **6c** (100%) as yellow solid. ¹H NMR (400 MHz, DMSO-d₆) δ 1.41-1.45 (t, 3H), 3.84 (s, 3H), 4.29-4.35 (q, 2H), 4.90 (s, 2H), 6.84-6.90 (m, 2H), 7.06 (s, 1H), 7.30 (s, 1H), 7.49-7.69 (m, 3H), 8.22 (s, 1H), 13.25 ppm (s, 1H); ¹³C NMR (126 MHz, DMSO-d₆) δ 15.85, 41.77, 55.92, 65.44, 97.97, 101.46, 106.68, 107.78, 111.98, 112.87, 113.30, 116.25, 125.40, 128.70, 131.11, 134.12, 145.04, 155.52, 165.16, 166.57, 169.96, 180.45 ppm.

(Z)-N-(1-((2-((1-ethyl-5-methoxy-1H-indol-3-yl)methylene)-3-oxo-2,3-

dihydrobenzofuran-6-yl)oxy)-2-oxo-6,9,12-trioxa-3-azatetradecan-14-yl)-5-(2-

oxohexahydro-1H-thieno[3,4-d]imidazol-4-yl)pentanamide (6d). To a 5 mL vial



containing 28 mg (0.072 mmol, 1.2 eq) of (Z)-2-((2-((1-ethyl-5-methoxy-1H-indol-3-yl)methylene)-3-oxo-2,3-dihydrobenzofuran-6-yl)oxy)acetic acid (**6c**) in 300 μ L of DMF was added 18 mg (0.096 mmol, 1.6 eq) of EDC (N-(3-Dimethylaminopropyl)-N'-ethylcarbodiimide) under stirring at 0 °C. After 20 min, 25 mg (0.06 mmol, 1 eq) of EZ-Link[®] Amine-PEGn-Biotin (Thermo Scientific, MA USA) was added. The mixture was stirred for 24 hours at room temperature, extracted with DCM, washed with brine, dried and purified on preparative silica plates by 1:13 methanol: dichloromethane ($R_f = 0.28$) to afford 20 mg (42%) of **6d** as yellow solid. ¹H NMR (400 MHz, DMSO-d₆) δ 1.23-1.6 (m, 9H), 2.02-2.06 (t, 2H), 3.85 (s, 3H), 2.54-2.57(d, 1H), 2.77-2.81 (dd, 1H), 3.0 (m, 1H), 3.14-3.5 (m, 16H), 4.10-4.11 (m, 1H), 4.26-4.32 (m, 3H), 4.69 (s, 2H), 6.35 (s, 1H), 6.40 (s, 1H), 6.88-7.70 (m, 7H), 7.80-7.83 (t, 1H), 8.21 (s, 1H), 8.22-8.25 ppm (t, 1H); ¹³C NMR (126 MHz, DMSO-d₆) δ 15.82, 25.68, 28.46, 28.62, 35.50, 38.83, 41.78, 55.85, 55.93, 59.58, 61.44, 67.74, 69.23, 69.57, 69.95, 70.0, 70.1, 98.23, 101.51, 106.78, 107.80, 111.99, 113.04, 113.30, 116.33, 125.37, 128.67, 131.14, 134.13, 145.00, 155.53, 163.12, 165.03, 166.52, 167.36, 172.54, 180.47 ppm.

Biology

The alpha-tubulin antibody was from GeneTex, Inc. (USA). The beta-tubulin antibody was from Developmental Studies Hybridoma Bank (Iowa city, IA USA). RO3306 was purchased from Cayman Chemical (Ann Arbor, MI, USA). TRITC-conjugated anti-rabbit antibody, DAPI and PI (propidium iodide) were from ThermoFisher (USA).

Cell lines and cell culture

PC-3, MCF-7, LS174T, HEK-293T and A549 cells were cultured in the medium recommended by American Type Culture Collection at 37°C with 5% CO₂ atmosphere in a water jacketed incubator (NuAire). Ovc8 and NCI/ADR-RES cells were gifts from Dr. Markos Leggas, University of Kentucky, Lexington, KY USA.

Cell proliferation inhibition assay

Cancer cells were seeded into 24-well plates at a density of 20,000 cells per well in 1 mL of culture medium and were cultured overnight at 37°C. Compounds and the vehicle control (DMSO) were added to the cells. After 6 days, the medium was removed, and 100 µL of trypsin was added. The cells were re-suspended in phosphate-buffered saline (PBS) and were counted by Vi-CELL XR 2.03 (Beckman Coulter, Inc. USA). The ratio R of the number of viable cells in the compound treatment group to the number of viable cells in DMSO treatment group was taken as relative growth, and the percentage growth inhibition was calculated as $(1-R)*100$. For initial testing, compounds were added to the cells at a final concentration of 10 µM. Active compounds at 10 µM were tested at lower concentrations than 10 µM.

Biotin-streptavidin pull-down assay

PC-3 cell lysates were collected and precleaned by incubation with 50 μ L of streptavidin mag sepharoseTM (GE Healthcare Bio-Sciences, Uppsala, Sweden) under shaking at 4 $^{\circ}$ C for 3 hours. Then the lysate was divided in two tubes. To the control tube, DMSO and 10 μ L of streptavidin mag sepharoseTM were added and to the binding reaction tube, compound **6d** and 10 μ L of streptavidin mag sepharoseTM were added. The two mixtures were incubated under shaking at 4 $^{\circ}$ C for 3 hours and washed with PBS for 4 times. The obtained samples were diluted with 2x loading buffer, boiled at 100 $^{\circ}$ C for 3 minutes, and resolved by 10% SDS-PAGE gel.

Silver staining

Silver staining was done following a published procedure³⁹.

NCI-60 cell lines

The lead compound aurone **5a** was submitted to the National Cancer Institute (Rockville, MD, USA) to test in the NCI-60 cell lines using cell proliferation inhibition assay.

Immunofluorescence imaging

Tubulin networks were examined by confocal immunofluorescence imaging. Briefly, PC3 cells were placed at a density of 80,000/mL to 24-well plates equipped with round microscope glass cover slides. After culturing at 37 $^{\circ}$ C for 24 hours, DMSO or compounds were added to the cells and incubated for additional 6 hours. Then the medium

was removed and the cells were washed with PBS three times. Primary anti- α -tubulin antibody was added and incubated overnight at 4°C. After additional washing, secondary TRITC-conjugated anti-rabbit antibody was added for 40 min, followed by additional washing and staining with DAPI. Final washing was performed and the cover slides were inverted onto glass slides. Images (40x) were taken using a Nikon confocal microscope with excitation at 557 nm and emission at 576 nm.

In vivo microtubule assembly assay

The amount of insoluble polymerized microtubules and soluble tubulin dimers in cells after exposure to aurones were detected using a reported method. Cells were seeded in 6-well plates at 50% confluency and cultured overnight. DMSO or aurones in DMSO solution were added, and the cells were incubated for additional 6 hours. The medium was removed, and cells were washed with PBS three times followed by the addition of a lysis buffer prepared from 20 mM Tris-HCl (pH 6.8), 1 mM MgCl₂, 2 mM ethylene glycol-bis(β -aminoethyl ether) (EGTA), 20 μ g/mL aprotinin, 20 μ g/mL leupeptin, 1 mM phenylmethylsulfonyl fluoride (PMSF), 1mM orthovanadate , and 0.5% NP40. The lysates were centrifuged at 12,000 g for 10 min to obtain supernatants and pellets that were mixed with loading buffer and heated to 100 °C. Standard western blotting against α -tubulin was performed as described previously⁴⁰.

In vitro tubulin polymerization assay

An *in vitro* tubulin polymerization assay was performed using a protocol from Cytoskeleton, Inc. (Denver, CO USA). Tubulin powder (Cytoskeleton Inc. Denver, CO

USA) was dissolved in a buffer prepared from 100 mM PIPES (pH 6.9), 2 mM MgCl₂, 1 mM GTP, and 5% glycerol at 0°C. Aliquots (80 μL, 3.75 μg/μL) of this tubulin solution were divided into the wells of a 96-well half-area plate (Corning Inc., NY USA). After adding either DMSO or testing compounds, the plate was mounted on a Spectra MR™ microplate spectrophotometer equipped with a thermal controller at 37°C (Dynex Technologies, Inc., Chantilly, VA USA). Readings at 350 nm were recorded every 30 s for 1 hour.

Molecular docking studies

An X-ray crystal structure of αβ-tubulin binding with colchicine (pdb: 4O2B) was downloaded from RCSB Protein Data Bank and manipulated using AutoDockTools-1.5.6 (Molecular Graphics Laboratory, The Scripps Research Institute, La Jolla, CA 92037 USA). The αβ-Tubulin dimer was separated from 4O2B using PyMOL (Version 1.7.4.5 Edu). Water molecules were removed, and polar hydrogens and Kollman charges were added. The docking pocket (colchicine-binding site) was defined as follows: Search space: 18 x 18 x 18 Å³; Center_x, y, z = 14.815, 9.422, - 20.186. The auronones **4d**, **5a**, and colchicine were manipulated by Openbabel. Molecular docking of **4d**, **5a**, and colchicine to the colchicine-binding site was executed using AutoDock vina-1.1.2 using the iterated gradient-based local search method with a Broyden–Fletcher–Goldfarb–Shanno (BFGS) method for local optimization⁴¹. Exhaustiveness was set at 14 and the number of modes was nine. Other parameters were left at default values.

Competitive tubulin binding assay

A competitive, tubulin-binding assay⁴² was performed as described to demonstrate that aurones bound to the colchicine-binding site of tubulins. The colchicine quantification was performed at the University of Kentucky Proteomics Core using a protocol modified from a previously published method. Liquid Chromatography-Electrospray Ionization-Tandem Mass Spectrometry (LC-MS/MS) analysis was carried out using a TSQ Vantage mass spectrometer (Thermo Fisher Scientific, Waltham, MA USA) coupled with a Shimadzu high performance liquid chromatography (HPLC) system (Shimadzu Scientific Instruments, Inc., Columbia, MD USA) through an electrospray ionization source. The colchicine-containing samples were separated with a Kinetex[®] reversed phase 2.6 μm XB-C18 100 \AA LC column (100 x 4.6 mm) (Phenomenex Inc., Torrance, CA USA) at a flow rate of 300 $\mu\text{L}/\text{min}$. Mobile phase A was water with 0.1% (v/v) formic acid while mobile phase B was acetonitrile with 0.1% (v/v) formic acid. A 16 min gradient condition was applied: initial 60% mobile phase B was increased linearly to 100% in 3 min, remained 100% for 3 min, and quickly (0.01min) decreased to 60% for re-equilibration. Multiple reaction monitoring (MRM) mode was used to scan from m/z 400 to m/z 310 in the positive mode to obtain the most sensitive signals for colchicine. The spraying voltage was set at 4000 V, vaporize temperature at 300 $^{\circ}\text{C}$, capillary temperature at 350 $^{\circ}\text{C}$ and sheath gas pressure at 45 (arbitrary units). Collision energies (CE) were set at 25 volts. Xcalibur software (Ver. 2.1.0, Thermo Fisher Scientific, Waltham, MA USA) was used for the data acquisition and quantitative processing. A series of colchicine at concentrations of 20, 40, 80, 200, 400, 800 nM were prepared to establish a linear calibration curve with a coefficient of correlation $R^2 = 0.9944$.

Cell cycle assay by flow cytometry

Briefly, a million of PC-3 cells were placed in 6-cm dishes and cultured at 37 °C for 24 hours. DMSO or compounds in DMSO were added to the cells and incubated for additional 16 hours. The cells were trypsinized, washed with ice cold PBS twice, and resuspended in 500 µL of PBS. This cell suspension was added to 5 mL of 70% ethanol dropwise in a 15 mL tube that was placed on vortex and kept at -20 °C overnight. The cells were further washed with PBS and 2 µL of 50 mg/ml RNase (final 0.2 mg/ml) and 2.5 µL of 4 mg/mL PI (final 20 µg/mL) were added. The mixture was incubated at dark for 45 min and filtered through 35 µm nylon mesh for analysis by the Flow Cytometry and Cell Sorting Shared Resource Facility of the University of Kentucky Markey Cancer Center.

hERG binding studies

An HEK-293 cell line stably expressing the hERG potassium channel (accession number U04270) referred to as hERG-HEK cells were received at passage 11 (P11) from Millipore (CYL3006, lot 2, Billerica, MA USA). [³H]-Dofetilide (specific activity of 80 Ci/mmol; labeled on the N-methyl group) was obtained from American Radiolabeled Chemicals, St. Louis, MO USA). Other chemicals and solvents were obtained from Sigma-Aldrich (Milwaukee, WI USA) with exceptions of polyethylenimine (PEI), which was obtained from Fluka/Sigma-Aldrich (St. Louis, MO USA), and Minimum Essential Medium (MEM) with GlutaMAX™ and phenol red, MEM non-essential amino acids solution (NEAA, 100X), G418 disulfate salt solution, fetal bovine serum (FBS), 0.05% Trypsin-Ethylenediaminetetraacetic acid (EDTA) 1X with phenol red, and Hank's

balanced salt solution (HBSS), which were obtained from Life Technologies (Carlsbad, CA USA).

hERG-HEK Cell Culture

The hERG-HEK cells were cultured according to the protocol provided by Merck Millipore (Burlington, MA USA). Cells were maintained in MEM (with glutamax and phenol red) supplemented with 10% FBS, 1% NEAA and 400 g/ml geneticin, and incubated at 37 °C in a humidified atmosphere with 5% CO₂. Frozen aliquots of cells were transferred into T-75 cm² flasks and allowed to adhere for 4-8 hours. The medium was replaced every 2 days. Passages were carried out at least 3 times after thawing at 6 day intervals. Cells were dissociated with trypsin/EDTA and seeded into new 150 x 25 mm dishes at 2-3 x 10⁶ cells per dish and placed at 30 °C, 5% CO₂, for 40-48 hours prior to membrane preparation. Membrane preparation occurred 6 days after the last passage (passage 20).

[³H]-Dofetilide binding assay

Membrane preparation

Cell membrane preparation was based on previous methods⁴³⁻⁴⁵. Cells were rinsed twice with HBSS at 37 °C and collected by scraping the dishes in *ca.* 20 mL of ice-cold 0.32 M sucrose and homogenized on ice with a Teflon pestle using a Maximal Digital homogenizer (Fisher Scientific, Pittsburgh, PA USA) at ~280 rpm for 30 sec. Homogenates were centrifuged at 300g and 800g for 4 min each at 4°C. Pellets were resuspended in 9 mL of ice-cold Milli-Q water and osmolarity restored by addition of 1 mL of 500 mM Tris buffer (pH 7.4) followed by suspension and centrifugation at 20,000g for 30 min at 4°C.

Pellets were homogenized in 2 mL assay buffer (50 mM Tris, 10 mM KCl, and 1 mM MgCl₂, 4°C) and aliquots of cell membrane suspensions were stored at -80°C and thawed the day of the [³H]-dofetilide binding assay. Protein content was determined prior to the assay using a Bradford protein assay with bovine albumin as the standard.

[³H]-Dofetilide binding assay

[³H]-Dofetilide binding assays using hERG-HEK293 cell membranes were based on previous methods. Assays determining concentration-response were performed in duplicate, and three independent assays were performed for each analog evaluated. Cell membrane suspension (5 µg) was added to duplicate tubes containing assay buffer, 25 µL of a single concentration of FIDAS agent (concentration range of 10 nM-100 µM for each experiment), and 25 µL of [³H]-dofetilide (5 nM, final concentration) for an assay volume of 250 µL. Binding occurred for 60 min at 25°C and was terminated by rapid filtration through Whatman GF/B filters, which were pre-soaked in 0.25% PEI overnight, using a Brandel cell/membrane harvester (M-48; Brandel Inc., Gaithersburg, MD USA). Filters were washed three times with *ca.* 1 mL of ice-cold assay buffer. Radioactivity was determined by liquid scintillation spectrometry using the Tri-Carb 2100-TR Liquid Scintillation Analyzer (Perkin-Elmer Life and Analytical Sciences).

In vivo evaluation of anti-leukemia activity in the zebrafish model

Zebrafish studies were carried out with approval from the Institutional Animal Care and Use Committee of the University of Kentucky (2015-2225). All methods were performed in accordance with the relevant guidelines and regulations governing research protocols involving animals. *Rag2: myc-GFP* zebrafish (n=8) at 21 days of age were

treated with DMSO, either aurones **5a** or **5r** in 1.5 mL of fish-system water in 12-well plates. Zebrafish were treated with compound for 2 days, removed from drug for 1 day, and treated for two more days with freshly prepared solutions of compound. Animals were imaged at the start and end of treatment using a fluorescence-equipped dissecting microscope at 350 ms exposure. The GFP image was overlaid onto the bright-field image of each animal in Photoshop, and the percent change in leukemia burden was calculated by normalizing the GFP+ area to the total area of the animal in ImageJ (National Institute of Health, USA).

In vivo evaluation of antineoplastic activity and gross toxicity in PC-3 xenografts

Mouse studies were carried out with approval from the Institutional Animal Care and Use Committee of the University of Kentucky (2009-1064). All methods were performed in accordance with the relevant guidelines and regulations according to protocols. PC-3 cells suspended in PBS were subcutaneously injected in the lower flanks of immune-deficient nude mice (5 mice in each group, two tumors on each mouse) at a density of 2×10^6 cells in 200 μ L of PBS. After tumors were established (in about two weeks), aurone **5a** formulated in a mixture of Tween-80 (5%), DMSO (10%), PEG400 (25%) and PBS (60%) was intraperitoneally administered to mice at a daily dose of 10 mg of aurone **5a**/kg (mouse). The first day of treatment was set as day 1. At day 18 treatment was ceased and mice were sacrificed. Blank vehicle was used as a control. Tumors and mouse weights were measured, and tumor volumes were calculated as $\text{Length} \times \text{width}^2/2$.

Statistics

Biological assays have been performed at least twice. Data were shown as mean \pm SD or the 95% confidence intervals were provided. For the mice study, five mice with two tumors on the lower flanks of each mouse were used in each treatment group. The data for the mouse study were analyzed by t-test. For the zebrafish study, eight fish were used in each treatment group.

Chapter 3 Structure-activity relationships of semisynthetic aurones

Introduction

Published studies of structure-activity relationships (SAR) in aurones as antineoplastic agents replaced the C-2 phenylmethylene subunit (*i.e.*, so-called “benzylidene” subunit) found in many naturally occurring aurones, such as sulfuretin (**1a**) and aureusidin (**1b**) (Figure 3.1 A), with a C-2 heteroarylmethylene group. For example, benzofuran-3(2*H*)-ones with 2-(coumarin-4-yl)methylene⁴⁶ groups or 2-(furan-2-yl)methylene⁴⁷ groups displayed *in vitro* activity against human leukemia K562 cells; benzofuran-3(2*H*)-ones with 2-(piperazin-1-yl)methylene groups possessed IC₅₀ values in the low micromolar range against various solid tumor cell lines⁴⁸; and benzofuran-3(2*H*)-ones with 2-(indol-3-yl)methylene groups inhibited cell proliferation in breast cancer MCF-7 and MDA-MB-231 cell lines⁴⁹. Another published study reported aurone (2*Z*)-2-benzylidene-4-hydroxy-6-methoxy-1-benzofuran-3(2*H*)-one as a P-glycoprotein inhibitor, and this compound modulated P-glycoprotein-mediated multiple drug resistance as an indirect antineoplastic agent⁵⁰. The 4' position of benzylidene was replaced by different halogens that resulted in different binding affinities to P-glycoprotein. Substitutions of the C-6 position of benzofuran-3(2*H*)-one have not been explored thoroughly for antineoplastic purposes. In addition, the relative potencies among these different C-2 heteroarylmethylene-substituted aurones were in the micromolar range. The *in vivo* activity of these aurones, and the specific biological target or targets in these cases were unclear.

In this chapter, we will discuss modifications that were made on the C-6 and C-2 positions of benzofuran-3(2*H*)-one to generate novel aurone analogs. Iterative synthesis and proliferation inhibition assays using PC-3 cells were used to determine the relative proliferation inhibition compared to the vehicle control, dimethyl sulfoxide (DMSO).

Results

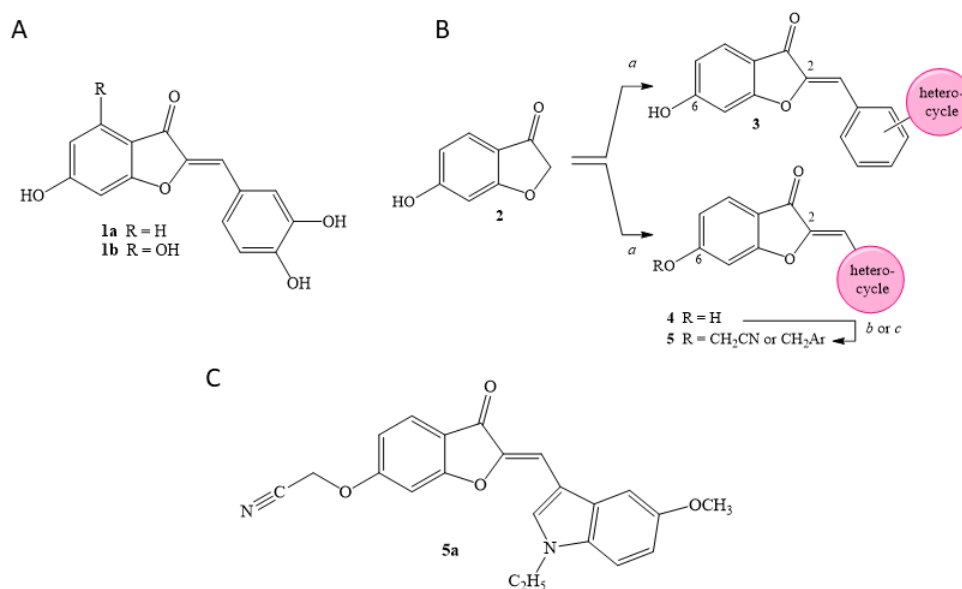


Figure 3.1: A, Representative, naturally occurring aurones, sulfuretin (**1a**) and aureusidin (**1b**). B, Synthesis of aurones **3-5**. Legend: *a*, heterocyclic-substituted benzaldehydes or heteroarylcarboxaldehydes, 50% aq. potassium hydroxide, 1:1 ethanol: *N,N*-dimethylformamide, *b*, bromoacetonitrile, potassium carbonate, *N,N*-dimethylformamide; *c*, halogenated benzyl bromide, potassium carbonate, *N,N*-dimethylformamide. C, Leading aurone candidate. (*Z*)-2-((2-((1-ethyl-5-methoxy-1*H*-indol-3-yl) methylene)-3-oxo-2,3-dihydrobenzofuran-6-yl) oxy) acetonitrile (**5a**).

Synthesis of semisynthetic aurones modified at C-2

Modifications of aurones were investigated in which either we attached a heterocyclic ring to the C-2 phenylmethylene group as in aurones **3** or we replaced the entire C-2 phenylmethylene group with a C-2 heteroarylmethylene group as in aurones **4** (Figure 3.1 B). The syntheses⁵¹ of 6-hydroxyaurones **3** and **4** involved the condensations of 6-hydroxybenzofuran-3(2*H*)-one (**2**) with heterocyclic-substituted benzaldehydes and heteroaryl carboxaldehydes, respectively (Figure 3.1 B). Although literature reports described various catalysts⁵²⁻⁵⁷ for similar condensations, we found that the use of 50% aqueous potassium hydroxide (2 eq) in 1:1 ethanol-*N,N*-dimethylformamide (DMF) furnished the 6-hydroxyaurones **3** and **4** in good yields. (*Z*)-Stereochemistry was in accord with prior acid or base-catalyzed condensations of benzofuran-3(2*H*)-ones with aromatic aldehydes^{50,58}. A reiterative process of synthesis and screening using *in vitro* prostate cancer PC-3 cell proliferation assays identified 4-(pyrrolidin-1-yl)phenylmethylene-substituted aurone **3a** and heteroarylmethylene-substituted aurones **4d**, **4e**, **4g** and **4l** with 1-isoquinolyl, 2-quinolyl, 8-methoxy-2-quinolyl, and 5-methoxy-*N*-ethyl-3-indolyl groups, respectively, as the most potent analogs at 10 μ M concentrations (**Table 1**). Only the latter heteroarylmethylene-substituted aurones **4** retained any activity at concentrations below 10 μ M. Comparable outcomes were observed using *in vitro* colorectal LS174T cell proliferation assays with the exception of aurone **3a** that showed no appreciable activity in this cell line even at 10 μ M concentration (data not shown for C-4 hydroxyl groups or C-7 methyl groups) failed to produce analogs with improved activity relative to their unsubstituted counterparts (data not shown). Among the heteroarylmethylene-substituted aurones **4**, the 3-indolylmethylene-substituted aurone **4l** warranted additional study based on a combination of modest potency in cell proliferation assays in the 1-10 μ M range.

Table 1. Abbreviated SAR study involving modifications aurone at the C-2 and C-6 positions using prostate cancer PC-3 cell proliferation assays

Aurone	Ar ¹	Inhibition of PC-3 Cells	
		10 μ M	1 μ M
3a	4-(pyrrolidin-1-yl)phenyl	95 \pm 4.7	2.1 \pm 7.1
3b	4-(morpholino-1-yl)phenyl	7.8 \pm 7.7	
3c	4-(4-methylpyridazin-1-yl)phenyl	42 \pm 14	
4a	2-pyridyl	8.8 \pm 15	
4b	3-pyridyl	0	
4c	4-pyridyl	20 \pm 5.4	
4d	1-isoquinolyl	88 \pm 5.5	
4e	2-quinolyl	99 \pm 0.2	26 \pm 8.6
4f	6-methoxy-2-quinolyl	8.4 \pm 33	
4g	8-methoxy-2-quinolyl	97 \pm 0.8	40 \pm 8.4
4h	4-quinolyl	63 \pm 7.2	16 \pm 3.5
4i	3-indolyl	20 \pm 6.8	
4j	<i>N</i> -methyl-3-indolyl	41 \pm 25	
4k	<i>N</i> -methyl-5-methoxy-3-indolyl	35 \pm 28	17 \pm 5.5
4l	<i>N</i> -ethyl-5-methoxy-3-indolyl	69 \pm 16	13 \pm 9.5

Synthesis of semisynthetic aurones modified at C-6

Alkylation of the C-6 hydroxyl group in heteroarylmethylene-substituted aurones **4** using various alkyl bromides and anhydrous potassium carbonate in *N,N*-dimethylformamide (DMF) led to the alkoxy-substituted aurones **5** (Figure 3.1 B). An SAR study involving dual modifications of the C-6 alkoxy group and the C-2 heteroarylmethylene group revealed a pattern favoring either a cyanomethoxy or a 2,6-

dichlorobenzyloxy group at C-6 and favoring one of the following C-2 heteroarylmethylene subunits: *N*-methyl-3-indolylmethylene, *N*-ethyl-3-indolylmethylene, 5-methoxy-*N*-methyl-3-indolylmethylene, or 5-methoxy-*N*-ethyl-3-indolylmethylene groups (**Table 2**). One candidate emerged with 90%⁺ inhibition of *in vitro* prostate cancer PC-3 cell proliferation at 300 nM concentration: (*Z*)-2-((2-((1-ethyl-5-methoxy-1*H*-indol-3-yl)methylene)-3-oxo-2,3-dihydrobenzofuran-6-yl)oxy)acetonitrile (**5a**) (Figure 3.1 C; **Table 2**). Modifications at other positions (*e.g.*, methyl groups at C-7 as in **5i** and **5m**) in addition to these modifications at C-2 and C-6 led to diminished activity relative to aurone **5a**.

The pairing of the cyanomethoxy group at C-6 with the (*N*-ethyl-5-methoxy-1*H*-indol-3-yl) methylene at C-2 in aurone **5a** and the pairing of the 2,6-dichlorobenzyloxy group at C-6 with the (pyridin-4-yl)methylene at C-2 in aurone **5r** were essential to potency. Alternate pairings, modification in the halogenation type and pattern in the 2,6-dichlorobenzyloxy group, changes in the *N*-ethyl-5-methoxy-1*H*-indol-3-yl group (*e.g.*, replacement of the *N*-ethyl with an *N*-methyl group; replacement of the 5-methoxy with a 5-hydroxy group), and modifications at still other positions in the benzofuran (*e.g.*, methyl groups at C-7) led to diminished activity in the prostate cancer PC-3 cell proliferation assay relative to aurones **5a** and **5r**.

Table 2. SAR study involving modifications of the C-6 alkoxy group in aurones **5** *versus* modifications of the C-2 heteroaryl-substituted methylene subunit using prostate cancer PC-3 cell proliferation assays.

Aurone	C-6	C-7	C-2 Heteroaryl Group	Inhibition of PC-3 Cells		
				10 μ M	1 μ M	300 nM
5a	OCH ₂ CN	H	<i>N</i> -ethyl-5-methoxy-3-indolyl		95±2.5	93±2.8
5b	OCH ₂ CN	H	<i>N</i> -ethyl-5-hydroxy-3-indolyl	96±1.6	96±2	24±11
5c	OCH ₂ CN	H	<i>N</i> -carboxymethyl-5-hydroxy-3-indolyl	0		
5d	OCH ₂ C ₆ H ₄ -2-F	H	<i>N</i> -methyl-3-indolyl	0		
5e	OCH ₂ C ₆ H ₄ -2-Cl	H	<i>N</i> -methyl-3-indolyl	20±6.6		
5f	OCH ₂ C ₆ H ₃ -2,6-F ₂	H	<i>N</i> -methyl-3-indolyl	82±4.3		
5g	OCH ₂ C ₆ H ₃ -2,6-Cl ₂	H	<i>N</i> -methyl-3-indolyl	96±1.4	80±8	28±4.4
5h	OCH ₂ C ₆ H ₃ -2-F-6-Cl	H	<i>N</i> -methyl-3-indolyl	31±40	0	
5i	OCH ₂ C ₆ H ₃ -2,6-Cl ₂	CH ₃	<i>N</i> -methyl-3-indolyl	7±35		
5j	OCH ₂ C ₆ H ₃ -2-F-4-Cl	H	<i>N</i> -methyl-5-methoxy-3-indolyl	8.6±12		
5k	OCH ₂ C ₆ H ₃ -2-F-6-Cl	H	<i>N</i> -methyl-5-methoxy-3-indolyl	57±18		
5l	OCH ₂ C ₆ H ₃ -2,6-Cl ₂	H	<i>N</i> -methyl-5-methoxy-3-indolyl	96±1.8	82±7.7	24±7.3
5m	OCH ₂ C ₆ H ₃ -2,6-Cl ₂	CH ₃	<i>N</i> -methyl-5-methoxy-3-indolyl	0		
5n	OCH ₂ C ₆ H ₄ -2-F	H	<i>N</i> -ethyl-5-methoxy-3-indolyl	52±23	28±15	
5o	OCH ₂ C ₆ H ₃ -2,6-Cl ₂	H	<i>N</i> -ethyl-5-methoxy-3-indolyl	96±1.1	67±5.8	3.9±11
5p	OCH ₂ C ₆ H ₃ -2-F-6-Cl	H	<i>N</i> -ethyl-3-indolyl	95±4.4	91±2.2	44±5.6
5q	OCH ₂ C ₆ H ₃ -2,6-Cl ₂	H	<i>N</i> -ethyl-3-indolyl	97±0.6	98±1	75±7.7
5r	OCH ₂ C ₆ H ₃ -2,6-Cl ₂	H	4-pyridyl		92±0.4	95±1.1

Aurones 5a and 5r showed broad antineoplastic activities

In addition to the prostate cancer PC-3 cell line in which aurone **5a** displayed an IC₅₀ of 57.8 ± 1.1 nM, I determined that aurone **5a** displayed inhibition of colorectal cancer LS174T, lung cancer A549, breast cancer MCF-7, and ovarian cancer OvcAR-8 and NCI/ADR-RES cell lines with IC₅₀ values in the low to mid-nanomolar range (Table 3). During a five-day treatment period, aurone **5a** showed potent, dose-dependent *in vitro* inhibition of these cancer cell lines. Treatment of a normal human embryo lung cell line HEL299 with aurone **5a** showed an IC₅₀ in the micromolar range (1.3 ± 0.2 μM), a finding that suggested aurone **5a** was selectively more toxic to cancer cell lines than normal cell lines.

Table 3. IC₅₀ values of aurones **5a** and **5r** in cancer cell line proliferation inhibition assays

Cell lines	IC ₅₀ (nM)	
	Aurone 5a	Aurone 5r
PC-3	58.7±1.1	66.0±1.1
LS174T	155.2±1.1	158.3±1.0
A549	173.6±1.0	113.0±1.0
MCF-7	244.3±1.2	185.6±1.1
NCI/ADR-res	85.9±1.0	190.3±1.1
OVCAR-8	181.9±1.0	257.7±1.1

Discussion

Previous SAR of aurones as antineoplastic agents focused on the substitution of the C-2 position of the benzofuran-3(2*H*)-one subunit and generated a number of aurone

analogs with limited potencies in the micromolar range⁴⁶⁻⁵⁰. The mechanisms of action of those aurone analogs were unclear, and the *in vivo* efficacy was not evaluated. Hence, further efforts were needed to improve the potency of aurone analogs. A reiterative process of synthesis and testing was used to guide the development of SAR relationships within the aurone pharmacophore. Aurones in which the C-2 position had either a heterocyclic-substituted phenylmethylene group as in aurone **3** or a heteroarylmethylene group as in aurone **4** (Figure 3.1 B) were examined. Using *in vitro* inhibitory activity in prostate cancer PC-3 cell proliferation assay as a readout, we established that the aurones **4** bearing either 1-isoquinolyl, 2-quinolyl, 8-methoxy-2-quinolyl, or 5-methoxy-*N*-ethyl-3-indolyl groups were more potent than most aurones **3** at 10 μ M concentrations (Table 1). Modifications of the benzofuran-3(2*H*)-one subunit in these heteroarylmethylene aurones **4** at other positions failed to produce aurones with improved activity relative to the heteroarylmethylene-substituted aurones **4d**, **4e**, **4g** and **4l** (Table 1).

The alkylation of the C-6 hydroxyl group in 3-indolylmethylene-substituted aurones **4** with various alkyl bromides secured the C-6 alkoxy 3-indolylmethylene-substituted aurones **5** (Figure 3.1 B). An SAR study involving modifications of the C-6 alkoxy group in concert with the 3-indolylmethylene subunit at C-2 revealed a synergistic effect favoring either a C-6 cyanomethoxy or a 2,6-dichlorobenzyloxy group and one of the following C-2 heteroarylmethylene subunits: *N*-methyl-3-indolylmethylene, *N*-ethyl-3-indolylmethylene; 5-methoxy-*N*-methyl-3-indolylmethylene or 5-methoxy-*N*-ethyl-3-indolylmethylene (Table 2). One candidate displayed significant inhibition (IC_{50} 58 ± 1.1 nM) on the *in vitro* proliferation of prostate cancer PC-3 cells: (*Z*)-2-((2-((1-ethyl-5-methoxy-1*H*-indol-3-yl)methylene)-3-oxo-2,3-dihydrobenzofuran-6-yl)oxy)acetonitrile

(5a) (Figure 3.1 C). Alkoxy groups other than the C-6 cyanomethoxy or 2,6-dichlorobenzyloxy groups possessed less activity than that of aurone **5a** and **5r**. Modifications of these C-6 cyanomethoxy- or 2,6-dichlorobenzyloxy-substituted 3-indolylmethylene-substituted aurones **5** with substituents at still other positions in the benzofuran-3(2*H*)-one pharmacophore (e.g., C-7 methyl groups as in **5i** and **5m**) also led to diminished activity in a prostate cancer PC-3 cell proliferation assay. Finally, although we focused our studies (Table 2) on heteroaryl-substituted aurones **5** in which the indo-3-ylmethylene was the preferred heteroaryl group, we examined other heteroaryl substituents and identified only one candidate, namely (*Z*)-6-((2,6-dichlorobenzyl)oxy)-2-(pyridin-4-ylmethylene)benzofuran-3(2*H*)-one (**5r**), that possessed a 4-pyridylmethylene group in place of the indo-3-ylmethylene group and that displayed nanomolar potency in cell proliferation assays.

In contrast to previous SAR of aurones that focused on the modification of C-2 position of the benzofuran-3(2*H*)-one subunit, we simultaneously substituted both C-6 and C-2 positions of the benzofuran-3(2*H*)-one subunit, which proved to be successful to improve the potency of aurones. The two leading aurone analogs **5a** and **5r** displayed subnanomolar activities toward a panel of cancer cell lines, demonstrating broad antineoplastic scope. The improved potency would benefit subsequent studies of mechanism of action and biological target(s) of these aurones, and *in vivo* studies.

Chapter 4 Mechanism of action of semisynthetic aurones

Introduction

Identifying the biological target(s) and understanding the mechanism of action of a bioactive compound is both challenging and important in drug discovery and pharmacological studies. Without the knowledge of a compound's target(s), improving a compound's physical properties and efficacy by iterative chemical synthesis and testing is not straightforward and is very time-consuming. It is also difficult to predict possible toxicities of a compound without knowing the compound's target(s). Therefore, different approaches for elucidating drug targets were developed and can be classified into three categories⁵⁹: direct biochemical methods, genetic methods, and computationally based methods.

Direct biochemical strategies rely on affinity binding between a compound and the protein target(s). Often a compound is chemically modified with biotin or photoactive groups to generate a bioactive probe that binds to a target and allows target purification or detection. Although the workflow for affinity-based target identification is straightforward, it is often difficult to generate a bioactive probe by chemically perturbing the original leading compound.

Unlike direct biochemical target identification, genetic-based methods do not require the chemical modification of the compound of interest. Instead, genetic-based methods utilize recent advances in molecular biology, including large-scale gene-perturbation and genomic measurements. The combination of small interfering RNA (siRNA)⁶⁰ or clustered regularly interspaced short palindromic repeats (CRISPR)⁶¹

libraries targeting the whole exome in mammalian cells and sub-lethal concentrations of a compound to enrich resistant cell colonies followed by next generation DNA sequencing would generate direct target(s) or target signaling pathways.

Computational methods have also been developed for uncovering biological targets for small molecules. One of the early examples is the NCI COMPARE algorithm⁶² from the National Cancer Institute (NCI). This algorithm leverages the idea that compounds that have similar mechanism of action should show similar dose-responses in a similar assay. The National Cancer Institute has determined the growth-inhibition profiles of more than 88,000 pure compounds and more than 34,000 crude extracts against the NCI-60 cancer cell line panel consisting of 60 human cancer cell lines. A compound with unknown target(s) is first tested against the NCI-60 cancer cell line panel and considered as a “seed”. The NCI COMPARE ranks the entire database of tested compounds in the order of similarity of the responses of the NCI-60 cell lines to the compounds in the database to the responses of the cell lines to the “seed compound”. The similarity is quantified as a Pearson correlation coefficient and highly ranked compounds may share a similar mechanism of action to the seed compound. For example, the leading compound, namely aurone **5a**, was submitted to NCI for testing in the NCI-60 cancer cell line panel.

Results

Attempted affinity-based approach to purify aurone 5a's binding partner

According to the structure-activity relationships that were discussed in the previous chapter, a biotinylated aurone **6d** was designed and synthesized using a multi-step procedure (Figure 4.1). This analog **6d** was tested in PC-3 cell proliferation assay and showed growth inhibitory activity at 10 and 30 μM (Figure 4.2), values that were judged to be sufficient for an effective probe in a pull-down assay.

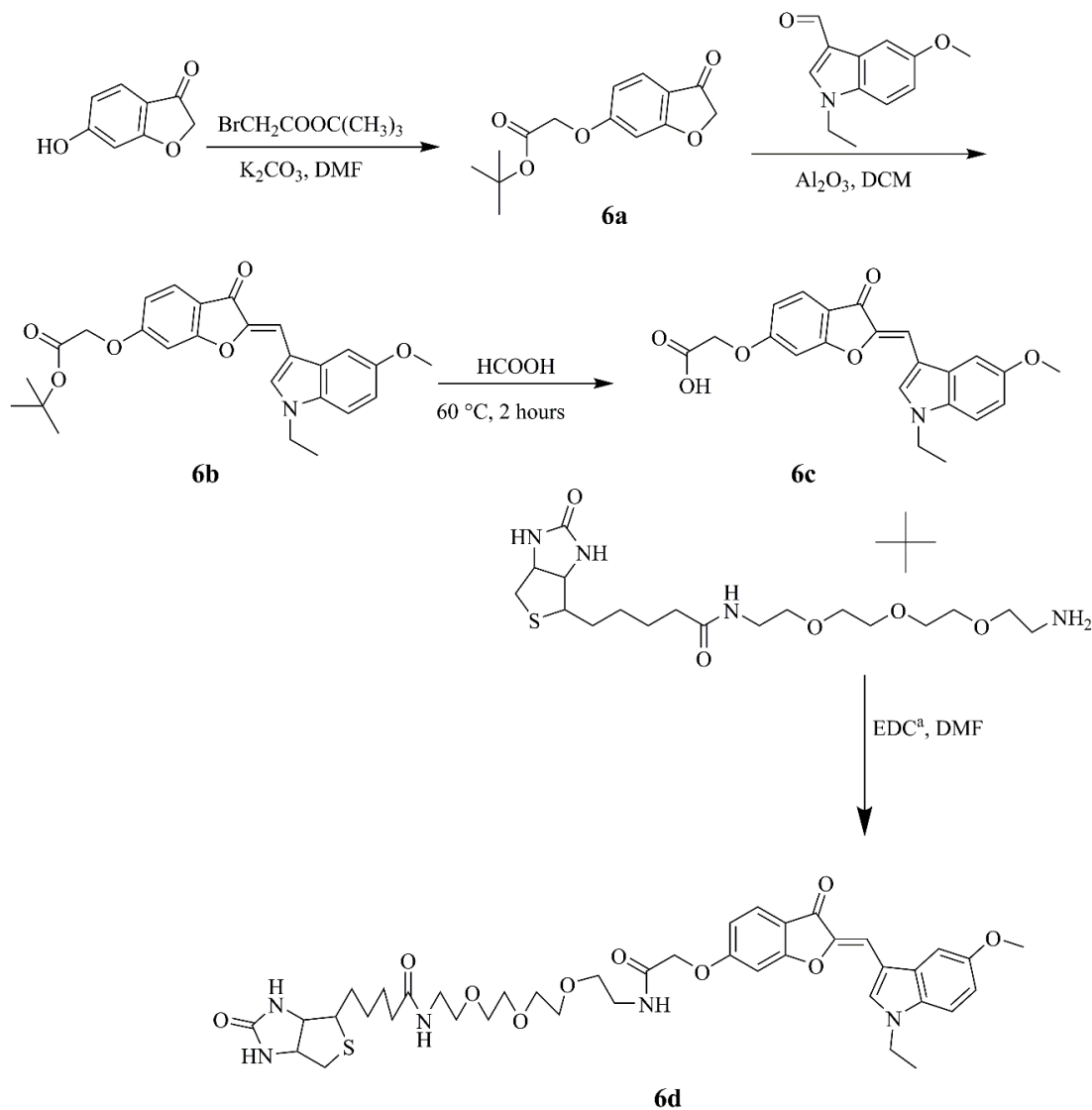


Figure 4.1: Synthesis scheme of biotinylated aurone analog **6d**. a, 1-ethyl-3-(3-dimethylaminopropyl)carbodiimide (EDC).

A streptavidin and biotin-based pull-down was performed using PC-3 cell lysates, and the results were visualized in by silver staining an SDS-PAGE gel (Figure 4.5), but unfortunately, this procedure did not reveal any targets. A possible reason why an active biotinylated probe did not pull down anything was that the binding site was at the interface of two protein monomers (in our case, tubulin alpha and beta monomers), so that the binding of biotinylated probe to the interface would destabilize the protein dimer.

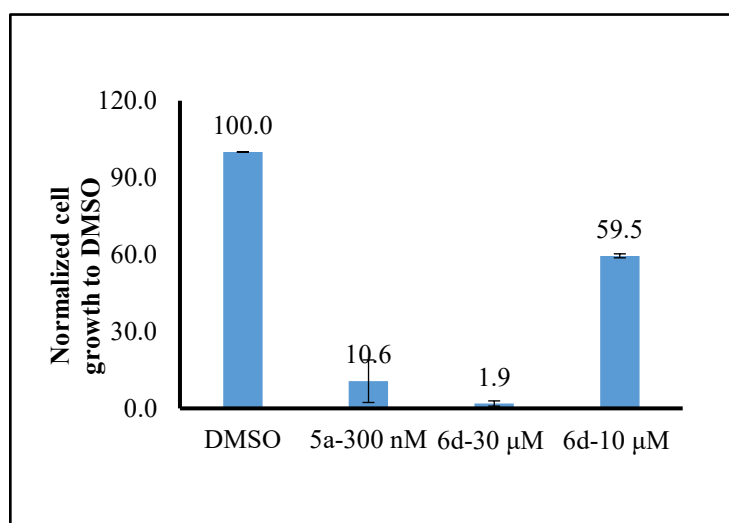


Figure 4.2: Biotinylated aurone analog **6d** inhibited PC-3 cell growth.

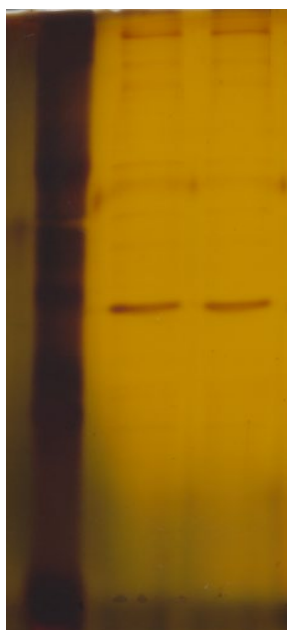


Figure 4.3: pull-down assay results. Left lane, DMSO; Right lane, biotinylated aurone analog **6d**.

Use of NCI COMPARE analysis

As noted above, the leading compound, aurone **5a**, was submitted to NCI for testing in the NCI-60 cancer cell line panel using cell proliferation inhibition assay. Results appear in Table 4. The majority of cancer cell lines in the NCI-60 panel were sensitive to aurone **5a**, and the data agreed well with the IC_{50} values of aurone **5a** in Table 2.

Table 4. IC₅₀ values of aurone **5a** in NCI-60 cell line proliferation inhibition assays (Data generated by the National Cancer Institute (Maryland, USA)).

Panel/Cell Line		Panel/Cell Line	
Leukemia	GI ₅₀ (nM)	Melanoma	GI ₅₀ (nM)
CCRG-CEM	289	LOX IMVI	696
HL-60(TB)	236	MALME-3M	> 100 μM
K-562	212	M14	319
MOLT-4	523	MDA-MB-435	174
RPMI-8226	352	SK-MEL-2	836
SR	275	SK-MEL-28	10.2 μM
Non-Small Cell		SK-MEL-5	405
Lung Cancer	GI ₅₀ (nM)	UACC-257	67.1 μM
A549(ATCC)	5.1 μM	UACC-62	499
EKVX	2.73 μM	Ovarian Cancer	
HOP-62	542	IGROV1	774
HOP-92	NA	OVCAR-3	377
NCI-H226	57.4 μM	OVCAR-4	19 μM
NCI-H23	812	OVCAR-5	2.52 μM
NCI-H322M	1.43 μM	OVCAR-8	483
NCI-H460	337	NCI/ADR-RES	406
NCI-H522	3.13 μM	SK-OV-3	669
Colon Cancer		Renal Cancer	
COLO 205	446	786-0	470
HCC-2998	3.44 μM	A498	10.3 μM
HCT-116	386	ACHN	794
HCT-15	399	RXF 393	182
HT29	356	SN 12C	763
KM12	546	TK-10	56.9 μM
SW-620	345	UO-31	864
CNS Cancer		Breast Cancer	
SF-268	848	MCF7	311
SF-295	307	MDA-MB-231	2.66 μM
SF-539	269	HS 578T	360
SNB-19	468	BT-549	571
SNB-75	5.65 μM	T-47D	NA
U251	453	MDA-MB-468	2.16 μM
Prostate Cancer			
PC-3	367		
DU-145	643		

NCI COMPARE analysis was used to explore possible mechanisms of action. The results are summarized in Table 5. The highly ranked compounds were tubulin inhibitors, and this finding first suggested that aurone **5a** was a tubulin inhibitor.

Table 5. Results of the NCI COMPARE analysis.

Rank	Correlation	NCI compounds
1	0.789	NSC S736992
2	0.78	NSC S736359
3	0.769	NSC S31708
4	0.736	NSC S330770
5	0.728	NSC S123528
6	0.728	NSC S650770

Disruption microtubule networks

As described in Chapter 1, tubulins polymerize into microtubules that are key components of the cell cytoskeleton. To test whether aurone **5a** and **5r** affected microtubule networks and cell morphology, studies of immunofluorescence imaging against alpha

tubulin were carried out, and as shown in Figure 4.4, the control, namely DMSO-treated cells, retained their normal microtubule network and an overall, shuttle-like morphology (Figure 4.4 A). On the other hand, aurone **5a** and **5r**-treated cells demonstrated significant microtubule depolymerization and adopted a round morphology (Figure 4.4 B, C, D, E). These results supported, but did not prove, the conclusion that aurone **5a** and **5r** were tubulin inhibitors.

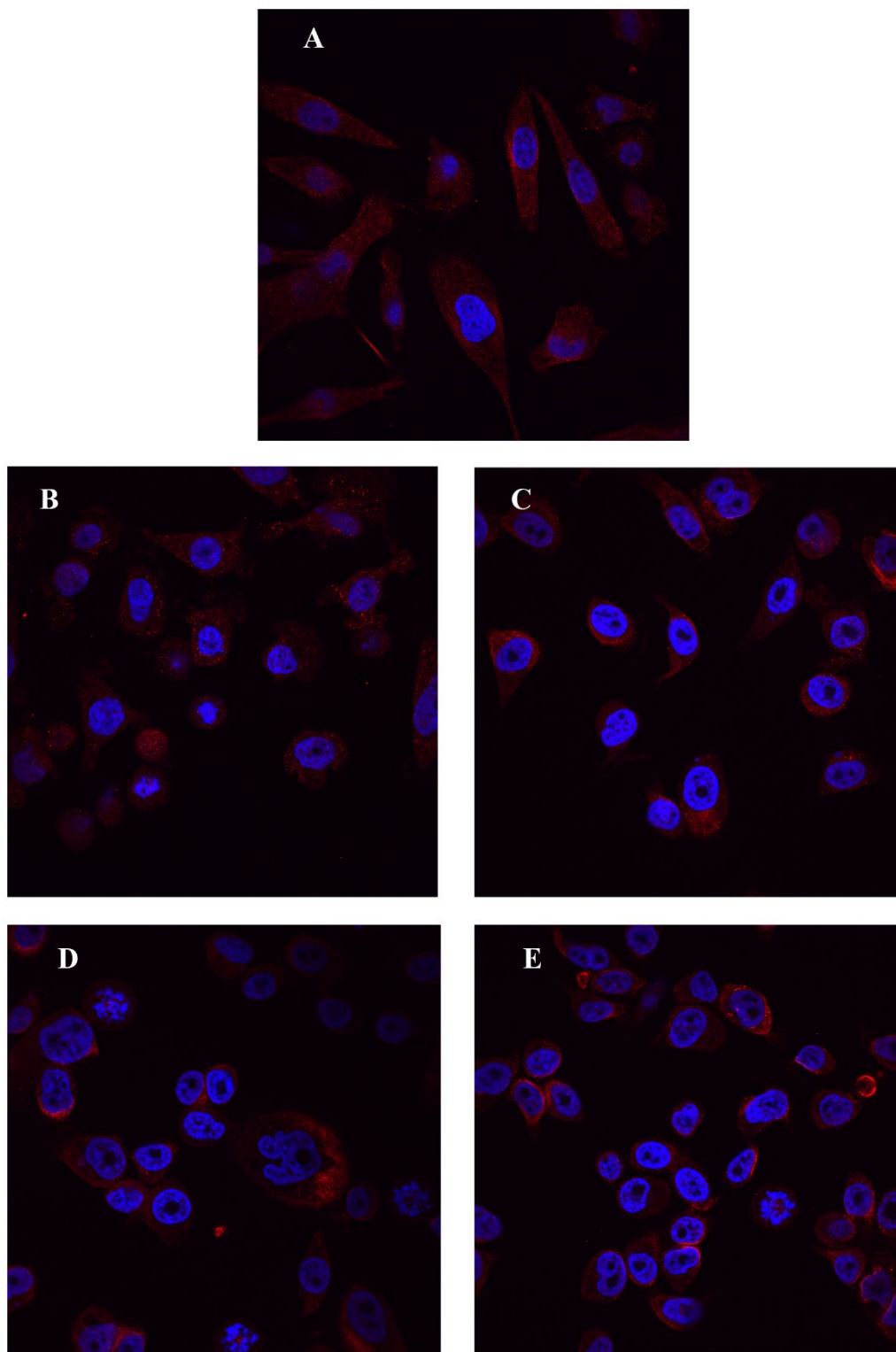


Figure 4.4: Aurone **5a** and **5r** treatment (6 hours) inhibited microtubule structures and caused cell morphology change in PC-3 cells as shown in panels A, DMSO; B, **5a** (1 μM); C, **5a** (300 nM); D, **5r** (1 μM); E, **5r** (300 nM). Red immunofluorescence: α -tubulin; blue: DAPI.

Effects on cell cycle

Because microtubules are the most abundant components of the mitotic spindle, a study of the effect of aurones **5a** and **5r** on cancer cell mitosis was warranted. Treatment of PC-3 cells with aurones **5a** and **5r**, and an analysis of the cell cycle by flow cytometry was performed. Compared to DMSO (Figure 4.5), aurones **5a** and **5r** induced significant cell cycle arrest to G2/M phase. These data again supported that aurones **5a** and **5r** inhibited tubulin polymerization.

Tubulin polymerization in vivo and in vitro

To further test whether aurone **5a** and **5r** were tubulin inhibitors, *in vivo* and *in vitro* tubulin polymerization assays were performed to investigate the level of tubulin polymerization in the presence or absence of aurones **5a** and **5r**.

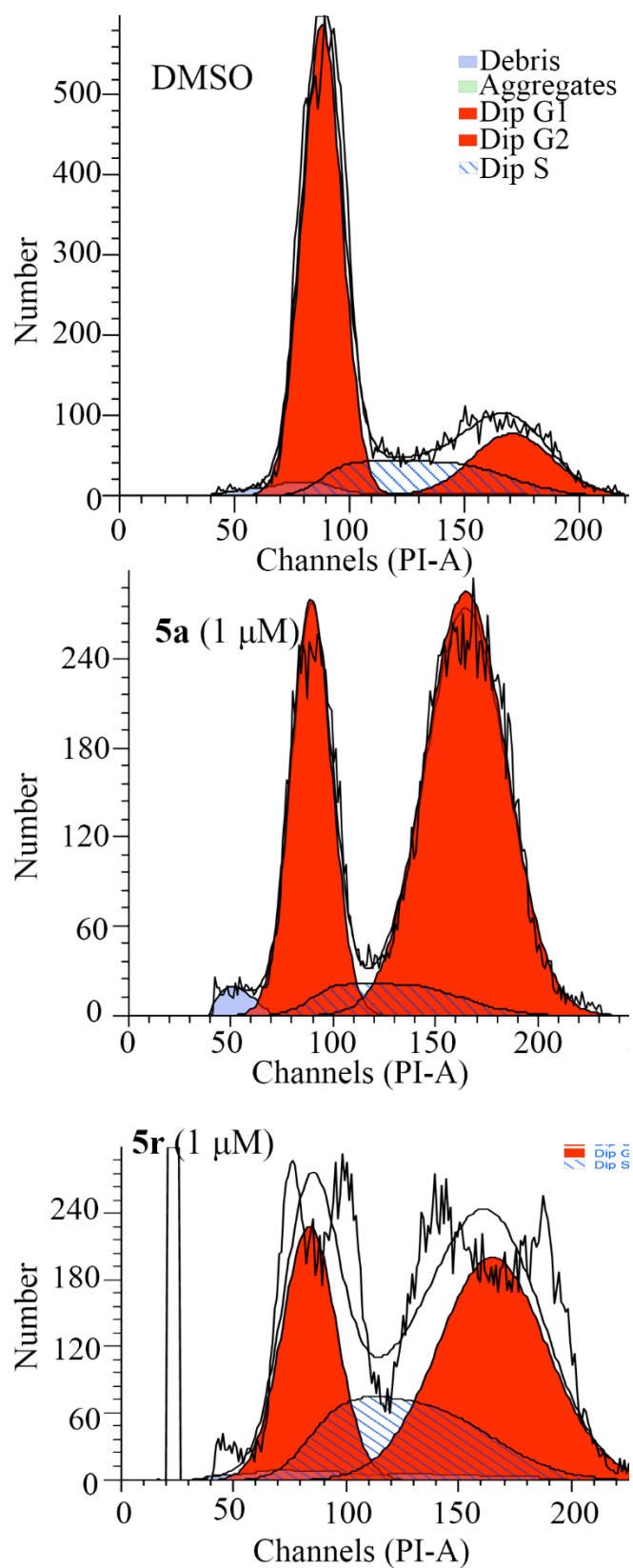


Figure 4.5: Aurones **5a** and **5r** induced cell cycle arrest in PC-3 cells.

For the *in vivo* tubulin polymerization assay, HEK293T cells were treated with aurone **5a** and **5r** at indicated concentrations (Figure 4.6). After cell treatment and lysis, cell lysates were separated by centrifugation into supernatants and pellets, which were individually subjected to western blotting using antibodies against β -tubulin. The idea behind this assay was that microtubules were “heavy” structures that would be in the pellets after centrifugation. After treatment with aurones **5a** and **5r** for 6 hours, the amount of tubulin in pellets was significantly less than that in cell lysates from DMSO-treatment alone, even at a concentration as low as 300 nM (Figure 4.6).

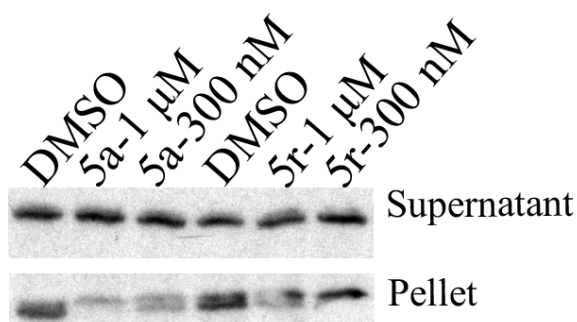


Figure 4.6: Aurones **5a** and **5r** decreased tubulin polymerization in HEK293T cells.

For the *in vitro* tubulin polymerization assay, a well-established tubulin inhibitor, colchicine, was chosen as a positive control. Polymerized microtubules showing absorbance at 340 nm were monitored in the presence of DMSO, colchicine (5 μ M), or aurone **5a** (5 μ M). In the presence of glycerol and guanosine triphosphate, either aurone **5a** at 5 μ M or colchicine at 5 μ M decreased the formation of microtubules in a similar fashion whereas a DMSO-treated control group showed, as expected, substantial tubulin

polymerization (Figure 4.7). Overall, these results were in agreement with the data of the NCI COMPARE analysis, the immunofluorescence imaging, and the cell cycle studies that suggested aurones **5a** and **5r** were tubulin inhibitors.

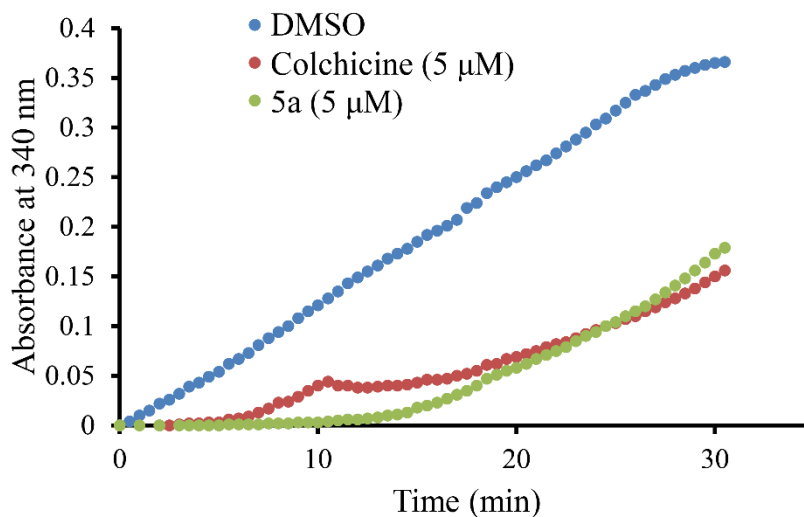


Figure 4.7: Aurone **5a** (5 μM) and colchicine (5 μM) inhibited tubulin polymerization *in vitro* in a similar fashion.

Molecular docking analysis

Molecular docking was performed using AutoDock Vina⁴¹ to explore the possible binding of aurone **5a** to the colchicine-binding site (CBS) on $\alpha\beta$ -tubulin heterodimers because this site was well known to host a plethora of chemically unrelated compounds⁶³. A less active aurone **4d** (Figure 4.8 A) than aurone **5a** and colchicine were also docked into the CBS for comparison. It was found that aurone **5a**, **4d** and colchicine occupied the CBS at the interface of the α -tubulin and β -tubulin heterodimer (Figure 4.8 B). A hydrophobic pocket formed by Ala, Ile and Leu residues from β -tubulin accommodated the hydrophobic indole moiety of aurone **5a** (Figure 4.8 C). The benzofuran-3(2*H*)-one and cyanomethoxy

groups in aurone **5a** participated in hydrophobic contacts with the loop T7 and helix H8 of β -tubulin and with the loops T3, T4 and T5 from α -tubulin (Figure 4.8 C)¹⁴. In addition, hydrogen-bonding interactions between the carbonyl oxygen of the benzofuran-3(2*H*)-one and β Asn258 and hydrogen-bonding interactions between the nitrogen of the cyanomethoxy group and α Tyr224 and α Gln11 provided additional binding stabilization (Figure 4.8 D).

The indole moiety and a portion of the benzofuran-3(2*H*)-one in aurone **5a** superimposed well with the colchicine A and B rings (Figure 4.8 E); however, aurone **5a** did not occupy the hydrophobic pocket within β -tubulin in which the colchicine C ring resided. Instead, aurone **5a** formed contacts with loops T3, T4, and T5 of α -tubulin using the benzofuran-3(2*H*)-one and cyanomethoxy groups. Additionally, a comparison of the binding poses of **5a** and **4d** revealed why **5a** possessed better potency than **4d**. Aurone **4d** had major interactions with β -tubulin but lacked the bifurcated, hydrogen-bonding between the nitrogen of the cyanomethoxy group and α Tyr224 and α Gln11 of α -tubulin. This deficiency weakened the binding affinity of aurone **4d** relative to the potent aurone **5a** (Figure 4.8 D).

Competitive binding assay showed aurones bound to the CBS site

A competitive, tubulin-binding assay⁴² confirmed that aurones **5a** and **5r** bound to the colchicine-binding site. Aurone **5a** or **5r** were added at various concentrations to a solution of α/β -tubulins (1.3 mg/mL) and colchicine (1.25 μ M). Unbound colchicine was separated from either tubulin-colchicine or tubulin-aurone complex by Amicon Ultra-0.5 mL Centrifugal Filters (30 kDa Cut-off). The level of unbound colchicine was measured

by liquid chromatography-electrospray ionization-tandem mass spectrometry (LC-MS/MS). Aurone **5a** and **5r** released colchicine from tubulin in a dose-dependent manner (Figure 4.9) that definitively indicated that aurones **5a** and **5r** bound to the colchicine-binding site on tubulin.

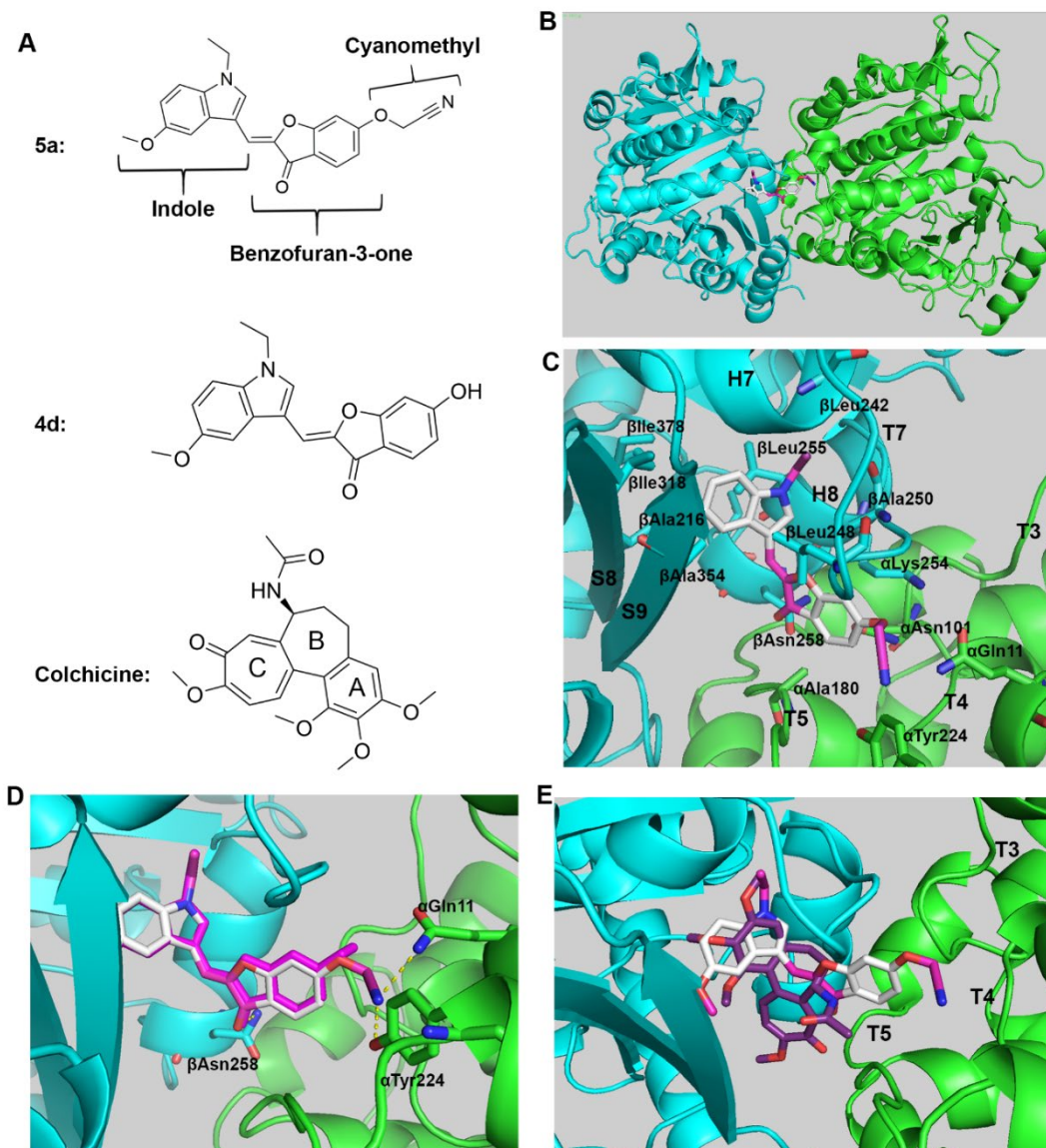


Figure 4.8: (A) Structures of aurone **5a**, aurone **4d**, and colchicine. (B) Aurone **5a** bound to the colchicine-binding site (CBS) in the interface of $\alpha\beta$ -tubulin dimers (cyan for β , green for α). (C) Close-up view of the interaction environment of **5a** (gray sticks) and tubulin (cartoon). (D) Superimposition of **5a** (gray sticks) and **4d** (magenta sticks) in the colchicine-binding site. Hydrogen bonding is represented by yellow, dashed lines. (E) Superimposition of **5a** (gray sticks) and colchicine (purple sticks) in the colchicine-binding site.

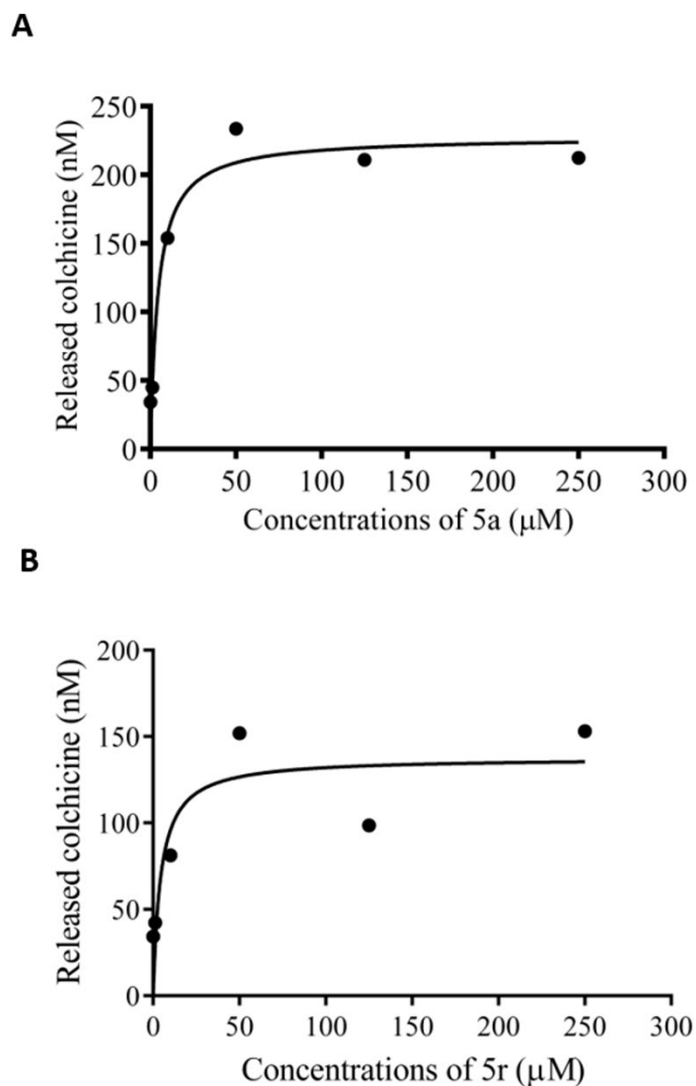


Figure 4.9: Competitive tubulin binding assay with colchicine in the presence of increasing concentrations of aurone **5a** and **5r**.

Synergistic effects of aurones with a cyclin dependent kinase inhibitor

The G2-to-M phase transition in the cell cycle is controlled by cdc2 (cdk1). Cdc2 is tightly regulated by cyclin association and by phosphorylation/dephosphorylation of Tyr 15 of cdc2. Phosphorylation of cdc2 at Tyr15 inactivates cdc2

and leads to mitosis delay, while dephosphorylation of Tyr 15 promotes G2 to M phase transition. Since aurone **5a** arrested cell cycle to G2/M, it is reasonable for cancer cells to dephosphorylate cdc2 at Tyr15 to push G2 to M phase transition as a feedback rescue upon aurone **5a** treatment.

To explore this, colon cancer LS174T cells and prostate cancer PC-3 cells were treated with aurone **5a**, and subject to western blot analysis against cdc2 Tyr15 phosphorylation. Compared with DMSO, aurone **5a** treatment decreased cdc2 Tyr15 phosphorylation (Figure 4.10), which could be explained as a feedback rescue of cancer cells upon aurone **5a** treatment.

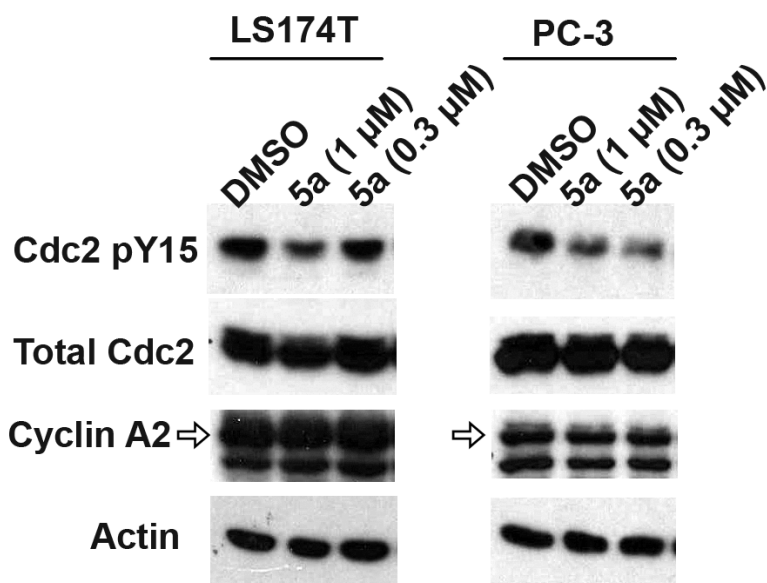


Figure 4.10: Aurone **5a** induced cdc2 (CDK1) activation by decreasing phosphorylation at tyrosine 15.

To confirm this, a cell-permeable and selective ATP-competitive reversible inhibitor of Cdk1, RO3306 was chosen to inhibit this feedback rescue. RO3306 shows preference for Cdk1/cyclin B₁ ($K_i = 35$ nM) over Cdk1/cyclin A ($K_i = 110$ nM), two CDK complexes which regulate cell cycling. LS174T colon and PC3 prostate cancer cells were treated with compounds at indicated combinations and concentrations, and relative cell growth was determined. As shown in figure 4.11, the combination of **5a** and RO3306 showed synergistic effects, indicating that the combination of tubulin inhibitors and cyclin dependent kinase inhibitors can achieve improved antineoplastic effects.

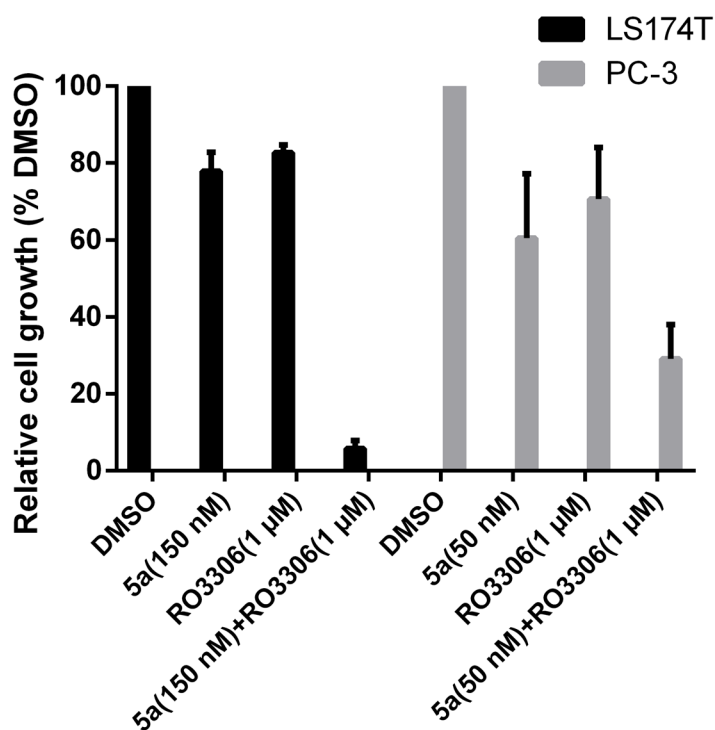


Figure 4.11: Aurone **5a** had synergistic effects with a cdc2 inhibitor RO3306 on the proliferation of LS174T colon and PC3 prostate cancer cells.

hERG inhibition

A frequent side effect of drug candidates is the drug-induced arrhythmia because of blocking the hERG K⁺ channel⁶⁴. The binding between aurones and the hERG K⁺ channel was determined by [³H]-dofetilide binding assays in collaboration with Dr. Linda P. Dwoskin at College of Pharmacy of University of Kentucky. The results showed that none of tested aurones were hERG inhibitors (data not shown).

Discussion

Two types of inhibitors target tubulin microtubule dynamics: stabilizing agents, such as paclitaxel, and destabilizing agents, such as the Vinca alkaloids and colchicine. These agents bind tubulin subunits at well-characterized binding sites, some of which find broad application in cancer therapeutics, including prostate cancer. Until recently, few agents were known that targeted the colchicine-binding site, but various pharmacophores^{10,19,65-69} now appear to exhibit excellent potency and selective binding to the colchicine-tubulin site. The impetus for developing these agents derives in part from the continuing need for new tubulin-targeting drugs to meet the needs of patients experiencing resistance or developing mutations that cripple the use of traditional taxol or Vinca-based therapies. The semisynthetic aurones reported here provide a new pharmacophore for the development of colchicine-targeting microtubule inhibitors for cancer treatment.

The SAR study led to the identification of two potent leading compound aurone **5a** and **5r**. A biotinylated aurone analog **6d** was synthesized and showed inhibitory effect in a PC-3 cell proliferation inhibition assay. However, the pull-down assay using biotinylated aurone analog **6d** did not reveal any potential target. The possible reasons why an active

biotinylated probe did not pull down anything was that the binding site was at the interface of two protein monomers (in our case, tubulin alpha and beta monomers).

Aurone **5a** was submitted to NCI for further testing on the NCI-60 cancer cell line panel. The NCI COMPARE analysis, a computational method for target identification, was chosen to probe the mechanism of action of the leading compound aurone **5a**. The NCI COMPARE analysis suggested that aurone **5a** is a tubulin inhibitor. This finding was confirmed by the *in vivo* and *in vitro* tubulin polymerization assay (Figures 4.6, 4.7). Consistent with this conclusion, aurone **5a** inhibited microtubule formation, disrupted cell cytoskeleton, and changed cell morphology shown by the immunofluorescence imaging studies (Figure 4.4). Similarly, aurone **5a** inhibited the most abundant component of mitotic spindle and arrested the cell cycle to G2/M phase (Figure 4.5).

Knowledge about the binding site between a ligand and its biological target is pivotal for structure-guided, rational design of compounds with improved properties including potency and solubility. Molecular docking studies showed that aurone **5a** binds to the colchicine-binding site between the α -tubulin and β -tubulin. The indole moiety and part of the benzofuran-3-one of aurone **5a** as well as the A and B rings of colchicine occupied a hydrophobic pocket in β -tubulin (Figure 4.8 C, E). However, aurone **5a** did not occupy another hydrophobic pocket in which the colchicine C ring normally resided. Instead, aurone **5a** interacted more with α -tubulin than β -tubulin and participated in bifurcated hydrogen-bonding between the nitrogen of the cyanomethoxy group and α Tyr224 and α Gln11 of α -tubulin (Figure 4.8 D). The relatively inactive aurone **4d** failed to form this same interaction because it lacked a cyanomethyl group.

To confirm that aurone **5a** and **5r** bound to the colchicine-binding site, a competitive tubulin-binding assay⁴² was performed. Aurone **5a** and **5r** bound to the CBS, resulting in an increased amount of unbound colchicine (Figure 4.9). These data were consistent with molecular docking results, and echoed the fact that the CBS would accommodate chemically diverse compounds. Mechanistically, previous crystallography studies show that free tubulin dimers are in a “straight” state and polymerized tubulin dimers in microtubules are in a “curved” conformation^{12,14,70,71}. During tubulin polymerization, tubulin dimers structurally transitioned from a straight state to a curved state, during which the T7 loop of β -tubulin flipped inwards into the CBS. As a mechanism of action, colchicine bound to the CBS, prevented the T7 loop flipping towards the CBS, and thus inhibited tubulin polymerization^{12,16}. Importantly, our leading compounds showed strong interaction with T7 loop (Figure 4.8 C, E) and reflected a similar mechanism of action seen with colchicine. As a result, aurone **5a** strongly inhibited cell cycle progression at G2/M phases (Figure 4.5) and disrupted microtubule networks in PC-3 cells (Figure 4.4).

In cell cycle, G2 to M phase transition is controlled by cdc2 (cdk1), which is tightly regulated by association with different kinds of cyclins, phosphorylation status of Tyr 15 of cdc2. Phosphorylation of cdc2 at Tyr15 inactivates cdc2 and leads to mitosis delay, while dephosphorylation of Tyr 15 promotes G2 to M phase transition. Aurone **5a** induced dephosphorylation of Tyr 15 and activated cdc2 (Figure 4.10), which could be explained as a feedback rescue under aurone **5a** treatment. Cdc2 can be inhibited by RO3306, a cell-permeable and selective ATP-competitive reversible inhibitor. Synergistic effects between RO3306 and aurone **5a** were observed (Figure 4.11), which provided molecular basis for

combination usage of tubulin inhibitors and cyclin dependent kinase inhibitors for better antineoplastic effects.

Chapter 5 *In vivo* evaluation of the antineoplastic activity of aurones

Introduction

Tubulins are a well-known, valid drug target in oncology, and four small-molecule binding sites in tubulins have been discovered to modulate the tubulin microtubule dynamics⁷². Representative molecules that bind to the four unique sites in tubulins include paclitaxel, Vinca alkaloids, colchicine, and laulimalide. Several tubulin inhibitors including taxanes and vinorelbine gained FDA approval for cancer chemotherapy¹⁵. Despite the fact that a large number of molecules that bind to the colchicine binding site (CBS) were identified, there is no FDA approved tubulin inhibitors targeting the CBS¹⁵.

A major obstacle of tubulin inhibitors as chemotherapy is the neurological toxicity induced by these agents⁷³, and consequently, the dosing regimen for tubulin inhibitors that target the CBS are crucial to avoid potential, unwanted neuropathy. Fortunately, our leading compound, aurone **5a**, possessed subnanomolar potency against cancer cells but showed an IC₅₀ in the micromolar range ($1.3 \pm 0.2 \mu\text{M}$) against a normal human embryo lung cell line HEL299, a finding that suggested aurone **5a** was selectively toxic to cancer cell lines rather than normal cell lines and was a suitable candidate for further *in vivo* studies.

Although our studies focused on developing agents for the treatment of prostate cancers, the prior report that aurones with 2-(coumarin-4-yl)methylene groups⁷⁴ or 2-(furan-2-yl)methylene groups⁷⁵ displayed *in vitro* activity against human leukemia K562 cells prompted a study of myc-induced T-cell acute lymphoblastic leukemia (T-ALL) in a

zebrafish model. Before testing aurone **5a** *in vivo*, several leukemia cell lines were treated with **5a** to assure that **5a** is effective for leukemia.

Results

Mouse xenograft model

The *in vivo* tumor inhibitory effect of aurone **5a** using prostate cancer PC-3 xenografts in immune-defective nude mice. PC-3 cells were subcutaneously injected into both flanks of nude mice. Two weeks after the inoculation, the mice were randomized to two groups (n=5), treated with aurone **5a** or control vehicle by intraperitoneal administration for about 3 weeks and then sacrificed. Compared to vehicle, the administration of **5a** at a low dose of 10 mg/kg/day showed significant, tumor-growth

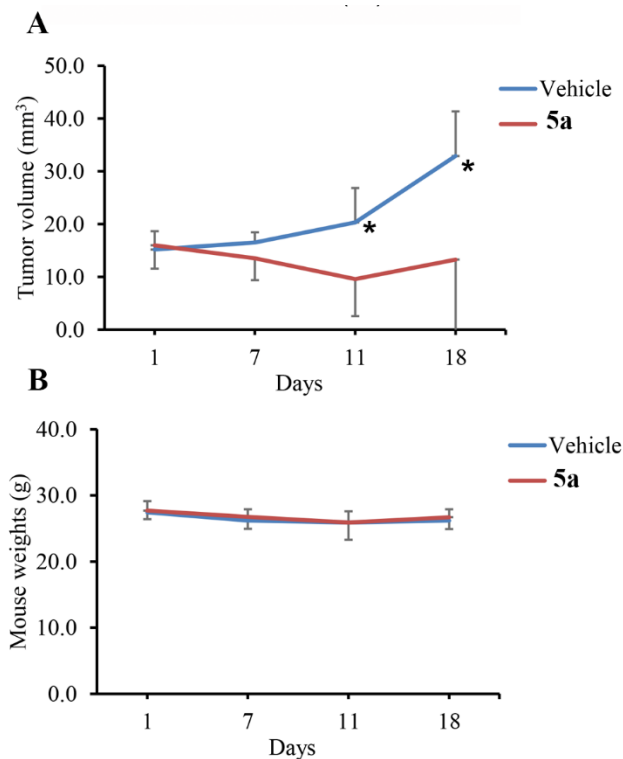


Figure 5.1: (A) Effects of aurone **5a** on PC-3 tumor xenografts in nude mice (n=5) at 10 mg/kg/day. (B) Effect on aurone **5a** on body weights of the treated mice: * $p < 0.05$, t-test.

suppression (Figure 5.1A). Importantly, aurone **5a** achieved tumor regression with no apparent gross toxicity as reflected by minimal changes in mice weights (Figure 5.1B).

Effects on leukemia cells and T-ALL

In addition to the *in vivo* PC-3 xenograft study in mice, we sought to test these aurones in a second species. Two prior reports indicated that aurones with 2-(coumarin-4-yl)methylene groups or 2-(furan-2-yl)methylene groups displayed *in vitro* activity against a leukemia cell line. Consequently, we tested various leukemia cell lines and found that the IC₅₀ values for aurone **5a** were in the mid-nanomolar range (**Table 6**). The IC₅₀ values of two normal B-lymphoblast cells were much higher than the leukemia cell lines and suggested a preferential toxicity of aurone **5a** toward leukemia cells.

Table 6. IC₅₀ values of aurone **5a** in leukemia cell line proliferation inhibition assays.

Cell Line	Cell Type	IC ₅₀ (nM)	95% Confidence Interval (nM)
CCRF-CEM	T-ALL	244	197-301
DND41	T-ALL	210	116-379
Jurkat	T-ALL	273	226-344
HBP-ALL	T-ALL	94	51-173
Loucy	T-ALL	334	285-391
Molt-4	T-ALL	241	114-402
Molt-16	T-ALL	234	218-250
RPMI8402	T-ALL	301	248-364
Nalm-16	B-ALL	272	248-291
REH	B-ALL	287	252-326
NCI-BL2009	Normal B-Lymphoblast	1,253	429-3,658
HCC1007-BL	Normal B-Lymphoblast	1,379	372-2,490

Because these leukemia cell lines had various mutations, we tested the activity of aurone **5a** *in vivo* using a genetically well-defined, zebrafish myc-induced T-ALL leukemia model^{76,77}. The zebrafish (*Danio rerio*) is a vertebrate system that develops tumors similar to those in humans and that provides a platform that is easy to manipulate for *in vivo* assays even in large-scale screens. According to previous studies^{76,77}, the zebrafish *Rag2* promoter controlling the *myc-GFP* transgene specifically targets gene expression to lymphoid cells. The *Rag2: myc-GFP* transgene was micro-injected into wild-type zebrafish embryos at the one-cell development stage, and a small fraction of injected embryos developed *c-myc* induced leukemia. GFP-labeled leukemia cells in zebrafish were treated with either DMSO (Figure 5.2A at day 0 and Figure 5.2D at day 5); aurone **5a** in DMSO (Figure 5.2B at day 0 and Figure 5.2E at day 5); or aurone **5r** in DMSO (Figure 5.2C at day 0 and Figure 5.2F at day 5). Since aurone **5a** had auto-fluorescence that interfered with visualizing the loss

of the GFP-labeled leukemia cells (Figure 5.2E), we selected aurone **5r** that lacked this auto-fluorescence and clearly displayed the loss of the GFP-labeled leukemia cells (Figure 5.2F). Aurone **5a** and **5r** significantly blocked the progression of T-ALL in zebrafish (Figure 5.2D *versus* Figure 5.2F, Figure 5.2G).

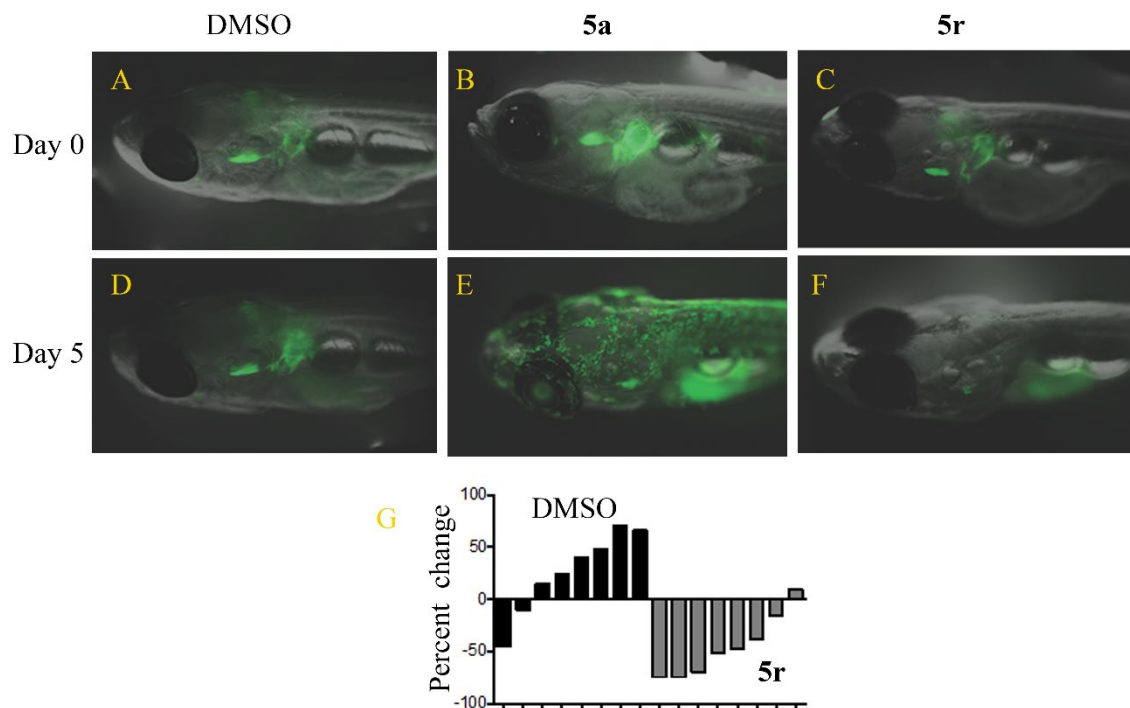


Figure 5.2: Aurones **5a** and **5r** inhibited myc-induce T-ALL in a zebrafish model. (A and D) Treatment of GFP-labeled thymic lymphoma cells with DMSO alone at day 0 and day 5, respectively. (B and E) Treatment of GFP-labeled thymic lymphoma cells with aurone **5a** in DMSO at day 0 and day 5, respectively. (C and F) Treatment of GFP-labeled thymic lymphoma cells with aurone **5r** at day 0 and day 5, respectively. (G) Percent change in fluorescence (*i.e.*, number of GFP-labeled thymic lymphoma cells) as a function of time from administration of DMSO alone to the administration of aurone **5r** in each zebrafish (n=8).

Discussion

The *in vitro* studies led to the identification of inhibiting tubulin polymerization as the mechanism of action of aurone **5a** and consequently the *in vivo* tumor inhibitory effects of aurone **5a** using prostate cancer PC-3 xenografts in immune-defective nude mice was evaluated. Compared to vehicle, the administration of aurone **5a** at a low dose of 10 mg/kg/day for 18 days showed significant, tumor-growth suppression (Figure 5.1A). Importantly, aurone **5a** achieved tumor regression with no apparent gross toxicity as reflected by minimal changes in mice weights (Figure 5.1B).

In addition to the *in vivo* PC-3 xenograft study in mice, we validated the *in vivo* anti-tumor efforts of these aurones in a second species. Because aurone **5a** showed nanomolar potency on several leukemia cell lines, we used a zebrafish T-ALL model to test these aurones. The zebrafish (*Danio rerio*) is a vertebrate system that develops tumors similar to those in humans and that provides a platform that is easy to manipulate for *in vivo* assays even in large-scale screens. No gross toxicity on zebrafish but significant inhibition of myc-induced T-ALL *in vivo* was observed (Figure 5.2). The zebrafish myc-induced T-ALL model could be an important *in vivo* tool to screen and characterize future aurone analogs. Overall, these *in vivo* data confirmed anti-tumor efficacy of aurones **5a** and **5r** *in vivo*, suggesting **5a** and **5r** could be potential chemotherapy drug candidates.

Chapter 6 Conclusions and future directions

Conclusions

Nature is the best chemist in terms of manipulating enzymes to make molecules necessary to sustain life processes. This evolutionary outcome provides an abundant reservoir of diverse chemical scaffolds that serve as departure points for drug discovery. A survey looking at natural products as sources of new drugs from 1981 to 2014 found that over 60% of current drugs are related to natural compounds⁷⁸. This project started from a less-distributed and less-studied flavone possessing the aurone scaffold³⁰, and we successfully identified potential drug candidates for cancer chemotherapy.

To generate these new aurone analogs, modifications were made on both C-6 and C-2 positions of benzofuran-3(2*H*)-one. Cell proliferation assays using PC-3 cells were carried out to determine the relative proliferation inhibition for new aurones compared to the vehicle control DMSO. Heterocyclic-substituted phenylmethylene groups or heteroarylmethylene groups were attached at C-2, and the C-6 position was modified with halogenated benzyls or cyanomethyl. Two candidates, (*Z*)-2-((2-((1-ethyl-5-methoxy-1*H*-indol-3-yl)methylene)-3-oxo-2,3-dihydrobenzofuran-6-yl)oxy)acetonitrile (**5a**) and (*Z*)-6-((2,6-dichlorobenzyl)oxy)-2-(pyridin-4-ylmethylene)benzofuran-3(2*H*)-one (**5r**), showed nanomolar potencies towards a panel of cancer cell lines.

One of the possible reasons why most published aurone analogs lack a clear mechanism of action is low potency. With the potent aurones **5a** and **5r** in hand, the combination of NCI-60 cell line panel assay and the NCI COMPARE analysis suggested that the biological target of aurone **5a** was tubulin. *In vivo* and *in vitro* tubulin polymerization assays confirmed that aurone **5a** inhibited tubulin polymerization. Because

microtubules are key components of cell cytoskeleton and mitotic spindle, aurone **5a** treatment resulted in abnormal cell morphology and cell cycle arrest at G2/M phases. These results further confirmed that tubulin was the biological target of aurone **5a**.

The colchicine-binding site resides at the interfaces of $\alpha\beta$ tubulins and binds a set of structurally diverse molecules. Molecular docking of aurone **5a**, a less active aurone **4d**, and a well-known CBS binder colchicine to the CBS revealed key interactions between aurone **5a** and $\alpha\beta$ tubulins. To confirm the binding site, a competitive binding assay in which aurone **5a** with increasing concentrations competed with fixed amount of colchicine for binding to the CBS was performed. Aurone **5a** resulted in decreased binding between tubulins and colchicine, showing that aurone **5a** is a CBS binder.

One interesting finding during the course of target identification was the synergistic effects between aurone **5a** and Cdk1 inhibitor RO3306. In cell cycle, the G2-to-M phase transition is controlled by cdc2 (cdk1). Cdc2 is tightly regulated by cyclin association and phosphorylation of Tyr 15 of cdc2. Phosphorylation of cdc2 at Tyr15 inactivates cdc2 and leads to mitosis delay, while dephosphorylation of Tyr 15 promotes G2 to M phase transition. Mechanistically, since aurone **5a** arrested cell cycle to G2/M, it's reasonable for cancer cells to dephosphorylate cdc2 at Tyr15 to push G2 to M phase transition as a feedback rescue upon aurone **5a** treatment. RO3306 inhibits cdc2 and the feedback rescue, thus showing synergistic effects with aurone **5a**.

The *in vivo* anti-tumor effects were confirmed in PC-3 mouse xenograft model and leukemia T-ALL zebrafish model. Compared to vehicle, the administration of aurone **5a** at 10 mg/kg/day showed significant tumor suppression. Importantly, aurone **5a** achieved tumor regression with no apparent gross toxicity as reflected by minimal changes in mice

weights. Because aurone **5a** possesses auto-fluorescence, the equally potent aurone **5r** was used in the zebrafish study and showed significant tumor growth inhibition.

Finally, aurone **5a** was selectively toxic for cancer cells, and was not a substrate of the hERG K⁺ channel and the P-glycoprotein that causing drug resistance. Considering that so far no colchicine-site binders have been approved by the FDA, aurone **5a** with strong potency, clear mechanism of action and *in vivo* anti-tumor efficacy could be a potential novel chemotherapy drug candidate as a colchicine-site binder.

Future directions

The pharmacokinetics of our aurones requires exploration. Bioavailability of the current leading aurone analogs is unknown. Determining the half-life and metabolites of aurones *in vivo* is a necessary next step in their potential development. How aurones are excreted from the body warrants further examination.

The solubility of current leading candidates requires further improvement and will probably require the synthesis of additional aurone analogs or the development of drug formulations such liposomes and nanoparticles.

Although molecular docking and competitive binding assay show that the leading two aurone analogs bind to the colchicine binding site of tubulins, how aurones and this binding pocket interact with each other is unknown. Co-crystallizing aurones and tubulins could potentially answer this question and allows the identification of critical amino acids residing the binding pocket that interact with aurones. This knowledge would provide information for rational design of next generation aurone analogs with improved potency and solubility.

Finally, while the drug combination with RO3306 is effective in tumor cell lines, it will be necessary to evaluate this combination *in vivo*. There are other FDA-approved cell cycle inhibitors such as Palbociclib (PD-0332991) (inhibitor of CDK4 and CDK6). It's interesting to test how these FDA-approved cell cycle inhibitors affect the activity of leading aurone candidates *in vivo*.

APPENDIX A: Abbreviations

CBS - colchicine binding site
CDK - cyclin dependent kinase
CRISPR - clustered regularly interspaced short palindromic repeats
DAPI - 4', 6-diamidino-2-phenylindole
DCM – dichloromethane
DMF - *N,N*-dimethylformamide
DMSO - dimethyl sulfoxide
EDC - *N*-(3-Dimethylaminopropyl)-*N'*-ethylcarbodiimide
EDTA - Ethylenediaminetetraacetic acid
EGFR - epidermal growth factor receptor
EGTA - ethylene glycol-bis(β -aminoethyl ether)
FDA - Food and Drug Administration
GDP - Guanosine diphosphate
GFP - green fluorescence protein
GTP - Guanosine triphosphate
HBSS - Hank's balanced salt solution
HESI - heated electrospray ionization
LC-MS/MS - liquid chromatography electrospray ionization tandem mass spectrometry
NCI - National Cancer Institute
NSCLC - Non-Small Cell Lung Cancer
PBS - phosphate-buffered saline
PI - propidium iodide
PIPES - piperazine-*N,N'*-bis(2-ethanesulfonic acid)
PMSF - phenylmethylsulfonyl fluoride
SDS-PAGE - sodium dodecyl sulfate polyacrylamide gel electrophoresis
siRNA - small interfering RNA

T-ALL - T-cell acute lymphoblastic leukemia

TKI - tyrosine kinase inhibitors

APPENDIX B: Collaborations

Several of my colleagues made contributions to this aurone project. Liliia M. Kril synthesized compounds **3a-f**. Mykhaylo S. Frasinuk synthesized **4a-l** and **5d-5r**. Vitaliy M. Sviripa characterized compounds **3a-f**, **4a-l** and **5d-5r**. Agripina Deaciuc performed hERG assay. Jing Chen run LC-MS/MS and Elizabeth Hausman did zebrafish study. I appreciate their input and welcomed their authorship in our recent publication in *Scientific Reports* (2019).

REFERENCES

- 1 McGuire, S. World Cancer Report 2014. Geneva, Switzerland: World Health Organization, International Agency for Research on Cancer, WHO Press, 2015. *Adv Nutr* **7**, 418-419, doi:10.3945/an.116.012211 (2016).
- 2 Mariotto, A. B., Yabroff, K. R., Shao, Y., Feuer, E. J. & Brown, M. L. Projections of the cost of cancer care in the United States: 2010-2020. *Journal of the National Cancer Institute* **103**, 117-128, doi:10.1093/jnci/djq495 (2011).
- 3 Scaltriti, M. & Baselga, J. The epidermal growth factor receptor pathway: a model for targeted therapy. *Clin Cancer Res* **12**, 5268-5272, doi:10.1158/1078-0432.CCR-05-1554 (2006).
- 4 Takezawa, K. *et al.* HER2 amplification: a potential mechanism of acquired resistance to EGFR inhibition in EGFR-mutant lung cancers that lack the second-site EGFR T790M mutation. *Cancer Discov* **2**, 922-933, doi:10.1158/2159-8290.CD-12-0108 (2012).
- 5 Zhou, W. *et al.* Novel mutant-selective EGFR kinase inhibitors against EGFR T790M. *Nature* **462**, 1070-1074, doi:10.1038/nature08622 (2009).
- 6 Walter, A. O. *et al.* Discovery of a mutant-selective covalent inhibitor of EGFR that overcomes T790M-mediated resistance in NSCLC. *Cancer Discov* **3**, 1404-1415, doi:10.1158/2159-8290.CD-13-0314 (2013).
- 7 Patel, H., Pawara, R., Ansari, A. & Surana, S. Recent updates on third generation EGFR inhibitors and emergence of fourth generation EGFR inhibitors to combat C797S resistance. *Eur J Med Chem* **142**, 32-47, doi:10.1016/j.ejmech.2017.05.027 (2017).
- 8 Jia, Y. *et al.* Overcoming EGFR(T790M) and EGFR(C797S) resistance with mutant-selective allosteric inhibitors. *Nature* **534**, 129-132, doi:10.1038/nature17960 (2016).
- 9 Andrews, A. Treating with Checkpoint Inhibitors-Figure \$1 Million per Patient. *Am Health Drug Benefits* **8**, 9 (2015).
- 10 Dumontet, C. & Jordan, M. A. Microtubule-binding agents: a dynamic field of cancer therapeutics. *Nat Rev Drug Discov* **9**, 790-803, doi:10.1038/nrd3253 (2010).
- 11 Jordan, M. A. & Wilson, L. Microtubules as a target for anticancer drugs. *Nat Rev Cancer* **4**, 253-265, doi:10.1038/nrc1317 (2004).
- 12 Ravelli, R. B. *et al.* Insight into tubulin regulation from a complex with colchicine and a stathmin-like domain. *Nature* **428**, 198-202, doi:10.1038/nature02393 (2004).
- 13 Vandecandelaere, A., Brune, M., Webb, M. R., Martin, S. R. & Bayley, P. M. Phosphate release during microtubule assembly: what stabilizes growing microtubules? *Biochemistry* **38**, 8179-8188, doi:10.1021/bi9830765 (1999).
- 14 Lowe, J., Li, H., Downing, K. H. & Nogales, E. Refined structure of alpha beta-tubulin at 3.5 Å resolution. *J Mol Biol* **313**, 1045-1057, doi:10.1006/jmbi.2001.5077 (2001).
- 15 Wu, X., Wang, Q. & Li, W. Recent Advances in Heterocyclic Tubulin Inhibitors Targeting the Colchicine Binding Site. *Anticancer Agents Med Chem* **16**, 1325-1338 (2016).

- 16 Dorleans, A. *et al.* Variations in the colchicine-binding domain provide insight into the structural switch of tubulin. *Proc Natl Acad Sci U S A* **106**, 13775-13779, doi:10.1073/pnas.0904223106 (2009).
- 17 Kavallaris, M. Microtubules and resistance to tubulin-binding agents. *Nat Rev Cancer* **10**, 194-204, doi:10.1038/nrc2803 (2010).
- 18 Perez, E. A. Microtubule inhibitors: Differentiating tubulin-inhibiting agents based on mechanisms of action, clinical activity, and resistance. *Mol Cancer Ther* **8**, 2086-2095, doi:10.1158/1535-7163.MCT-09-0366 (2009).
- 19 Lu, Y., Chen, J., Xiao, M., Li, W. & Miller, D. D. An overview of tubulin inhibitors that interact with the colchicine binding site. *Pharm Res* **29**, 2943-2971, doi:10.1007/s11095-012-0828-z (2012).
- 20 <https://www.drugs.com/monograph/vinblastine-sulfate.html>.
- 21 Shekelle, P. G. *et al.* Management of Gout: A Systematic Review in Support of an American College of Physicians Clinical Practice Guideline. *Ann Intern Med* **166**, 37-51, doi:10.7326/M16-0461 (2017).
- 22 <https://clinicaltrials.gov/ct2/results?term=CA4P&Search=Search>.
- 23 Seve, P. *et al.* Expression of class III {beta}-tubulin is predictive of patient outcome in patients with non-small cell lung cancer receiving vinorelbine-based chemotherapy. *Clin Cancer Res* **11**, 5481-5486, doi:10.1158/1078-0432.CCR-05-0285 (2005).
- 24 Kamath, K., Wilson, L., Cabral, F. & Jordan, M. A. BetaIII-tubulin induces paclitaxel resistance in association with reduced effects on microtubule dynamic instability. *J Biol Chem* **280**, 12902-12907, doi:10.1074/jbc.M414477200 (2005).
- 25 Alli, E., Bash-Babula, J., Yang, J. M. & Hait, W. N. Effect of stathmin on the sensitivity to antimicrotubule drugs in human breast cancer. *Cancer Res* **62**, 6864-6869 (2002).
- 26 Zhang, C. C. *et al.* The role of MAP4 expression in the sensitivity to paclitaxel and resistance to vinca alkaloids in p53 mutant cells. *Oncogene* **16**, 1617-1624, doi:10.1038/sj.onc.1201658 (1998).
- 27 Vogt, T. Phenylpropanoid biosynthesis. *Mol Plant* **3**, 2-20, doi:10.1093/mp/ssp106 (2010).
- 28 Nakayama, T. Enzymology of aurone biosynthesis. *J Biosci Bioeng* **94**, 487-491 (2002).
- 29 Nakayama, T. *et al.* Specificity analysis and mechanism of aurone synthesis catalyzed by aureusidin synthase, a polyphenol oxidase homolog responsible for flower coloration. *FEBS Lett* **499**, 107-111 (2001).
- 30 Boumendjel, A. Aurones: a subclass of flavones with promising biological potential. *Curr Med Chem* **10**, 2621-2630 (2003).
- 31 Zwergel, C. *et al.* Aurones: interesting natural and synthetic compounds with emerging biological potential. *Nat Prod Commun* **7**, 389-394 (2012).
- 32 Amin, M. L. P-glycoprotein Inhibition for Optimal Drug Delivery. *Drug Target Insights* **7**, 27-34, doi:10.4137/DTI.S12519 (2013).
- 33 Boumendjel, A. *et al.* 4-Hydroxy-6-methoxyaurones with high-affinity binding to cytosolic domain of P-glycoprotein. *Chem Pharm Bull (Tokyo)* **50**, 854-856 (2002).

- 34 Asghar, U., Witkiewicz, A. K., Turner, N. C. & Knudsen, E. S. The history and future of targeting cyclin-dependent kinases in cancer therapy. *Nat Rev Drug Discov* **14**, 130-146, doi:10.1038/nrd4504 (2015).
- 35 <https://www.ascopost.com/News/16151>. (2014).
- 36 Schoepfer, J. *et al.* Structure-based design and synthesis of 2-benzylidenebenzofuran-3-ones as flavopiridol mimics. *J Med Chem* **45**, 1741-1747 (2002).
- 37 Ait-Aissa, K., Ebben, J. D., Kadlec, A. O. & Beyer, A. M. Friend or foe? Telomerase as a pharmacological target in cancer and cardiovascular disease. *Pharmacol Res* **111**, 422-433, doi:10.1016/j.phrs.2016.07.003 (2016).
- 38 Bursavich, M. G. *et al.* Novel benzofuran-3-one indole inhibitors of PI3 kinase-alpha and the mammalian target of rapamycin: hit to lead studies. *Bioorg Med Chem Lett* **20**, 2586-2590, doi:10.1016/j.bmcl.2010.02.082 (2010).
- 39 Nesterenko, M. V., Tilley, M. & Upton, S. J. A simple modification of Blum's silver stain method allows for 30 minute detection of proteins in polyacrylamide gels. *J Biochem Biophys Methods* **28**, 239-242 (1994).
- 40 Zhang, W. *et al.* Fluorinated N,N-dialkylaminostilbenes repress colon cancer by targeting methionine S-adenosyltransferase 2A. *ACS chemical biology* **8**, 796-803, doi:10.1021/cb3005353 (2013).
- 41 Trott, O. & Olson, A. J. AutoDock Vina: improving the speed and accuracy of docking with a new scoring function, efficient optimization, and multithreading. *J Comput Chem* **31**, 455-461, doi:10.1002/jcc.21334 (2010).
- 42 Li, C. M. *et al.* Competitive mass spectrometry binding assay for characterization of three binding sites of tubulin. *J Mass Spectrom* **45**, 1160-1166, doi:10.1002/jms.1804 (2010).
- 43 Greengrass, P. M. S., M.; Wood, C.M. Affinity-assay for the human ERG potassium channel. (2003).
- 44 Jo, S. H., Youm, J. B., Lee, C. O., Earm, Y. E. & Ho, W. K. Blockade of the HERG human cardiac K(+) channel by the antidepressant drug amitriptyline. *Br J Pharmacol* **129**, 1474-1480, doi:10.1038/sj.bjp.0703222 (2000).
- 45 Chen, T. *A Practical Guide to Assay Development and High-throughput Screening in Drug Discovery*. (CRC Press Taylor and Francis Group, 2010).
- 46 Zwergel, C. V., S.; Salvato, A.; Xu, Z.; Talhi, O.; Mai, A.; Silva, A.; Altucci, L.; Kirsch, G. Novel benzofuran-chromone and -coumarin derivatives: synthesis and biological activity in K562 human leukemia cells. *Med. Chem. Commun.* **4**, 1571-1579 (2013).
- 47 Guo, Q. N. L., L.; Zhou, Y.; Yu, P.; Teng, Y. Design, synthesis and biological evaluation of the novel antitumor agent aurone derivatives. *Ad. Mat. Res.* **781-784**, 1235-1239 (2013).
- 48 Huang, W., Liu, M. Z., Li, Y., Tan, Y. & Yang, G. F. Design, syntheses, and antitumor activity of novel chromone and aurone derivatives. *Bioorg Med Chem* **15**, 5191-5197, doi:10.1016/j.bmc.2007.05.022 (2007).
- 49 Pathak, N. P., J. Design and synthesis of indole integrated aurones as potent anti breast cancer agents. *Ind. J. App. Res.* **6**, 800-802 (2016).
- 50 Hastings, J. & Heller, H. The stereochemistry of aurones [2-substituted benzylidenebenzofuran-3 (2 H)-ones]. *Journal of the Chemical Society, Perkin Transactions 1*, 2128-2132 (1972).

- 51 Jagtap, S. V. K., A.A. Synthesis and biological activities of aurones: A review. *Int. J. Pure App. Biosci.* **4**, 137-155 (2016).
- 52 Zheng, X. W., H.; Liu, Y.-M.; Yao, X.; Tong, M.; Wang, Y.-H.; Liao, D.-F. Synthesis, characterization and anticancer effect of trifluoromethylated aurone derivatives. *J. Heterocyclic Chem.* **52**, 296-301 (2015).
- 53 Chen, H. Q., X.-D.; Qui, P. . A novel synthesis of aurones: Their in vitro anticancer activity against breast cancer cell lines and effect on cell cycle, apoptosis and mitochondrial membrane potential. *Bangladesh J. Pharmacol.* **9**, 501-510 (2014).
- 54 Okombi, S. *et al.* Discovery of benzylidenebenzofuran-3(2H)-one (aurones) as inhibitors of tyrosinase derived from human melanocytes. *J Med Chem* **49**, 329-333, doi:10.1021/jm050715i (2006).
- 55 Lee, C. Y., Chew, E. H. & Go, M. L. Functionalized aurones as inducers of NAD(P)H:quinone oxidoreductase 1 that activate AhR/XRE and Nrf2/ARE signaling pathways: synthesis, evaluation and SAR. *Eur J Med Chem* **45**, 2957-2971, doi:10.1016/j.ejmech.2010.03.023 (2010).
- 56 Haudecoeur, R. *et al.* Discovery of naturally occurring aurones that are potent allosteric inhibitors of hepatitis C virus RNA-dependent RNA polymerase. *J Med Chem* **54**, 5395-5402, doi:10.1021/jm200242p (2011).
- 57 Sheng, R. *et al.* Design, synthesis and AChE inhibitory activity of indanone and aurone derivatives. *Eur J Med Chem* **44**, 7-17, doi:10.1016/j.ejmech.2008.03.003 (2009).
- 58 King, T. J., Hastings, J. S. & Heller, H. G. X-Ray analysis of (Z)-2-p-methoxyphenylmethylenebenzofuran-3 (2 H)-one. *Journal of the Chemical Society, Perkin Transactions 1*, 1455-1457 (1975).
- 59 Schenone, M., Dancik, V., Wagner, B. K. & Clemons, P. A. Target identification and mechanism of action in chemical biology and drug discovery. *Nat Chem Biol* **9**, 232-240, doi:10.1038/nchembio.1199 (2013).
- 60 Boutros, M. & Ahringer, J. The art and design of genetic screens: RNA interference. *Nat Rev Genet* **9**, 554-566, doi:10.1038/nrg2364 (2008).
- 61 Kasap, C., Elemento, O. & Kapoor, T. M. DrugTargetSeqR: a genomics- and CRISPR-Cas9-based method to analyze drug targets. *Nat Chem Biol* **10**, 626-628, doi:10.1038/nchembio.1551 (2014).
- 62 Paull, K. D. *et al.* Display and analysis of patterns of differential activity of drugs against human tumor cell lines: development of mean graph and COMPARE algorithm. *Journal of the National Cancer Institute* **81**, 1088-1092 (1989).
- 63 Sanghai, N. *et al.* Combretastatin A-4 inspired novel 2-aryl-3-arylamino-imidazo-pyridines/pyrazines as tubulin polymerization inhibitors, antimetabolic and anticancer agents. *MedChemComm* **5**, 766-782 (2014).
- 64 Yu, Z., AP, I. J. & Heitman, L. H. Kv 11.1 (hERG)-induced cardiotoxicity: a molecular insight from a binding kinetics study of prototypical Kv 11.1 (hERG) inhibitors. *Br J Pharmacol* **172**, 940-955, doi:10.1111/bph.12967 (2015).
- 65 Dong, M., Liu, F., Zhou, H., Zhai, S. & Yan, B. Novel Natural Product- and Privileged Scaffold-Based Tubulin Inhibitors Targeting the Colchicine Binding Site. *Molecules* **21**, doi:10.3390/molecules21101375 (2016).

- 66 Li, W., Sun, H., Xu, S., Zhu, Z. & Xu, J. Tubulin inhibitors targeting the colchicine binding site: a perspective of privileged structures. *Future Med Chem* **9**, 1765-1794, doi:10.4155/fmc-2017-0100 (2017).
- 67 Mirzaei, H. & Emami, S. Recent advances of cytotoxic chalconoids targeting tubulin polymerization: Synthesis and biological activity. *Eur J Med Chem* **121**, 610-639, doi:10.1016/j.ejmech.2016.05.067 (2016).
- 68 Ji, Y. T., Liu, Y. N. & Liu, Z. P. Tubulin colchicine binding site inhibitors as vascular disrupting agents in clinical developments. *Curr Med Chem* **22**, 1348-1360 (2015).
- 69 Bueno, O. *et al.* High-affinity ligands of the colchicine domain in tubulin based on a structure-guided design. *Sci Rep* **8**, 4242, doi:10.1038/s41598-018-22382-x (2018).
- 70 Prota, A. E. *et al.* The novel microtubule-destabilizing drug BAL27862 binds to the colchicine site of tubulin with distinct effects on microtubule organization. *J Mol Biol* **426**, 1848-1860, doi:10.1016/j.jmb.2014.02.005 (2014).
- 71 Ayaz, P., Ye, X., Huddleston, P., Brautigam, C. A. & Rice, L. M. A TOG:alphabeta-tubulin complex structure reveals conformation-based mechanisms for a microtubule polymerase. *Science* **337**, 857-860, doi:10.1126/science.1221698 (2012).
- 72 Li, L. *et al.* Recent advances in trimethoxyphenyl (TMP) based tubulin inhibitors targeting the colchicine binding site. *Eur J Med Chem* **151**, 482-494, doi:10.1016/j.ejmech.2018.04.011 (2018).
- 73 Canta, A., Chiorazzi, A. & Cavaletti, G. Tubulin: a target for antineoplastic drugs into the cancer cells but also in the peripheral nervous system. *Curr Med Chem* **16**, 1315-1324 (2009).
- 74 Zwergel, C. V., S.; Salvato, A.; Xu, Z.; Talhi, Q.; Mai, A.; Silva, A.; Altucci, L.; Kirsch, G. Novel benzofuran-chromone and -coumarin derivatives: synthesis and biological activity in K562 human leukemia cells. *MedChemComm* **4**, 1571-1579 (2013).
- 75 Guo, Q. N. L., L.; Zhou, Y.; Yu, P.; Teng, Y. Design, synthesis and biological evaluation of the novel antitumor agent aurone derivatives. *Adv. Mat. Res.* **781-784**, 1235-1239 (2013).
- 76 Blackburn, J. S. *et al.* Notch signaling expands a pre-malignant pool of T-cell acute lymphoblastic leukemia clones without affecting leukemia-propagating cell frequency. *Leukemia* **26**, 2069-2078, doi:10.1038/leu.2012.116 (2012).
- 77 Langenau, D. M. *et al.* Myc-induced T cell leukemia in transgenic zebrafish. *Science* **299**, 887-890, doi:10.1126/science.1080280 (2003).
- 78 Newman, D. J. & Cragg, G. M. Natural Products as Sources of New Drugs from 1981 to 2014. *J Nat Prod* **79**, 629-661, doi:10.1021/acs.jnatprod.5b01055 (2016).

VITA

1. Educational institutions attended and degrees already awarded:

Bachelor of Science in Pharmacy

Sun Yat-sen University, Guangzhou, China, 2013

2. No professional positions held.
3. No scholastic and professional honors.
4. Professional publications:

Xie, Yanqi, et al. "Semisynthetic aurones inhibit tubulin polymerization at the colchicine-binding site and repress PC-3 tumor xenografts in nude mice and myc-induced T-ALL in zebrafish." *Scientific reports* 9.1 (2019): 6439.

Sviripa, V. M., Kril, L. M., Zhang, W., Xie, Y., Wyrebek, P., Ponomareva, L., ... & Liu, C. (2018). Phenylethynyl-substituted heterocycles inhibit cyclin D1 and induce the expression of cyclin-dependent kinase inhibitor p21 Wif1/Cip1 in colorectal cancer cells. *MedChemComm*, 9(1), 87-99.

Frasinyuk, M.S., Zhang, W., Wyrebek, P., Yu, T., Xu, X., Sviripa, V.M., Bondarenko, S.P., Xie, Y., Ngo, H.X., Morris, A.J. and Mohler, J.L. et al. "Developing Antineoplastic Agents that Targeting Peroxisomal Enzymes: Cytisine-linked Isoflavonoids as Inhibitors of Hydroxysteroid 17-beta-dehydrogenase-4 (HSD17B4)." *Organic & Biomolecular Chemistry* (2017).

Popova, A. V., Frasinyuk, M. S., Bondarenko, S. P., Zhang, W., Xie, Y., Martin, Z. M., ... & Watt, D. S. Efficient synthesis of aurone Mannich bases and evaluation of their antineoplastic activity in PC-3 prostate cancer cells. *Chem. Pap.* (2018) 72: 2443.

5. Yanqi Xie